DISSERTATION

SPATIALLY-SELECTIVE OPTICAL PUMPING COOLING AND TWO-ISOTOPE

COLLISION-ASSISTED ZEEMAN COOLING

Submitted by

Rebekah Ferrier Wilson

Department of Physics

In partial fulfillment of the requirements

For the Degree of Doctor of Philosophy

Colorado State University

Fort Collins, Colorado

Spring 2014

Doctoral Committee:

Advisor: Jacob Roberts

David Krueger
Stephen Lundeen
Mario Marconi

ABSTRACT

SPATIALLY-SELECTIVE OPTICAL PUMPING COOLING AND TWO-ISOTOPE
COLLISION-ASSISTED ZEEMAN COOLING

In this thesis I describe two non-evaporative cooling schemes for cooling Rb atoms. The first is a Sisyphus-like ultracold gas cooling scheme called Spatially-selecTive Optical Pumping (STOP) cooling. In principle, STOP cooling has wide applicability to both atoms and molecules. STOP cooling works by exploiting the fact that atoms or molecules in a confining potential can be optically pumped out of an otherwise dark state in a spatially-selective way. Selecting atoms or molecules for optical pumping out of a dark state in a region of high potential energy and then waiting a fixed time after the optical pumping allows for the creation of a group of high kinetic energy atoms or molecules moving in a known direction. These can then be slowed using external fields (such as the scattering force from a resonant laser beam) and optically pumped back into the dark state, cooling the gas and closing the cooling cycle. I present theoretical modeling of the STOP cooling technique, including predictions of achievable cooling rates. I have conducted an experimental study of the cooling technique for a single cooling cycle, observing one dimensional cooling rates in excess of 100 μK per second in an ultracold gas of ^{87}Rb atoms. I will also comment on the prospects for improving the cooling performance beyond that presented in this work.

The second cooling scheme I investigated is called Two-Isotope Collision Assisted Zeeman (2-CAZ) cooling. Through a combination of spin-exchange collisions in a magnetic field and optical pumping, it is possible to cool a gas of atoms without requiring the loss of atoms from the gas. I investigated 2-CAZ cooling using ^{85}Rb and ^{87}Rb. I was able to experimentally confirm that the measured 2-CAZ cooling rate agreed with a cooling rate predicted though a simple analytic model. As part of the measured cooling rate, I quantitatively characterized the heating rates associated with our actual implementation of this cooling technique and found hyperfine-changing collisions to be a significant limitation for the $^{85/87}$Rb gas mixture. Possible improvements to this experiment will be discussed as well as the prospects for improved cooling performance using an atom without hyperfine structure as the optically pumped atom.

ACKNOWLEDGEMENTS

I would like to take this opportunity to thank the many people who have made the completion of this thesis possible.

Throughout this whole process my husband Truman has been a constant support. He helped me with much of my work in the lab, from lending an extra set of hands during laser alignment to suggesting better ways to optimize my measurement techniques. Without his help I would never have been able to complete the experiments I performed. He was also always there to listen when I wanted to complain about the experiment. Without that outlet I probably would have lost my sanity a long time ago. He has also been a great help in the thesis writing process. Without his help and friendship I would not have completed this thesis and degree.

I have also been supported by a wonderful family. My family in Oregon has been a great resource. They were always there to listen when I wanted to vent about this or that or when I wasnt sure I wanted to complete this degree. Without their help I would not be where I am today. My Colorado family has also been a great encouragement to me. They have also been extremely generous in sharing their home with me for the many weeks when I was without a Colorado apartment. Without the help of all of my family I could never have finished this work.

Last, but certainly not least, I would like to thank my adviser, Jake Roberts. He has provided me with a great deal of scientific guidance throughout this process. From the daily data analysis and interpretation work to the more general investigation of scientific topics, his help has been invaluable. He was always willing to take the time to explain the scientific details involved in a particular problem or walk me through a complicated calculation. In addition to his great scientific ability, Jake is also a great human being. He treats everyone with kindness and respect, including his graduate students. This made working for him a very pleasant experience. I will always be thankful that I had an adviser who was not only an excellent physicist but also a great person to work with and for.

TABLE OF CONTENTS

Chapter 1

History of Laser Cooling and Relevant Physics

Major strides have been made in the last few decades in the field of laser cooling resulting in the ability to cool and trap atoms at micro-Kelvin temperatures [1, 2]. The field of Atomic Molecular and Optical (AMO) Physics includes a wide range of techniques and applications of laser cooling, from the Cesium clocks [3] to the use of ionized ultracold atoms to create focused ion beams [4], to quantum degenerate gases [5, 6] to list just a few. I will begin this chapter by discussing some of the history of laser cooling and several laser cooling techniques that relate to the work done in this thesis. I will then briefly overview the two cooling experiments that I performed. Finally, I will discuss some of the relevant physics that will be required to understand the remaining chapters.

1.1 History of Laser Cooling and Laser Cooling Techniques

When atoms or ions are cooled to very cold temperatures they, by necessity, are much slower than a room temperature atom or ion. The prospect of being able to work with atoms that are traveling just a few meters per second or less was a large part of the motivation for the development of laser cooling. If an atom is traveling slowly and is confined, one is then able to determine properties of the atom without having to worry about the Doppler shift or relativistic time dilation. Once atoms are cooled significantly they allow for the study of cold collision dynamics and quantum behavior that is qualitatively different from the behavior of room temperature gases.

The idea for laser cooling was proposed in 1975 by two separate groups [7, 8], but it wasn't until a few years later in 1978 that the very first experiment demonstrating the technique with ions was accomplished [9]. Within the next few years additional techniques using more than just the radiative force of light were developed. I will discuss several light-based cooling techniques, specifically Doppler cooling since it has been one of the most successful all optical techniques, and several other techniques to cool below the temperatures achievable with Doppler cooling.

Another common technique used to cool atoms to very low temperatures is evaporative cooling. It has been the most successful method for cooling ultracold atoms to the lowest possible tempera-

tures to date. It was used to create the first Bose-Einstein Condensate (BEC) in 1995 [1, 2]. I will discuss some of the details of evaporative cooling after I discuss the optical cooling techniques.

1.1.1 Doppler Cooling and Optical Molasses

To understand how a laser can be used to cool an atom it is important to first understand the force that can be exerted on an atom by a laser. If we consider the scattering rate from a laser with intensity I for a two level atom we find the scattering rate is given by [10]

$$\gamma_p = 2\pi\Gamma/2\frac{I/I_{sat}}{1 + I/I_{sat} + (2\Delta/\Gamma)^2} \tag{1.1}$$

where Γ is the natural linewidth of the transition in Hz, I_{sat} is the saturation intensity and Δ is the laser frequency detuning from the natural transition. In our case, Γ is about 6 MHz for the cooling transition in Rb and I_{sat} is 1.6 mW/cm^2 for circularly polarized light resonant with the cycling transition and the atoms spin polarized by that light [11]. If an atom absorbs a photon from a laser it will receive a momentum kick of $\hbar k$ in the direction of the laser. When the atom then emits the photon it will get another momentum kick of $\hbar k$, but this time in a random direction. Over many photon scatters, the momentum kick from the spontaneously emitted photon will average to zero, making the average momentum kick per photon scatter $\hbar k$ in the direction of laser propagation. So the average force on the atom from a laser will be

$$F = \hbar k \gamma_p = \hbar k 2\pi\Gamma/2\frac{I/I_{sat}}{1 + I/I_{sat} + (2\Delta/\Gamma)^2} \tag{1.2}$$

where k is the wave number of the photon from the laser light.

This force can now be used to cool an atom as long as certain considerations are taken to ensure that this force results in cooling instead of heating. To insure that cooling occurs, the Doppler effect is used in conjunction with the variation of γ_p as a function of detuning, Δ (shown in Figure 1.1). Figure 1.1 shows that a decrease in γ_p occurs when the laser is detuned from resonance. To see how this can lead to cooling, consider a laser detuned slightly red of resonance and consider an atom traveling towards that laser. In this case, the laser light will be Doppler shifted closer to resonance with the atom, meaning it will be more likely to scatter photons that will slow it down. If an atom

2
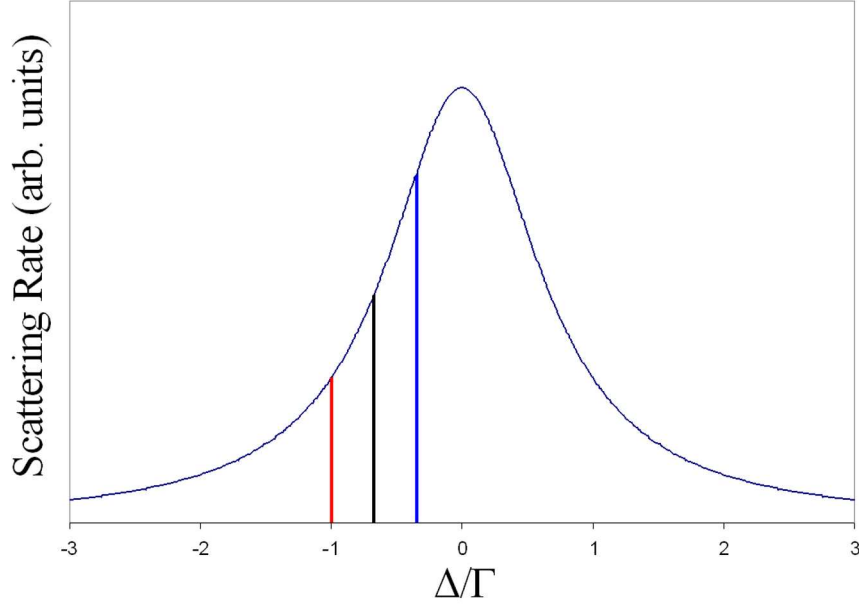
Figure 1.1: The scattering rate, γ_p, as a function of detuning is shown. The laser frequency is indicated by the dashed line and the red and blue shifted frequencies seen by a traveling atom are indicated by the red and blue lines. This figure was taken from [14].

is traveling away from the laser, the laser light will be Doppler shifted further from resonance, decreasing the likelihood of a photon scatter. This decreases the chance of scattering photons that increase the atom's kinetic energy. Counter-propagating two red shifted beams cools atoms in one dimension. This set-up provides a velocity dependent damping force on the atoms and is known as an optical molasses [13].

1.1.2 Sub-Doppler Cooling Techniques

There are a number of non-evaporative cooling techniques, but only one has been successful at reaching BEC temperatures [12]. The pursuit of a non-evaporative cooling technique is what led us to investigate both of the cooling experiments that I will discuss in future chapters. Before I go on to describe the cooling techniques that I investigated, I want to first mention a few of the non-evaporative cooling schemes that have been tried in the last few decades, including one technique, Sisyphus cooling, that relates closely to one of the experiments I did. The following techniques are meant to be at an overview level to simply give a sense of the types of techniques that exist. For a

more in depth description of any of these techniques, I suggest reading *Laser Cooling and Trapping* [10].

Raman Cooling

Raman Cooling was first demonstrated in 1992 by Mark Kasevich and Steven Chu [15] and was also expanded in 1995 as described in Ref. [16]. It has been one of the most successful of the sub-Doppler cooling techniques, but has still not been able to reach BEC temperatures. In its most basic realization the technique uses two counter-propagating laser beams. The most straightforward implementation of this cooling technique relies on velocity selection, so the detuning of each beam is very important. The first step in a cooling cycle is a phase-coherent stimulated-emission-based population transfer from one internal state to another. Without spontaneous emission, the linewidth of the Raman transition can be much smaller than the Doppler width of ultracold atoms, meaning that this transfer can be accomplished in a velocity-sensitive way. The detuning is chosen so that when an atom absorbs and emits a photon from the two beams, known as undergoing a Raman pulse, its momentum is reduced by $2\hbar k$. The Raman pulse not only changes the velocity of the atoms, but changes the magnetic spin state as well. Thus, while the kinetic energy decreases, the entropy associated with the magnetic spin state increases. The atoms are then optically pumped back to the initial magnetic spin state to close the cooling cycle and remove entropy from the gas. A simple diagram of Raman cooling is shown in Figure 1.2. Later implementations of this technique replaced the phase-coherent external Raman beams with Raman transitions driven by the optical trap light confining the atoms, simplifying the laser requirements at the expense of requiring an additional magnetic field [17].

Velocity Selective Coherent Population Transfer (VSCPT)

Velocity Selective Coherent Population Transfer (VSCPT) is also a velocity selective technique like Raman cooling. It was first demonstrated in three dimensions in 1995 [19]. To understand VSCPT it is useful to discuss coherent population trapping. Consider a three level system that is driven by two lasers with frequencies such that an atom can be pumped from one ground state to the other by a stimulated Raman process, similar to that shown in Figure 1.2. This means the atoms are pumped to a virtual excited state when being transferred from one ground state to the other.
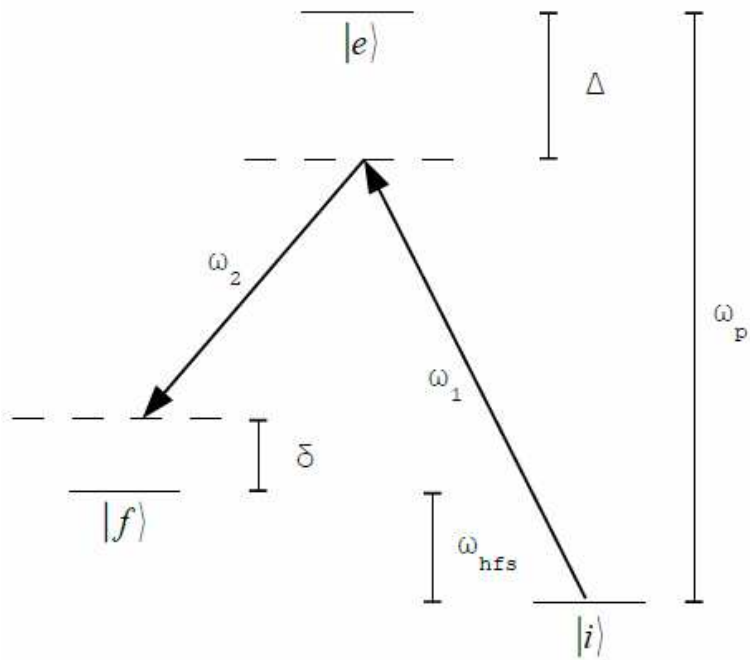
Figure 1.2: This figure shows a a simple diagram of Raman cooling. The two counter-propagating beams have angular frequencies of ω_1 and ω_2 that are used to drive that atoms from the initial state (i) to the final state (f) through and excited state (e). The initial and final state are separated by a hyperfine splitting indicated by ω_{hfs}. The beams are detuned by Δ and δ so that they only interact with chosen velocity classes. This figure was taken from [18]

This process results in the atoms being coherently transferred from one ground state to another. In addition, spontaneous scatters occur.

Because of the Doppler effect, VSCPT can make use of the detuning of the stimulated Raman process' proportionality to the atoms' velocity. Spontaneous scatters during VSCPT can pump atoms into a dark state(a state which does not interact with the laser light), which exists only for states with zero angular momentum. When the atoms have a non-zero velocity, however, such a dark state is not stable as kinetic energy differences result in phase shifts that prevent the states from remaining dark. When photon scattering occurs, the atom is more likely to scatter a photon from the laser toward which it is moving and so in general will move closer to zero velocity through spontaneous emission. Eventually, optical pumping in this configuration will result in an atom being in a state where the velocity of the atom is zero and where the phase of the two ground states is such that the atom no longer couples to the laser light due to destructive interference(i.e. the atoms are pumped into the dark state). Such an atom will then remain in that state and be "trapped" at zero average velocity. If however the atom's momentum is non-zero the atom can be excited and scatter additional photons that may reduce its velocity. The result is that atoms with non-zero velocity will continue to be excited and scatter photons until they are pumped by random walk into the zero momentum dark state. While VSCPT was demonstrated experimentally, it worked effectively only in gases with small atom numbers that were optically transparent[19].

Sisyphus Cooling

Finally consider non-evaporative Sisyphus cooling. This technique has not been able to reach sub-recoil temperatures to the same degree as the other techniques listed above, but it is quite robust and relatively easy to implement. It also has similarities to the first experimental cooling technique that I will discuss in this thesis. In both cases atoms are optically pumped at a turning point in a confining potential and then optically pumped at the center of this confining potential. The main difference between my technique and Sisyphus cooling is that my technique does not rely on the atoms moving "uphill" more than "downhill" in the potential to achieve cooling. The name "Sisyphus cooling" comes from the Greek myth of Sisyphus who was punished by the gods and forced to roll a boulder up a hill. Every time he got the boulder to the top, it would roll back down
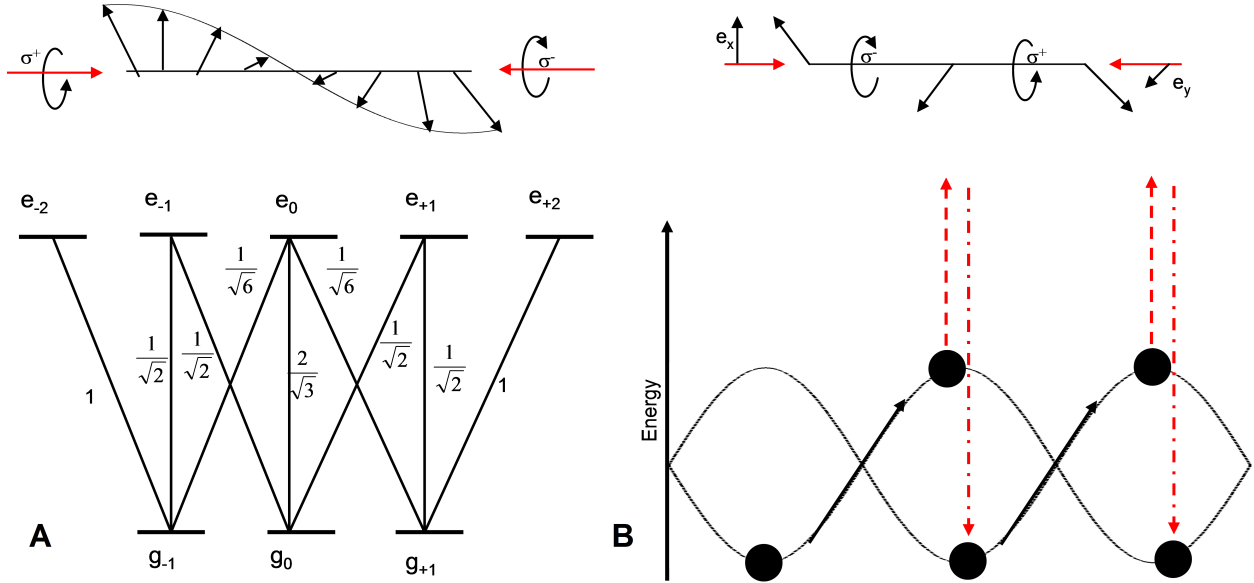
Figure 1.3: This figure shows a cartoon of the laser polarization (top) and energy variation (bottom) associated with $\sigma^+ - \sigma^-$ polarization gradient cooling (A) and lin $\perp$ lin Sisyphus cooling (B). As shown, the goal is to have an atom continually climb a potential hill. This figure was taken from [20]

and he would have to start over. This gives us a simplistic picture of Sisyphus cooling; forcing an atom to continually climb a potential hill in order to cool it.

There are two types of Sisyphus cooling [21], lin $\perp$ lin cooling and induced orientation cooling (also known as $\sigma^+ - \sigma^-$ polarization gradient cooling). The physics of the two techniques are different, but both are important. I will first discuss lin $\perp$ lin cooling and then induced orientation cooling.

Both techniques make use of two counter propagating laser beams tuned to the red side of an atomic resonance. Also, an atom needs to have internal state structure in the ground state for either of these techniques to work. Lin $\perp$ lin cooling is so named since the two beams of light used have orthogonal linear polarization. The polarization of the light field that results is shown in Figure 1.3B. The two beams are counter-propagated, as shown, creating a light field whose polarization varies in space. The combined polarization of the standing wave pattern varies between linear at z=0, to circularly polarized (σ^-) at z=λ/8, back to linear at z=λ/4, then opposite handed circularly polarized (σ^+) at z=3λ/8 and finally back to linear at z=λ/2.

The position variation in polarization also leads to a position variation in the light shift of the magnetic sub-states. This variation occurs since with σ^+ polarization $\Delta m_F = +1$ transitions are driven, with σ^- polarization $\Delta m_F = -1$ transitions are driven and with linear polarization $\Delta m_F = \pm 1$ transitions are driven equally. This variation results in a shift in the ground state energies that is position and spin state dependent and is shown at the bottom of Figure 1.3B. It is this variation in the energy that allows the atoms to see potential "hills" just like Sisyphus. This variation in ground state energy comes from different strengths of $\Delta m_F = +1$ and -1 transitions due to the different Clebsch-Gordan coefficients associated with those transitions.

From the atoms' perspective it sees the ground state energy oscillating with position for a given magnetic sublevel. When the atom climbs the potential hill it loses much of its kinetic energy and slows down. Since it is slower at the top of the hill it ends up spending more time at the top than at other positions in the potential. It is then much more likely that the atom will absorb a photon while at the top of the hill. Once excited it can either stay at the top of the potential by radiating back into the initial state (and thus there is no change in the potential) or it winds up in the lower state and has to climb uphill again. On average, the atom will climb uphill more than downhill, and thus will cool.

Induced orientation cooling again makes use of two counter-propagating laser beams tuned to the red side of an atomic resonance. In this case the two beams are circularly polarized beams of different handedness (σ^+ and σ^-). When these two beams are overlapped the result is a polarization field that appears linear to the atom, but the linear polarization rotates in space, as shown in Figure 1.3A. This linear polarization vector rotates in a helix through space. The linear light drives $\Delta m = 0$ transitions in a local frame where the z axis is taken to be along the light polarization direction. Because of the Clebsh-Gordan coefficients an atom with zero velocity would see a build up in the center of the m_F distribution after many photon scatters. This build up is always in the center of the m_F distribution, as long as the m_F states are defined locally by the direction of the linear magnetic field. But when an atom moves, the quantization axis changes, and so the atoms have to scatter photons to readjust. In so doing, the atom scatters more photons from the beam towards which it is moving, resulting in a force that opposes the atom's motion. In this way, this technique is much like Doppler cooling, although this technique can reach temperatures below those reached by Doppler cooling alone.

As an interesting historical note, the technique of induced orientation cooling was discovered by accident in 1987 [22]. During some of the first experiments implementing Doppler cooling with Sodium atoms it was discovered that the temperature of the atoms was significantly lower then that predicted by the Doppler limit. Additionally, the measured temperature was found to be dependent on the polarization of the laser beams used and the size of any ambient magnetic field. The predicted Doppler limit was derived for a two level atom, so the initial investigation into the measured temperature discrepancy focused on the differences between Sodium and a two level system. The observed dependence on polarization and magnetic field also suggested that the multi-level nature of Sodium was important, specifically the Zeeman sublevels. Through additional observation and detailed calculations, the technique of induced orientation cooling was identified and described. A detailed history of this discovery can be found in the Nobel lectures of Phillips [22], Chu [23] and Cohen-Tannoudji [24].

Disadvantages of These Techniques

While these techniques perform well in gases with relatively low density, the performance degrades as the density is increased. This limitation has prevented most techniques from reaching near BEC temperatures. The mechanism limiting these techniques is reabsorption [25]. Reabsorption becomes important as the optical thickness of a gas increases due to increasing density. If the sample is dense enough, when an atom absorbs and re-emits a photon, that photon cannot easily escape the dense cloud of atoms. It is instead likely to be reabsorbed by another atom, causing heat, but also interfering with the cooling mechanisms by driving atoms to unwanted internal states. Reabsorption is generally the primary limiting factor for all-optical cooling techniques.

Additionally, these techniques have also been limited by light assisted collisional loss [26]. This loss occurs when a pair of atoms in the ground state absorbs a photon and is excited to a bound excited state potential. In this upper potential the atoms are accelerated towards one another due to induced dipole forces and their kinetic energy is increased. Eventually they emit a photon and de-excite back to the ground state. The energy of the emitted photon is less than the absorbed photon so the overall kinetic energy of the pair is increased. This increase leads to heating and loss. A desire for a new method that would not be as easily limited by these two heating mechanisms led us to perform the experiments described in this thesis.

1.1.3 Evaporative Cooling

Evaporation occurs naturally in many systems. One simple example is the case of a hot cup of coffee. Under typical conditions, if you leave a hot cup of coffee on a table it will immediately begin to cool down. In part this is because the most energetic coffee particles are evaporating and leaving the coffee as steam. As they leave, the rest of the coffee cools down since the particles that leave have more energy than the average particles in the liquid. In fact, it only takes a small portion of the hot coffee particles leaving to reduce the coffee temperature significantly. This is an example of how evaporative cooling works in general. Evaporative cooling of atoms works in much the same way and this method was first applied to cold atoms in 1988 [27].

Evaporative cooling of trapped atoms works in just the same way as described above–by allowing the atoms with the highest energy to leave so that the remaining atoms have a lower average energy. Once the remaining atoms re-establish thermal equilibrium, the gas will then be colder than before. At some point, enough of the high energy atoms will have left and the remaining atoms will be confined to the trap with only a vanishingly small number of atoms with enough energy to escape. The final group of atoms will have a lower temperature and possibly a higher density than the initial group of atoms depending on the nature of the confining potential.

Evaporation can be used to cool atoms in a trap of finite depth either through controlling the depth of the confining potential or by introducing losses for atoms that have more than a chosen amount of energy (e.g. driving magnetic trap loss via resonant spin flips at a chosen magnetic field [28]). By reducing the trap depth or inducing loss in higher energy atoms, more and more of the higher energy atoms are allowed to escape thereby reducing the temperature of the cloud significantly and increasing the density for commonly used ultracold atom traps. This technique is called forced evaporation.

Advantages and Disadvantages

Evaporative cooling has one main advantage over all other cooling methods. This advantage is that the energy scale associated with evaporation is determined by the energy of the gas. This means that evaporation will continue to work even as the temperature of the gas is lowered since the energy scale of the cooling follows the energy scale of the gas. Other cooling techniques have some

fixed energy scale associated with them (such as the recoil energy) and once the temperature of the gas gets close to that scale the cooling works less effectively, oftentimes limiting the final achievable temperature. Before this last year [12], evaporative cooling was the only technique that would allow atoms to be cooled to cold enough temperatures to create a BEC. Although this is the most common cooling method that can currently be used to achieve a BEC, there are several disadvantages to the technique. One of the major disadvantages is that most of the atoms (90-95%) are required to leave the sample in order to reach the desired temperature. Also this technique is slow as compared to optical cooling techniques. Finally, the cooling is linked strongly to the potential used to confine the atoms, leading to less flexibility in the potentials that could possibly be used. These disadvantages have led researchers to continue to search for non-evaporative methods that can reach BEC temperatures.

1.2 My Non-Evaporative Cooling Experiments

The desire for a successful non-evaporative cooling method, especially one with the possibility of mitigating reabsorbtion, led our lab to begin investigating Two Isotope Collision Assisted Zeeman (2-CAZ) Cooling. I took over this experiment part way through its implementation and completed the experiment. My work with the 2-CAZ experiment led to the investigation of another novel cooling technique called Spatially selecTive Optical Pump (STOP) Cooling. I will briefly describe the two cooling methods at an overview level. Both of these experiments will then be discussed at greater length in the remaining chapters of this thesis.

For the experiments discussed in this thesis, I have worked with Rb since it has transitions that are easily accessible using readily available and low cost diode lasers. Figure 1.4 shows the relevant ^{85}Rb and ^{87}Rb transitions that I used for both experiments, including the main trapping transitions ($5S_{1/2}$ $F=2$ to $5P_{3/2}$ $F=3$ for ^{87}Rb and $5S_{1/2}$ $F=3$ to $5P_{3/2}$ $F=4$ for ^{85}Rb) and the repump transitions ($5S_{1/2}$ $F=1$ to $5P_{1/2}$ $F=2$ for ^{87}Rb and $5S_{1/2}$ $F=2$ to $5P_{1/2}$ $F=3$ for ^{85}Rb). The STOP cooling experiment used only ^{87}Rb, but the CAZ cooling experiment, discussed in Chapters 5-7 used both ^{85}Rb and ^{87}Rb simultaneously. Previous iterations of the experiment used 795 nm diode lasers to repump the atoms out of the lower hyperfine state for both isotopes [18, 20], but during my time on the experiment all of the lasers were converted to 780 nm lasers. When using a

11
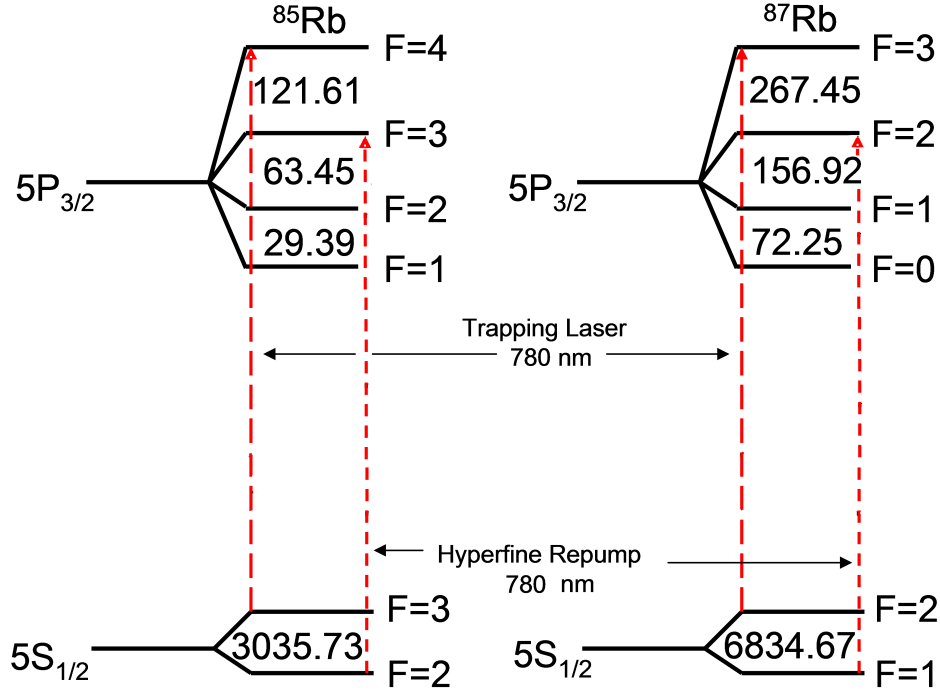
Figure 1.4: The hyperfine splitting for [87]Rb and [85]Rb are shown in MHz. The main trapping and repump transitions are indicated in the figure. For both isotopes, the repump can also be from the $5S_{1/2}$ to $5P_{3/2}$. This figure was taken from [20]

780 nm laser the main repump transition is from the $5S_{1/2}$ F=2 state to the $5P_{3/2}$ F=3 state for [85]Rb and from the $5S_{1/2}$ F=1 to the $5P_{3/2}$ F=2 state for [87]Rb.

1.2.1 Spatially selecTive Optical Pumping (STOP) Cooling

The first experiment that will be described in this thesis (Chapters 2-4) is Spatially selecTive Optical Pumping (STOP) Cooling. STOP Cooling is a Sisyphus-like ultracold gas cooling scheme. In principle, STOP cooling has wide applicability to both atoms and molecules. STOP cooling works by exploiting the fact that atoms or molecules in a confining potential can be optically pumped out of an otherwise dark internal state, with respect to a particular transition, in a spatially-selective way. Selecting atoms or molecules for optical pumping out of a dark state in a region of high potential energy and then waiting a fixed time after the optical pumping allows one to create a group of high kinetic energy atoms or molecules moving in a known direction. These atoms can

then be slowed using external fields (such as the scattering force from a resonant laser beam) and optically pumped back into the dark state, cooling the gas and closing the cooling cycle.

STOP cooling is a simple cooling technique that can be applied to any atom or molecule that has a dark state and can be trapped. The simple requirements for what can be cooled indicates that it has the potential to be a wide ranging cooling technique. In this thesis I will present a single cycle STOP cooling experiment with ^{87}Rb in an optical dipole trap. From this experiment I was able to confirm the predicted cooling rates that were suggested by the model I created.

There are many advantages to STOP cooling, including its simplicity, but by far the most intriguing advantage is its potential to cool a wide range of atoms and molecules. There has been a great deal of recent interest in cold and ultracold molecules due to the predicted usefulness of molecules in investigating many-body physics studies in the presence of long-range interactions [29, 30], fundamental physics studies such as parity violation and electron dipole measurement searches [32–35], and potential applications in quantum information and quantum simulation [36–38]. Many of these lines of investigation benefit from either cold temperatures and/or high phase-space density, and so a widely applicable cooling technique would be useful in these studies. More detail about how STOP cooling could be applied to molecules will be discussed in Chapter 4.

1.2.2 Two Isotope Collision Assisted Zeeman (2-CAZ) Cooling

The second experiment that will be described in this thesis is Two Isotope Collision Assisted Zeeman (2-CAZ) Cooling. 2-CAZ cooling is a non-evaporative cooling technique that has the potential to avoid some of the reabsorbtion limitations that have plagued the other non-evaporative cooling techniques. 2-CAZ cooling can best be thought of as a two step process. The first step is for two atoms to undergo a spin-exchange collision in the presence of a magnetic field that converts their kinetic energy to magnetic energy. Once this has occurred, the second step is for optical pumping to be used to remove this increased magnetic energy and pump the atoms back to their original state. This results in a lower kinetic energy for the atoms, meaning they are at a lower temperature than when they started. This technique will be described in greater detail in Chapter 5. This technique has similarities to demagnetization cooling [39], and spin gradient demagnetization cooling [40].

This cooling technique was originally proposed using one isotope [41], but we have extended the cooling technique to two isotopes. I will discuss some of the advantages of 2-CAZ cooling over

single isotope CAZ cooling in Chapter 5. I will also discuss some of the challenges we encountered during the experiment. Some of these challenges prevented us from achieving the hoped for cooling from 2-CAZ, but these challenges did lead us to try STOP cooling which proved to be a much more successful cooling technique.

1.3   Outline of Thesis

In the rest of this chapter I will discuss the background physics that is needed to understand the cooling experiments that I performed. This includes some basic laser cooling physics, specifically the making of a Magneto-Optic Trap (MOT) and a Far-Off Resonance Trap (FORT). I will also discuss spin-exchange collisions and Zeeman shifts as they relate to the 2-CAZ experiment.

In the next three chapters (Chapters 2-4) I will discuss in detail the STOP cooling experiment. I will first cover the model that was created to describe the cooling in Chapter 2 and then I will move on to discuss the actual experiment in Chapter 3. Finally, I will describe the results of the experiment in Chapter 4.

In Chapter 5-7, I will describe the 2-CAZ cooling experiment. I will start by describing the theory of 2-CAZ cooling and single isotope CAZ cooling in Chapter 5 and will then discuss the experiment in Chapter 6. I will then describe the results of the 2-CAZ experiment in Chapter 7. Finally, I will briefly summarize the work presented in this thesis and discuss the future of both experiments in Chapter 8.

1.4   Overview of Relevant Physics

In the previous sections, STOP cooling, CAZ cooling and other cooling techniques were briefly discussed, but thus far I have not discussed any of the general techniques that would be required to actually implement this type of cooling. It is important to go into some detail about these subjects so that the remaining chapters can be well understood. There are also several other important physics concepts that will be used throughout the remainder of the thesis that will be discussed here. I will first discuss some basic atomic physics specifically related to magnetic fields. This information is needed to understand 2-CAZ cooling. I will also discuss some basics of laser cooling

physics that will help the reader to understand how the initial conditions necessary for both the STOP and 2-CAZ cooling experiments were obtained.

1.4.1 Zeeman Effect

In a magnetic field, quantum states with a net magnetic moment experience an energy shift and this energy shift with magnetic field is called the Zeeman Effect. One manifestation of this effect is the splitting of a spectral line in the presence of a magnetic field. The Zeeman energy shift occurs because of an interaction between an atom's magnetic moment and an externally applied magnetic field. The Hamiltonian that describes this interaction is

$$H_{Zeeman} = -\overline{\mu} \cdot \overline{B} \tag{1.3}$$

where μ is the magnetic moment and B is the magnetic field strength. The shift in the energy levels due to the Zeeman effect are given to first order as

$$\Delta E_{Zeeman} = -g_F \mu_B B m_F \tag{1.4}$$

where μ_B is the Bohr magneton, m_F is the magnetic sublevel of the atoms and g_F is the gyromagnetic ratio of the atoms' states. g_F is defined for a particular set of magnetic sublevel states and depends on several quantum numbers, including the total atom angular momentum (which is denoted as F). This g_F term is described in more detail in [18]. The g_F factor is -1/3 for ^{85}Rb in the lower hyperfine ground state and -1/2 for ^{87}Rb in the lower hyperfine ground state. For 2-CAZ cooling we are only concerned with first order Zeeman shifts. Single isotope CAZ cooling, which will be discussed in Chapter 5, also makes use of second order Zeeman shifts. The second order Zeeman shift for an alkali atom with hyperfine structure is given by

$$\Delta E_{Zeeman2} = (-1)^F \hbar \omega_{HF} (4 - m_F^2) \left(\frac{\mu_B B}{2\hbar \omega_{HF}} \right)^2 \tag{1.5}$$

where $\hbar \omega_{HF}$ is the energy splitting of the ground state hyperfine levels without a magnetic field present. The previous equations were taken from [18]. One thing to note about the first and second order Zeeman shift is that the first order shifts are uniform with respect to adjacent m_F states

15

since the shifts are proportional to m_F, but since the second order shift is proportional to $(4 - m_F^2)$ the second order shifts are not uniform. Also, as their names imply the first order shift is more relevant at low magnetic field and the second order shift becomes relevant at high magnetic fields.

1.4.2 Spin-Exchange Collisions

Spin-exchange collisions are an integral part of one and two isotope CAZ cooling. A spin-exchange collision is a collision between two atoms in which both atoms' final spin state is different from their initial spin state and the total spin projection along a quantization axis of the atoms in the collision is conserved. This requirement that spin-exchange collisions preserve the total atom spin along a quantization axis differentiates spin-exchange collisions from other types of collisions where the spin of the atoms can change (e.g. dipole exchange collisions [31]).

To understand this in more detail, consider two different atoms each with a single valence electron, which is the case for Rb atoms. For two atoms far away from one another, a good set of basis states is one where the individual atom spins are each specified independently. We can consider the specific case where one atom's electron is in the spin up state, and the other atom's electron is in the spin down state. When the atoms are close together, like during a collision, it is no longer correct to describe the states in this way. Instead, the electrons are best described in a set of basis states consisting of a singlet and triplet states since the energies of these states are very different due to different amounts of electron overlap due to quantum statistics. The singlet state and the triplet states have different scattering lengths since the associated interatomic potentials are different. These different scattering lengths lead to a difference in phase shift during a collision. After the collisions, the atoms can be thought of as effectively being projected back on the original (i.e. large separation) basis states and so the phase difference between the singlet and triplet portions of the wavefunction will produce a change in the individual atoms' spin. In general, the triplet and singlet phase shifts depend on the details of the interatomic potential so these rates are difficult to predict from first principles in many cases. The addition of nuclear spin complicates the situation, but the essential physics described here for spin-exchange collisions still holds.

1.4.3   Magneto-Optical Trap (MOT)

Laser cooling and trapping has enabled a wide range of interesting research using ultracold atoms ranging from very fundamental measurements like the measurement of the electron dipole moment [32–35] to more applicable technology like atomic clocks [3]. The majority of experiments in atomic physics make use of one of several standard techniques, namely magneto-optical traps (MOTs), optical dipole traps or magnetic traps. I will discuss magneto-optical traps and a specific type of optical dipole trap, the far-off resonance trap (FORT), in this section and the following.

Although an optical molasses can be very useful, it does not actually provide a way to trap atoms in space. Since the damping force provided by the lasers is not position dependent, the atoms will eventually drift out of the cooling region. However, magneto-optical forces can be used to create spatial confinement in addition to Doppler cooling [42]. To illustrate how this works consider a two level system with a $J=0$ ground state and $J=1$ excited state with possible excited state sublevels of $m = \pm 1, 0$. In order to create the needed position dependent force to trap the atoms, a magnetic field with linear spatial variation is added. When the magnetic field is applied the m states are shifted in energy. As shown in Figure 1.5, the $m=+1$ state is shifted up for B>0 and the $m=-1$ state is shifted down. Because of this shift the $\Delta m=-1$ transition is tuned closer to resonance and the $\Delta m=+1$ is tuned further from resonance since the light is detuned to the red of the transition as part of Doppler cooling. Now if the laser polarization is chosen to be σ^- from the right and σ^+ from the left, then the atoms will scatter more photons from the laser they are traveling towards. An atom that is located to the right of the B=0 point will then feel a net force to the left due to the scattering from the left-going σ^- laser beam being greater than the right-going σ^+ laser beam. In this situation of σ^+ from the left, σ^- from the right, and red detuning in the magnetic field gradient, there will be both a velocity damping force from Doppler cooling given the red detuning and a position-dependent restoring force. This allows atoms to be confined to a specific region in space as well as be cooled.

This technique can be easily extended to three dimensions by simply applying this one dimensional setup along three axes. A simple schematic of this type of setup is shown in Figure 1.6. A set of anti-Helmholtz coils was used to create the needed magnetic field. This three dimensional MOT is what is used in our experiment.
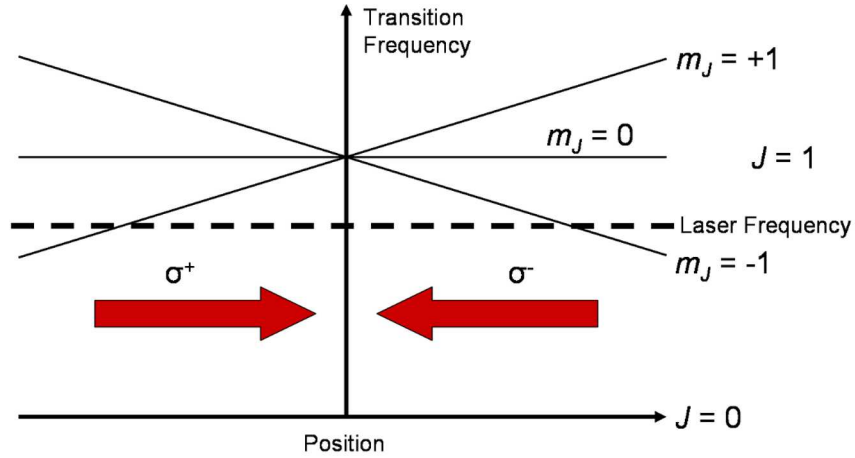
Figure 1.5: This figure shows the energy levels for a 1-D MOT as a function of position. The counter propagating circularly polarized lasers used are shown in red. These beams push atoms towards the center of the trap. This figure was taken from [14].
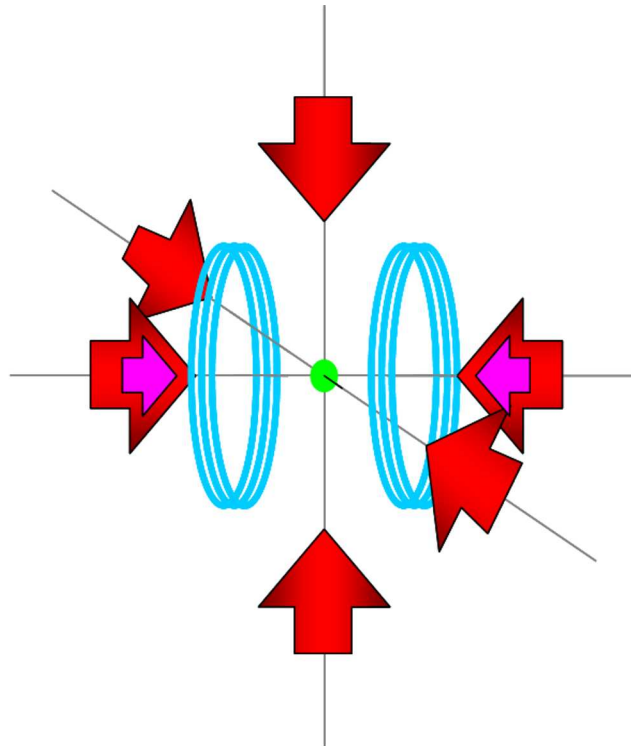
Figure 1.6: A simply cartoon of a typical MOT set-up is shown. The main trapping lasers are shown in red and the repump laser is shown in pink. The blue coils represent the Anti-Helmholtz pair of coils used to create the needed magnetic field.

At this point the atoms can be trapped and will allow us to perform experiments, but they are still relatively warm (100s of μK) and not very dense. Most experiments that use MOTs, including ours, also use an additional trapping method to improve the density or allow additional cooling of the atoms by removing the limits to the lowest achievable temperatures associated with continuous scattering of light as occurs in the MOT. These trapping methods include magnetic traps and optical dipole traps [43, 44]. We use a type of optical dipole trap called a Far-Off Resonant Trap (FORT) which will be discussed in detail in the following section.

1.4.4   Far-Off Resonance Trap

As the name suggests, an optical dipole trap takes advantage of an atom's electric dipole moment in order to trap the atom. If we consider an atom in a light field, the induced dipole moment will look like

$$\overline{p} = \alpha \overline{E} \tag{1.6}$$

where α is the atom's polarizability constant and E is the electric field. For time-varying fields α in general depends on the detuning and can be positive or negative. The potential associated with this dipole is proportional to $-\overline{p} \cdot \overline{E}$. If we substitute in for $\overline{p}$ we can see that the potential is proportional to E^2 or the intensity of the laser. We can write an explicit equation for the potential in terms of the detuning [20]

$$U_0 = \frac{\hbar \Delta}{2} ln \left(1 + \frac{\Omega_1^2/2}{\Delta^2 + (\Gamma^2/4)} \right) \tag{1.7}$$

where Ω_1 is the Rabi frequency associated with the laser and Γ and Δ are the same as in equation 1.1. For a value of $\Delta < 0$ (red detuning) the potential is attractive, for $\Delta = 0$ the potential vanishes and for $\Delta > 0$ the potential becomes repulsive. The above equation is for a simple two-level system and doesn't exactly describe the FORT we used, but it does indicate the relevant general result that would allow a high intensity beam to be used to trap atoms. In this experiment a CO_2 laser with a wavelength of 10.6 microns was used. The resulting detuning is so great that the electric field of the laser can be treated as a DC electric field in terms of the Rb atoms' response and the polarizability, α, is equal to the DC electric field polarizability of the ground state to a good

approximation. More details about the strength and loading physics of such an optical dipole trap can be found in [20]

There are several advantages to using a FORT. One of the main advantages over a MOT is that a FORT can allow for significantly higher atoms densities and colder temperatures because there are no radiation forces from light scattering since there is little light scattering in the FORT. Also a FORT doesn't require a magnetic field which can sometimes be beneficial. Additionally a FORT is experimentally simple in that it only requires the use of one laser beam to create a three dimensional trapping potential. It is important to note that far-detuned optical dipole traps do not provide any cooling, so it is usually necessary to load atoms that have already been cooled into them. In our case, we load our FORT from the MOT by overlapping them in space for several milliseconds and then turning off the MOT, leaving only the trapped FORT atoms. More detail about the specifics of our FORT will be discussed in later sections.

1.5   Conclusion

In this chapter I have provided a brief overview of the field of laser cooling including several of the standard cooling techniques that are used to cool atoms. I have also introduced several of the important physics concepts that will be used to analyze and understand the two experiments that I performed. In the following chapters I will build on the basic physics that has been discussed here beginning with the STOP cooling experiment. In Chapters 5-7, I will then discuss the details of the 2-CAZ cooling experiment.

References for Chapter 1

[1] Anderson, M. H., J. R. Ensher, M. R. Matthews, C. E. Wieman, and E. A. Cornell, 1995, Science 269, 198.

[2] Davis, K. B., M.-O. Mewes, M. R. Andrews, N. J. van Druten, D. S. Durfee, D. M. Kurn, and W. Ketterle, 1995, Phys. Rev. Lett. 75, 3969.

[3] D. M. Meekhof, S. R. Jefferts, M. Stepanovc, and T. E. Parker, 2001. IEEE T. Instrumentation and Measurement, Vol 50 507-509

[4] B. Knuffman et al, AIP Conf. Proc. 1395, 85 (2011).

[5] K Aikawa et al 2009 New J. Phys. 11 055035

[6] S. Giorgini, L. Pitaevskii, and S. Stringari, Rev. Mod. Phys. 80, 1215 (2008).

[7] Hänsch, T., and A. Schawlow, 1975, Opt. Commun. 13, 68.

[8] Wineland, D., and H. Dehmelt, 1975, Bull. Am. Phys. Soc. 20, 637.

[9] Wineland, D., R. Drullinger, and F. Walls, 1978, Phys. Rev. Lett. 40, 1639.

[10] H. J. Metcalf and P. van der Straten, Laser Cooling and Trapping (Springer-Verlag, New York, 1999).

[11] Daniel A. Steck, Rubidium 85 D Line Data, available online at http://steck.us/alkalidata (revision 0.1.1, 2 May 2008).

[12] S. Stellmer, B. Pasquiou, R. Grimm, and F. Schreck, Phys. Rev. Lett. 110, 263003 (2013)

[13] S. Chu, and L. Hollberg, J. Bjorkholm, A. Cable, and A. Ashkin, Phys. Rev. Lett. 55, 48 (1985).

[14] Truman Wilson, Ph. D. Thesis, Colorado State University (2013).

[15] H. Lee, C. Adams, M. Kasevich, and S. Chu, Phys. Rev. Lett. 76, 2658 (1996).

[16] J. Reichel, F. Bardou, M. B. Dahan, E. Peik, S. Rand, C. Salomon, and C. Cohen-Tannoudji, Phys. Rev. Lett. 75, 4575 (1995).

[17] A. Kerman, V. Vuleti, C. Chin, and S. Chu, Phys. Rev. Lett. 84, 439 (2000).

[18] Mathew Hamilton, Ph. D. Thesis, Colorado State University (2013).

[19] J. Lawall et al., Phys. Rev. Lett. 75, 4194 (1995).

[20] Anthony Gorges, Ph. D. Thesis, Colorado State University (2010).

[21] J. Dalibard and C. Cohen-Tannoudji, J. Opt. Soc. Am. B 6, 2023 (1989).

[22] William D. Phillips. Rev. of Mod. Phys., Vol. 70, No. 3,721-741, July (1998).

[23] Steven Chu. Rev. of Mod. Phys., Vol. 70, No. 3, 685-706, July (1998).

[24] Claude N. Cohen-Tannoudji. Rev. of Mod. Phys., Vol. 70, No. 3,707-719, July (1998).

[25] Y. Castin, J. Cirac, and M. Lewenstein, Phys. Rev. Lett. 80, 5305 (1999).

[26] J. Weiner, V. Bagnato, S. Zilio, P. Julienne, Rev. Mod. Phys. 71, 1 (1999).

[27] N Masuhara, JM Doyle, JC Sandberg, D Kleppner, TJ Greytak, HF Hess, GP Kochanski,Phys. Rev. Lett. 61, 935 (1988)

[28] H. Lewandowski, D. Harber, D. Whitaker, and E. Cornell, J. Low Temp. Phys. 132, 516 (2003).

[29] M. Cavagnero and C. Newell, New J. Phys. **11**, 055040 (2009)

[30] J. L. Bohn, M. Cavagnero, C. Ticknor, **11**, New J. Phys. 055039 (2009)

[31] James Patrick Burke, Jr., Ph. D. Thesis, University of Colorado (1999).

[32] D. DeMille, F. Bay, S. Bickman, D. Kawall, D. Krause, S. E. Maxwell, and L. R. Hunter, Phys. Rev. A **61**, 052507 (2000)

[33] E. R. Meyer and J. L. Bohn, Phys. Rev. A **78**, 010502 (2008)

[34] D. Cho, K. Sangster, and E. A. Hinds, Phys. Rev. A **44**, 2783 (1991)

[35] M.G. Kozlov, L.N. Labzovskii, and A.O. Mitrushchenkov, Sov. Phys. JETP **73**, 415, (1991)

[36] A. Pe'er, E. A. Shapiro, M. C. Stowe, M. Shapiro, and J. Ye, Phys. Rev. Lett. **98**, 113004 (2007)

[37] E. A. Shapiro, A. Peer, J. Ye, and M. Shapiro, Phys. Rev. Lett. **101**, 023601 (2008)

[38] M. Ortner, A. Micheli, G. Pupillo, and P. Zoller, New J. Phys. **11**, 055045 (2009)

[39] M. Fattori et al., Nature Physics 2, 765 (2006).

[40] P. Medley, D. Weld, H. Miyake, D. Pritchard and W. Ketterle, Phys. Rev. Lett. 106, 195301 (2011).

[41] G. Ferrari, Eur. Phys. J. D 13, 67-70 (2001).

[42] E. L. Raab, M. Prentiss, A. Cable, S. Chu, and D. E. Pritchard, Phys. Rev. Lett. 59, 2631 (1987).

[43] J. D. Miller, R. A. Cline, and D. J. Heinzen Phys. Rev. A 59, R922 (1998).

[44] J. M. Doyle, J. C. Sandberg, D. Kleppner, Th. J. Greytak,H.F. Hess and G. P. Kochanski, Naoto Masuhara, Phys. Rev. Lett. 61, 935, 1988.

Chapter 2

Spatially-selecTive Optical Pumping (STOP) Cooling Model

In this chapter, I will discuss the basic theory of Spatially-selecTive Optical Pumping (STOP) cooling. I will start by discussing the basic cooling steps of STOP cooing and then I will detail a few of the potential advantages of this cooling technique. Then, I will describe the details of a harmonic potential model that was created to predict STOP cooling rates. Finally, I will discuss an anharmonic potential model that was developed to model the cooling in an ideal optical trap potential. Throughout this chapter and the next two, I will discuss STOP cooling in terms of atoms, but these general considerations can be adapted to the cooling of molecules as well.

2.1 Basic Cooling Steps

This cooling technique consists of three distinct steps as shown in Figure 2.1. The first step is to select a fraction of the highest energy atoms in a trapped gas and optically pump them into a different internal state than the rest of the atoms. In the following discussion, I will refer to this optical pumping process as "up-pumping". These high-energy atoms are selected by exploiting the relationship between the position of an atom in a confining potential and its potential energy; by optically pumping atoms only at the edge of the gas where the potential energy is the highest, it is ensured that high energy atoms are selected. The internal state optical pumping can be accomplished in an alkali atom, for instance, by optically pumping atoms from the lower hyperfine ground state to the upper hyperfine ground state, or by optically pumping a molecule from one or more initial vibrational states to another selected set of vibrational states. Once "up-pumping" has been completed, the second step is to wait until the atoms have moved into the center of the trap (thus converting their potential energy to kinetic energy) and then apply a "stopping pulse" to slow these atoms(or molecules). The stopping pulse slows the atoms by transferring linear momentum from the light of the stopping pulse to the atoms in the direction opposite the atoms' motion. Several mechanisms can be used to affect this momentum transfer, including spontaneous scattering of a laser beam directed opposite the atoms' motion or driving appropriately directed coherent Raman
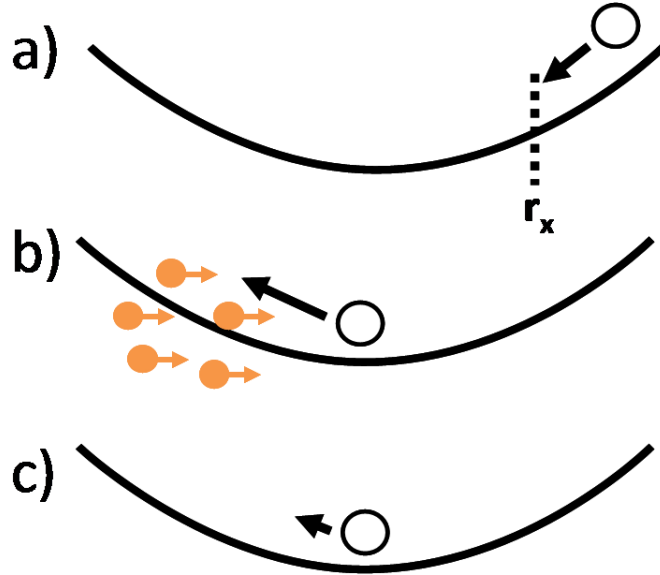
Figure 2.1: The Spatially-selecTive Optical Pump Cooling sequence is shown. This technique relies on three steps; a) applying a spatially selective beam to select atoms beyond some axial cutoff, r_x, to pump the selected atoms into a different state, b) applying a pulse to oppose the atoms' velocity once at the center of the trap and slow them down, and c) applying a pulse to pump the atoms back to their original state and remove the entropy from the system.

transitions. Finally, after the stopping pulse the atoms need to be optically "down-pumped" back to their original state or states to complete the cycle and remove the entropy from the system.

2.2 Potential Advantages

There are several potential advantages associated with STOP Cooling. One major advantage is that cooling rates well in excess of evaporative cooling rates are predicted. In fact, predicted cooling rates are comparable to or faster than other non-evaporative cooling rates. For a sample case of ^{87}Rb, one-dimensional cooling rates are expected to initially be 100s of μK per second. Additionally, this technique should be widely applicable. The only requirements regarding what can be cooled are that the atom or molecule can be trapped and has a dark state. Closed or nearly-closed transitions are helpful in implementation of this technique, but they are not required.

Like all light-based cooling, there is a potential for both light-induced trap losses and reabsorption [1]. However, there are some advantages in this regard to these mechanisms for STOP cooling. One potential advantage with regard to reabsorption is that there can be a range of internal states

in the atoms selected for the cooling. This reduces the influence of reabsorption if there is an energy difference between these states due to either internal energy shifts or externally applied fields that produces transition frequency differences on the order of the stopping pulse scattering rate [1]. For some systems, specifically molecules, there may in fact be many internal states, greatly mitigating expected reabsorption problems.

Light-induced losses were observed in our system and will be described in more detail in Chapter 4. Losses of this nature will be very atom-and transition-dependent [2]. In STOP cooling, however, there is a great deal of freedom in choosing the atomic or molecular transition used to stop the atoms or molecules. Therefore, there is a corresponding ability to reduce the loss through selecting favorable transitions and parameters (e.g. intensity and detuning) for the beam used to stop the atoms. The detuning of this beam can be blue or red, for instance. Additionally, stimulated off-resonant techniques are viable. The required photon scattering rate is also much smaller than for many other forms of laser cooling. Since the atoms direction of motion is known, the momentum transfer is "maximally efficient" in that the photon momentum is always directed opposite the atom motion. This is not the case for other laser cooling that relies on a velocity-selective scattering [4–7]. Thus, while light-induced losses and reabsorption will likely pose problems, there is reason to believe that there are advantages intrinsic to this cooling technique that help mitigate them.

2.3 Simple Estimate of STOP Cooling Rate

Simple estimates can be performed to examine the cooling potential of this technique. Consider an optically-trapped cloud of atoms at a temperature T. A simple estimate of the cooling power of this technique can be performed through assuming that the cooling cycle removes axial potential energy from a set of selected high-energy atoms such that their kinetic energy at the center of the trap is reduced to $1/2k_BT$ (i.e. the high-energy atoms have their kinetic energy reduced to the average kinetic energy in the gas). The cooling rate is then given by the average energy of the atoms removed in one cooling cycle divided by the time it takes the atoms to travel from the edge of the high-energy selection region to the center of the optical trap.

Following the parameters typical of an optical trap of the type used in our experiments, the upper 10% of the atoms have an average potential energy of about 170 μK. This value is multiplied

by an average excitation rate of 0.7 and divided by 2 to convert from axial potential energy to total energy. For our experimental parameters of a 50 μK ^{87}Rb gas trapped in an axial potential with an oscillation period of 80 ms, this simple estimate produces a one-dimensional cooling rate of about 200 μK/sec when 10% of the atoms are selected. On the basis of the cooling rates derived from these estimates, we determined that it was worthwhile to model the cooling process in more detail.

2.4 Harmonic Model

Beyond this simple estimate, it is possible to model the basic physics of STOP cooling to obtain predicted cooling rates in a straightforward way. To do so, we used parameters for STOP cooling appropriate to ^{87}Rb on its $5S_{1/2}$ to $5P_{3/2}$ λ=780 nm cycling transition as the stopping pulse. The results of these calculations, however, can be applied directly to a good approximation to other atoms or molecules with a closed or nearly-closed transition. The only variation between such atoms or molecules occurs due to a slight dependence of the predicted cooling on the stopping pulse photon momentum and the mass of the atom or molecule. We started our calculations by assuming the ideal case of a harmonic confining potential. One of the first inputs into the model is the fraction of higher-energy atoms that are to be optically pumped in the first step of the cooling cycle. We calculated a cut-off axial distance based on Maxwell-Boltzmann thermal distributions, labeled r_x in Figure 2.1, for a specified up-pump fraction. That is, by assuming a density proportional to $\exp(-U/k_B T)$ we could compute the value of r_x such that a selected fraction of atoms would be selected for up-pumping. Further, we assumed that the up-pumping occurred at time t=0. Using the basic equations of motion for a simple harmonic oscillator, Equations (2.1) and (2.2) below, and the one-dimensional Maxwell-Boltzmann thermal phase space density describing the position and velocity distribution at time t=0, Equation (2.3), the energy ($E(n,t)$) of the selected atoms after n directed photon absorptions at time t is calculated in Equation (2.4). For each photon that was absorbed, we assumed that an $\hbar k$ of momentum was transferred to the atom in the direction of the stopping pulse light, where $k = \frac{2\pi}{\lambda}$ and λ is the wavelength of the light.

$$x = x_0 \cos(\omega t) + \frac{v_0}{\omega} \sin(\omega t) \tag{2.1}$$

26

$$v = v_0 \cos(\omega t) - x_0 \omega \sin(\omega t) \tag{2.2}$$

$$f = \frac{m\omega}{2\pi kT} exp(-\frac{m\omega^2 x_0^2}{2kT} - \frac{mv_0^2}{2kT}) \tag{2.3}$$

$$E(n,t) = \int_{-\infty}^{\infty} dv_0 \int_{x_c}^{\infty} dx_0 f[\frac{1}{2}m\omega^2 x^2 + \frac{1}{2}m(v + n\frac{\hbar k}{m})^2] \tag{2.4}$$

Note that the integration in equation (2.4) is over the initial condition variables x_0 and v_0.

Once this energy as a function of n was determined, the total energy removed by n photon scatters could be calculated. This was done by calculating the change in energy $\Delta E = E(n,t) - E(0,t) + n(\hbar k)^2/2m$. The last term in ΔE models the recoil energy increase from a spontaneously-emitted photon that occurs after each absorption. Such a term is present for some forms of the stopping pulse (e.g. resonant scattering) but not others (e.g. sequences of stimulated Raman transitions with appropriately directed pairs of beams). We also assume the down-pump beam propagates in the same direction as the stopping pulse. Ideally, each atom would scatter a precisely-controlled number of photons, and for some stopping pulse mechanisms that would indeed be the case. However, we chose to assume that the stopping pulse and down-pump pulse consisted of light resonantly scattered and so the number of photons scattered varied randomly from atom to atom. We assumed that each atom scattered a number of photons according to a Poisson distribution, which is approximately correct for below-saturation intensities. The parameter representing the average number of photons scattered in the Poisson distribution was optimized to produce the most cooling. The net result of this calculation was a prediction of the amount of energy removed in one cooling cycle.

The results of our calculations for several selection fractions and temperatures are shown in Figure 2.2. These calculations used the ideal delay time between optical pumping and the application of the stopping pulse for a single cycle of cooling ($\frac{1}{4}$ period of the atoms' oscillation in the trap). Of the prediction shown, the 25% selection fraction has the highest cooling rate, although the 15% fraction prediction is only slightly lower. The corresponding cooling rate for the 25% selected fraction at 44 μK for a trap period of 60 ms is 422 μK/sec. At higher temperatures, the
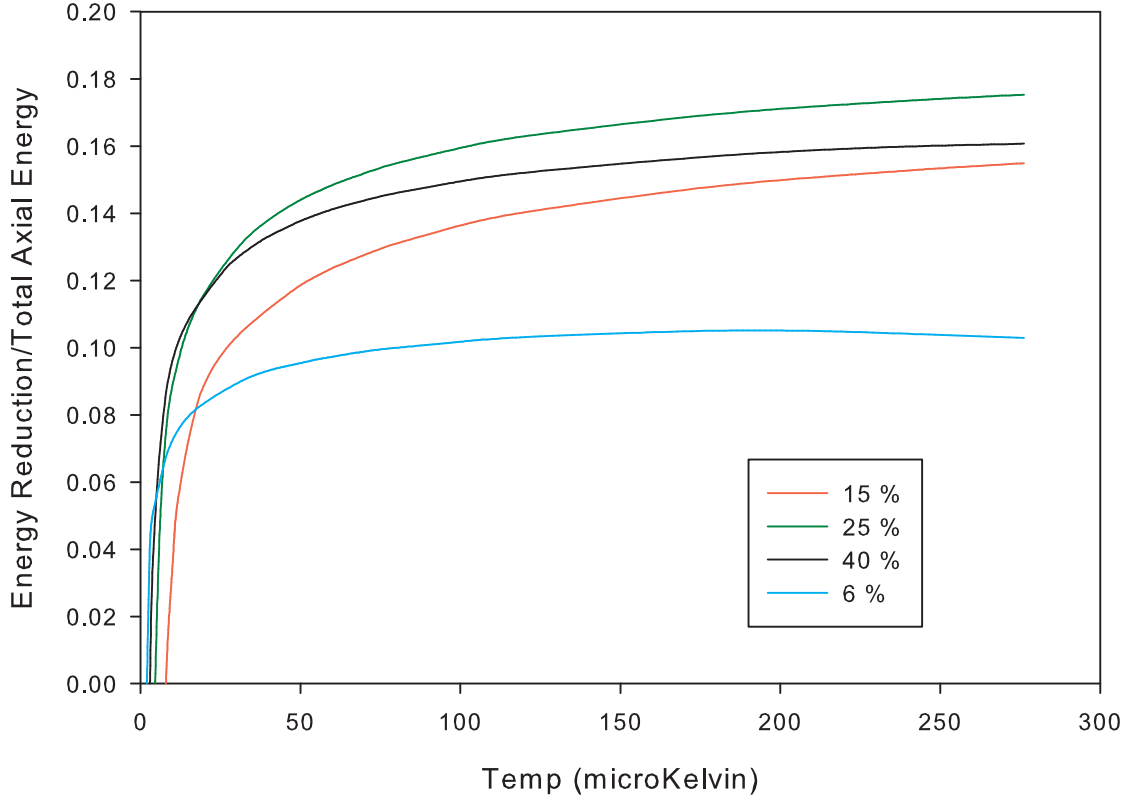
Figure 2.2: Cooling achieved in a single cycle as determined by the energy removed in a single cycle divided by the total one-dimensional thermal energy in the gas (i.e. Nk_BT for N atoms in a harmonic confining potential). The cooling amount for a 40% initial up-pump fraction is represented by the black curve , a 25% initial up-pump fraction is represented by the green curve, a 15% initial up-pump fraction is represented by the red curve and a 6% initial up-pump fraction is represented by the blue curve.

energy removed in a single cycle is proportional to temperature, as it should be. As expected, as the temperature decreases the cooling becomes less efficient as the heat imparted by random recoils during scattering becomes relatively more important. However, from these calculations we found that even at lower temperatures there is still significant cooling. Assuming that the selected fraction can be controlled as cooling proceeds, at T=1.2 μK the achievable energy reduction fraction is still about $\frac{1}{e} = 36.8\%$ of the maximum possible energy reduction fraction.

In addition to extracting cooling rates and ideal selection fractions, we also used the harmonic model to check on the influence of other possible variations that could occur experimentally. The effect from a change in down-pump probability was investigated first. In the calculation reported

above, we assumed a down pump probability of 50% to match the probability of down pumping on the $5S_{1/2}$ $F=2$ to $5P_{3/2}$ $F'=2$ transition in ^{87}Rb, which was the primary transition that we used to optically repump the atoms after the stopping pulse. The detuning of the down pump laser was actually slightly below the $5S_{1/2}$ $F=2$ to $5P_{3/2}$ $F'=2$ transition meaning that the down pump probability was between the 50% expected for the $F=2$ to $F'=2$ transition and the 80% expected for the $F=2$ to $F'=2$ transition. With this in mind, we adjusted the down-pump probability in the model between 50% and 90% and looked at the resulting cooling. The model indicated that this variation in the fraction changed the cooling by less than 3% for a gas temperature of 38 μK.

2.5   Influence of Anharmonicity on Predicted Cooling Rates

In addition to considering the ideal case of a harmonic potential we also performed a similar computation for an anharmonic potential because the cooling rate considerations in an anharmonic potential are different. While the up-pumped atoms initially may be traveling towards the center of the trap or away from it, in a harmonic potential after one-quarter oscillation period, the kinetic and potential energy of all of the atoms in the gas will have been exchanged. This means that regardless of the initial direction or magnitude of the velocity of an up-pumped atom, after one-quarter cycle the atom will be moving in a direction determined solely by its position and so all of the high-potential energy atoms will be moving towards the stopping pulse. This is not the case in an anharmonic potential. Because the period in such a potential is dependent on the energy of the particle, the exchange between potential and kinetic energy will occur at different times for different atoms. This introduces a complication in the cooling since some atoms will not have converted all of their potential energy to kinetic motion directed towards the stopping pulse. This reduces cooling effectiveness. It also complicates any measurement technique that relies on a regular exchange of kinetic and potential energy at the same time for all atoms, such as will be described in Chapter 4.

Optical trap potentials are not harmonic since they have a finite depth. For this model we considered an ideal optical trap potential along the axial direction of the form

$$U = \frac{U_0}{\sqrt{1 + z^2/z_0^2}} \tag{2.5}$$

where $z_0 = \pi w_0^2/\lambda$, w_0 is the minimum spot size and U_0 is the maximum trap depth. Developing a model for an optical trap potential was useful to investigate the possible influence of anharmonicity on the predicted cooling. Our experimental potential actually deviated significantly from an ideal optical trapping potential. Thus, the predictions in this section are not directly applicable to our measurements and a different analysis had to be used to compare our results to theory, as described in Section 4.3. However, the predictions concerning a more idealized anharmonic potential are included here so that the influence of the anharmonicity in a more ideal situation can be evaluated. This is relevant to future experiments that should have a potential closer to the ideal optical trap potential and not have as much distortion from lens aberrations.

One of the first inputs into the model is the fraction of higher-energy atoms that are to be optically pumped in the first step of the cooling cycle. We calculated the cut off axial distance, labeled r_x in Figure 2.1, where this occurs for a specified optical-pump fraction based on Maxwell-Boltzmann thermal distributions and the shape of the potential energy as a function of position. We then considered eleven initial atom positions, ranging from r_x to an upper trap cut-off location chosen to span the range of distances where there was significant atom population outside of r_x. A cut-off had to be introduced into the Maxwell-Boltzmann distribution to account for the finite trap depth. The potential was assumed to be one-dimensional and of the form of Equation 2.5. The velocities were also one-dimensional. At each position, a maximum trappable velocity was computed by setting $1/2 m v_c^2 = U_0 - U$ where v_c is the cut-off velocity, U_0 is the overall trap depth and U is the potential energy at the position in question. The integral of $\exp(-mv^2/(2k_B T))\sqrt{m/(2\pi k_B T)}$ from $-v_c$ to v_c was performed to compute the thermal density in the presence of the finite trap depth. These velocities were used in conjunction with the associated position to create a group of position/velocity combinations that were then weighted by the above mentioned thermal density for each combination. Once the array of positions and velocities was determined, we propagated the atoms' motion in the trap using the equations of motion associated with the potential. After waiting a chosen amount of time, the original position/velocity combinations evolved into new position/velocity values.

Once this array of new velocities and positions was computed, a stopping pulse and down-pump pulse were applied theoretically. The model assumes the down-pump beam propagates in the same direction as the stopping pulse and thus has some stopping power, and these effects are

30

included in our calculation. Due to the finite size of the momentum carried by a single photon the importance of the stopping action of the down-pump pulse will increase as the temperature of the gas decreases. Again, we chose to assume that the stopping pulse and down-pump pulse consisted of light spontaneously scattered on a closed transition and so the number of photons scattered will vary from atom to atom due to the random nature of the scattering process. To model these pulses, we assumed that each atom scattered photons according to a Poisson probability distribution. For each photon that was scattered, we assumed that an $\hbar k$ of momentum was transferred to the atom in the direction of the stopping pulse light. We also assumed that the energy of the atom increased by $\hbar^2 k^2/(2m)$ on average as a result of the random recoil of the atom during the spontaneous scattering process. To find the optimum predicted cooling, the value of the average number of photons scattered that was input to the Poisson distribution was changed to find the optimum cooling value. The net result of this calculation is a prediction of the amount of energy removed in one cooling cycle. This model was done assuming a trap depth of 280 μK(k_B), which was consistent with measurements of our system.

The model showed that at sufficiently high temperatures in an anharmonic potential of the type expected in an optical trap formed from a Gaussian beam, a non-negligible fraction of the "up-pump" selected atoms were still traveling away from the center of the trap at the time the cooling pulse was applied even under optimal cooling conditions, meaning those atoms' energy could not be reduced. An example trajectory of one of these atoms is shown in Figure 2.3. It is clear from this figure that it can take tens of milliseconds before the atoms turn around, which is much longer than the delay before the cooling pulse would be applied. We can also see a problem when we examine the cooling rate. In Figure 2.4 a clear reduction in the cooling rate can be seen at higher temperatures. Since the 6% initial selection fraction is most affected by the anharmonicites of the trap it is not surprising that the most drastic reduction was seen for that case. A reduction is still evident for both the 15% and 25% initial selection fractions. Such a problem is absent in the harmonic case. The degree to which this reduction in cooling due to anharmonicities is present is dependent on the temperature of the gas in the trap. The colder the gas, the closer to harmonic the trapping potential. This means that for ideal cooling, the ratio of the gas temperature to trap depth is an important parameter, and needs to be considered in future designs for improved cooling.

31
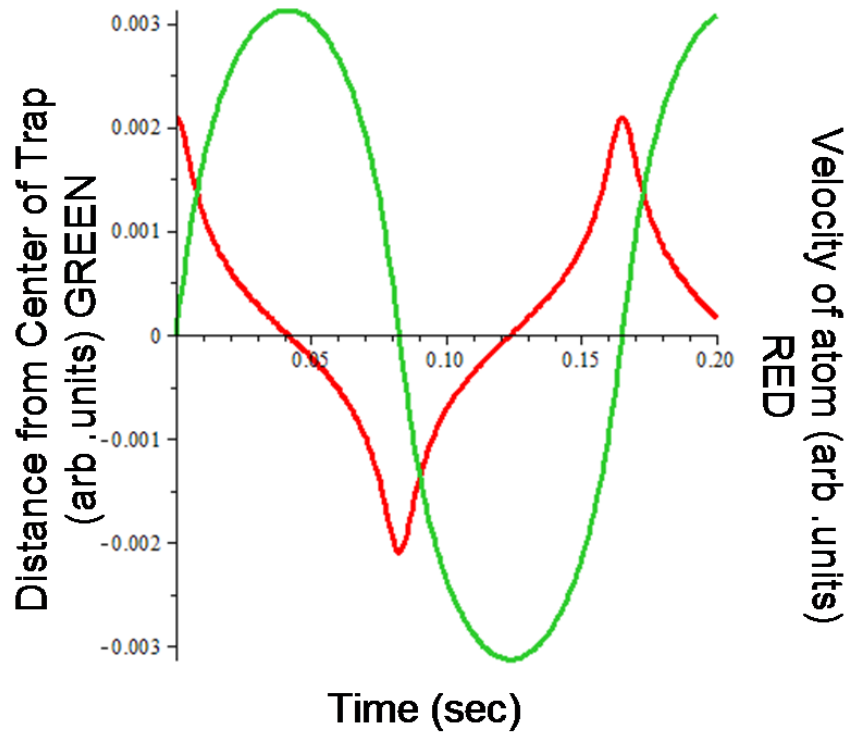
Figure 2.3: Trajectory of an atom initially heading away from the center of the trap with the maximum possible velocity that can be contained in the trap. The atoms position is shown in green while its velocity us shown in red. This calculation was done with a typical gas temperature of 50 μK.
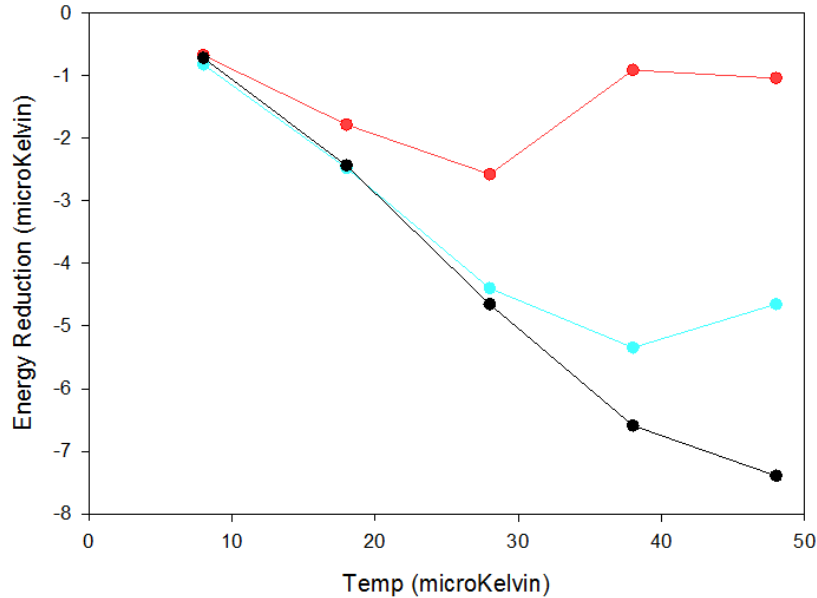
Figure 2.4: Single Cycle Cooling for the case of an anharmonic potential is shown. The simulation results for the 6% initial selection fraction are shown in red, the results for 15% are shown in blue and the results for 25% are shown in black.

An additional model will be described in Chapter 4 that allowed us to compare our measured results to expectations. This additional model was used primarily to confirm that the results we were seeing were reasonable and to extract the total energy reduction from a measured reduction in just the potential energy of the gas due to the cooling sequence. Details will be presented in Section 4.3.

2.6 Alternative Optical Pumping Options

It is important to note that we did not take into account any information about the m_F state of the atoms. We assume all of the atoms regardless which m_F state they are in scatter approximately the same number of photons. If different internal states of the selected atoms have different scattering rates, the Poisson distribution is not a correct description of the probability distribution of scattered photons. For instance, in the case of ^{87}Rb the square of the Clebsch-Gordan coefficients vary by up to factors of 15 if circularly polarized light is considered (we used linearly polarized light in our measurements so that the range of coefficients would not be so broad in our experiments).

If the probability distribution was widened to more accurately reflect the possible scattering rate variations the cooling would be reduced(but not eliminated).

Spontaneous scattering is not theoretically the ideal way to slow the atoms, due to the randomness in the number of scatters. A more ideal system would be one where, for instance, a Stimulated Raman Adiabatic Passage (STIRAP) pulse could be used for the stopping pulses [3]. For each STIRAP pulse there would ideally be exactly one excitation and subsequent spontaneous scatter. Multiple STIRAP pulses would then be used to obtain the desired number of scattering events for a given set of experimental conditions. This technique would remove the randomness of the number of stopping pulse photons scattered. This would be particularly useful in systems with a wide variety of transition strengths arising from different internal state coupling strengths if in those systems there was a distribution across such states arising from the first-cooling-stage optical pumping pulse. We adapted our ideal harmonic model for such a situation to have each atom scatter the exact same number of photons from the cooling pulse. The model showed that the energy reduction fraction was improved by 7% for a 25% initial selection fraction and an initial axial temperature of 50 μK. The model also showed that this improvement increased at lower temperatures. For an initial axial energy of 5 μK the improvement in cooling rate was almost 21%. Thus, improvements in the cooling rate are expected to contribute most strongly at low temperatures.

2.7 Cooling Rate

Additionally, we calculated the cooling rate (rather than single-cycle energy removal fraction) as a function of time between the up-pump and stopping pulses for a 25% initial up-pump fraction at $T = 40\mu$K. Near the optical trap potential minimum, the velocity of the atoms does not change much with time. By applying the stopping and down pump pulses slightly before the atoms reach the minimum of the trapping potential, the energy that can be removed decreases only slightly while the cooling cycle time decreases linearly. Thus, a larger cooling rate can be obtained by reducing the cooling cycle time without a significant reduction in the amount of energy removed. This result, shown in Figure 2.5, is graphed as a function of the fraction of the ideal single-cycle delay time between up-pump and stopping pulses. It is clear that to achieve the maximum possible
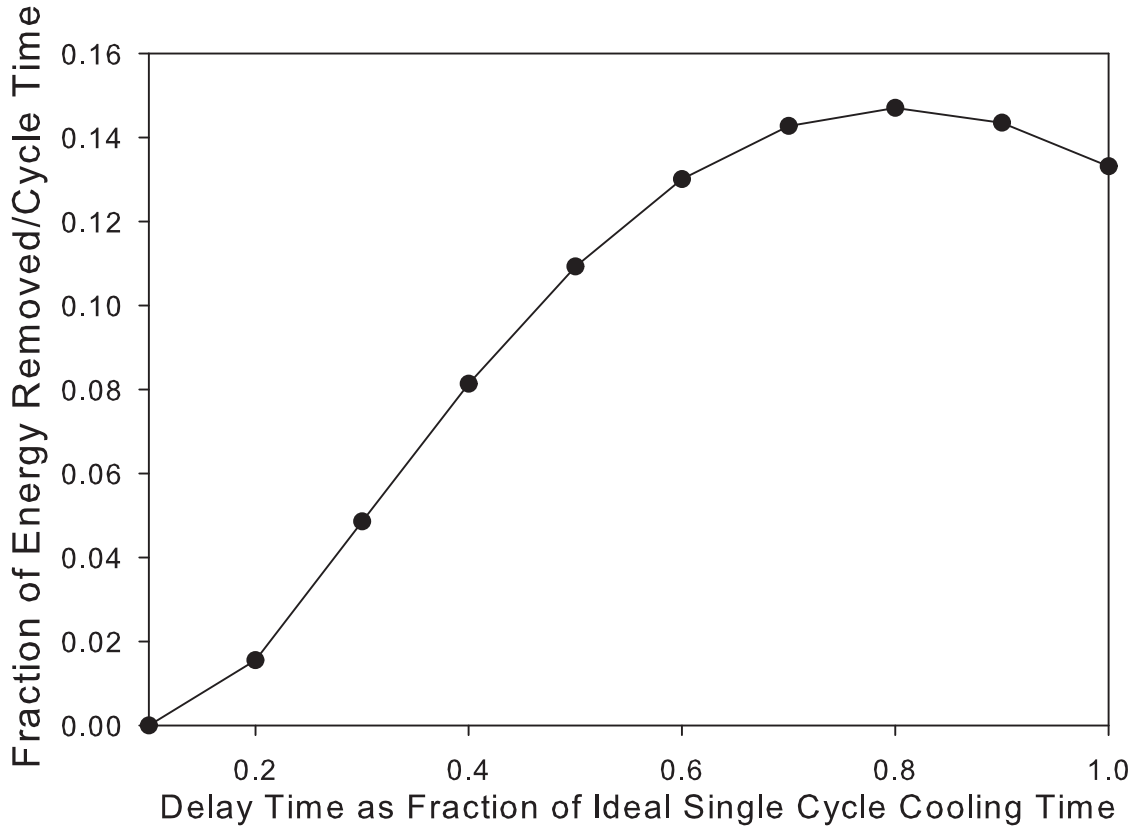
Figure 2.5: The cooling rate(energy removed per cycle divided by the cycle time) is shown as a function of the delay time as a fraction of the cycle time. The cycle time is normalized to a 1/4 period for both the x and y axes in the figure. This cooling rate is calculated for a 25% initial up pump fraction and a temperature of 40 μK. It is clear that the maximum cooling rate occurs for a cycle time that is below the time expected for maximum single cycle cooling. By decreasing the cycle time to 80% of the ideal single cycle cooling time the number of cycle can be increased thus increasing the cooling rate by several percent.

cooling rate for multiple cycles the delay time should be shorter than the one-cycle ideal time. The gains in doing so, however, are relatively slight.

2.8 Conclusion

From these models we were able to conclude that this cooling technique has the potential to cool atoms at rates of hundreds of microKelvin per second. We also saw that the trap shape, whether harmonic or anharmonic, plays an important role in the expected amount of cooling. In particular, the dynamics of the cooling in an ideal optical trap confining potential show that a sufficient trap

depth to atom temperature ratio is required for efficient cooling. The ideal cooling rate as a function of cooling cycle time was also calculated. In the next chapter I will discuss the techniques used to perform the experiment. Then in Chapter 4 I will discuss the results of the experiment including the model used to confirm that our results were reasonable.

References for Chapter 2

[1] Y. Castin, J. Cirac, and M. Lewenstein, Phys. Rev. Lett. 80, 5305 (1999).

[2] A. R. Gorges, N. S. Bingham, M. K. DeAngelo, M. S. Hamilton, and J. L. Roberts, Phys. Rev. A **78**, 033420 (2008)

[3] K. Bergmann, H. Theuer, and B. W. Shore, Rev. Mod. Phys. 70, 1003 (1998)

[4] D Boiron, A Michaud, P Lemonde, Y Castin, C Salomon, SWeyers, K Szymaniec, L Cognet, A Clairon, Phys. Rev. A 53, R3734 (1996)

[5] A. Aspect, E. Arimondo, R. Kaiser, N. Vansteenkiste, and C. Cohen-Tannoudji, Phys. Rev. Lett. 61, 826 (1988)

[6] S. Chu, L. Hollberg, J. E. Bjorkholm, A. Cable, and A. Ashkin, Phys. Rev. Lett. 55, 48 (1985)

[7] J. Dalibard, and C. Cohen-Tannoudji, J. Opt. Soc. Am. B 6, 2023 (1989)

Chapter 3

Spatially-selecTive Optical Pumping (STOP) Cooling Experiment

In Chapter 1, I presented an overview of some of the techniques used in the initial trapping and cooling of atoms as the starting point for the experiments described in this thesis. In Chapter 2, an overview of Spatially-selecTive Optical Pumping (STOP) cooling was also presented. I now want to discuss more of the specific details of the STOP cooling experimental apparatus. The STOP cooling experiment and the 2-CAZ cooling experiment used the same initial optical trap loading experimental sequence and much of the same experimental equipment. I will start by discussing the equipment and experimental techniques that are common to both. Then I will discuss the STOP cooling techniques in detail. In Chapter 6, I will discuss the additions to the basic experimental setup that were made in order to perform the 2-CAZ experiment.

3.1   Common Experimental Equipment

Several parts of the experimental apparatus that I used have been described in other theses [1, 2]. When appropriate, references will be made to those theses for additional details that will not be repeated in this thesis.

3.1.1   Vacuum Chamber

All of the experiments described in this thesis occurred within a multi-port vacuum chamber. It is made of stainless steel and has eight 2.75 inch diameter conflat windows, six of which are used to create a MOT and two of which are used to create the FORT. The two windows through which the CO_2 beam enters the vacuum chamber to create the FORT are made of Zinc Selenide (ZnSe) instead of the standard fused silica windows used for the MOT beams. This is because of the significant absorption of the 10.6 μm light from the CO_2 laser through fused silica. Additionally there are many other smaller ports in the vacuum chamber that are used for imaging and optically pumping the atoms. The chamber is kept at ultahigh vacuum (10^{-9} Torr) in order for the MOT to

function properly and to ensure sufficiently few background gas collisions during optical trapping. More detail about the vacuum chamber can be found in [1].

3.1.2 Diode Lasers

In order to create the MOT and image the atoms it was essential that we have access to frequency stabilized diode lasers. These lasers were used for many aspects of both the STOP and 2-CAZ experiments: from the initial atom cooling and trapping, to optical trap loading, to the required optical pumping and slowing in STOP cooling and even to perform the absorption imaging. These diode lasers have several specific requirements for our use. It was crucial that we could tune these lasers to specific chosen frequencies over a wide range of optical transitions in Rb and it was important that we could keep them at that specific frequency for long periods of time.

The diode lasers that we used were 70 mW ADL-78901TX from Roithner LaserTechnik for the 780 nm lasers and Photonic DL7141035A for the 795 nm lasers. During all but the first few months of my time on the experiment, I used only the 780 nm diodes. The diode lasers were used in an external cavity configuration (ECDL)[3], allowing us to tune the frequency of the lasers. The diodes can produce up to 70 mW of total power and can be tuned over a range of 10-14 nm from their center frequency of 785 nm. Thorlabs LT230P-B collimation tubes were used to collimate and thus limit the output divergence of the beam. The specific ECDL configuration that we used was the Littrow configuration to control the frequency of the laser [4]. The Littrow configuration works by placing a diffraction grating in the path of the diode laser beam such that the m=-1 diffraction order is fed back into the laser. By feeding back this light, the loss at the wavelength of the m=-1 diffraction order is reduced, improving the net gain at that wavelength. Since the angle of the m=-1 diffraction order is wavelength-dependent, adjusting the grating angle tunes the wavelength of light that will be fed back into the laser. The angle of the diffraction grating is precisely controlled by a piezo-electric transducer (PZT). With this setup the laser frequency can to be stabilized to a narrow range ($\sim$0.5 MHz in our system, limited primarily by vibration and electronic noise) and tuned precisely by adjusting the PZT voltage. In addition to using this feedback configuration we also temperature control the diode lasers to about 5 mK precision to achieve additional stability.

Although our Littrow configuration for the diode lasers allows us to stabilize the output frequency, an external frequency reference is needed to set the laser frequency to the desired values
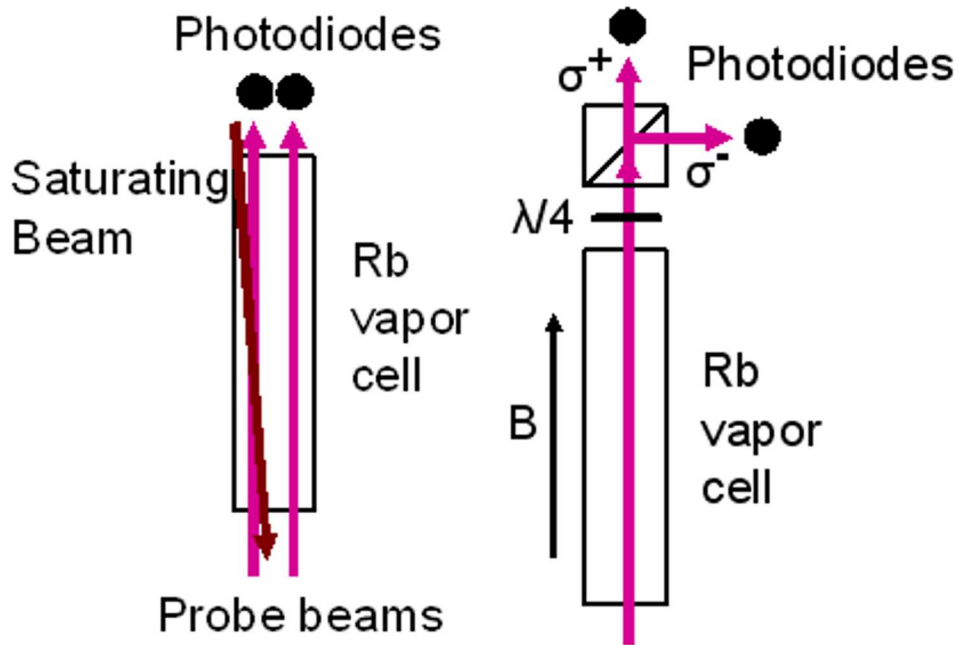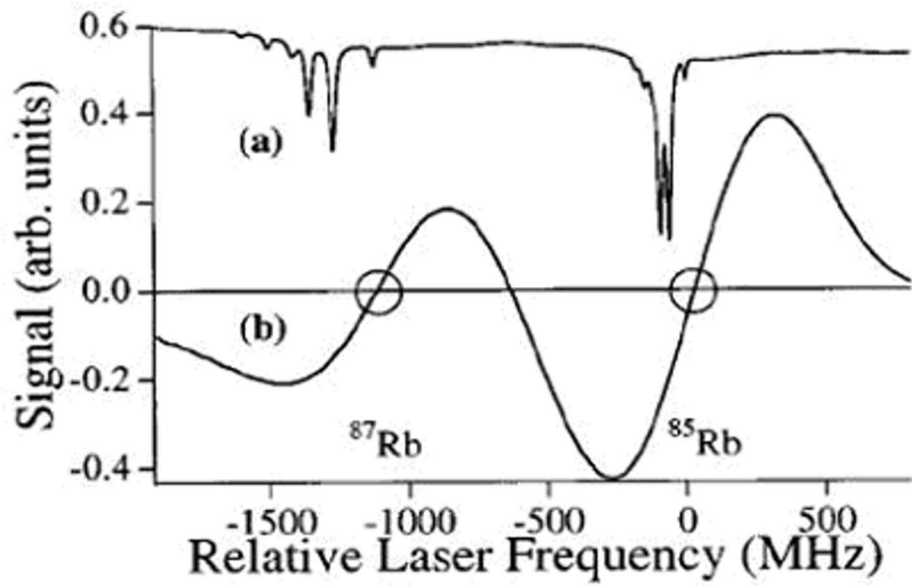
Figure 3.1: A sample Saturated Absorption (SA) signal and DAVLL signal are shown in the top figure, trace a and b respectively. The bottom left image shows a typical set up for a SA. The bottom right image shows the typical set up for a DAVLL. The top image was taken from [5].

at the necessary precision. To do this we used both a Saturated Absorption (SA) signal and a Dichroic Atomic Vapor Laser Lock (DAVLL)[5] signal. The DAVLL signal was used as the primary frequency servo reference and was fed into a sidelock servo circuit to control the laser frequency [6]. The SA signal was used as a more stable long-term reference that was necessary due to drifts in the DAVLL signal over time. Typical signals from a SA and DAVLL are shown in Figure 3.1. This image is not from our apparatus, but our signal looks very similar to these published images.

For our SA setup we send two low intensity beams through a Rb vapor cell and onto two photodiodes. Near resonance the Rb vapor absorbs a significant fraction of the light from these beams. We also counter-propagate a high intensity beam along one of the two low intensity beams as shown in Figure 3.1. This beam saturates the Rb transitions when both beams are resonant with the same velocity class of atoms and decreases the amount of light that is absorbed from the low intensity beam. The SA signal output consists of the difference between the power in the two low intensity beams as measured by a pair of photodiodes. A typical SA signal is shown at the top of Figure 3.1.

To create the DAVLL signal we also use a Rb vapor cell, but this one is placed in a uniform 150 G magnetic field. This magnetic field induces Zeeman shifts such that the center frequency of the absorption profile for light with σ^+ circular polarization is different than that with σ^- circular polarization. When a beam that consists of a combination of these two polarizations is sent through the cell, the absorption of the σ^+ and σ^- components will be different at almost all frequencies near resonance owing to the Zeeman shift. These two polarizations can be sent into the cell through using linearly polarized light whose polarization is perpendicular to the magnetic field. At the output of the cell, a quarter-waveplate and polarizing beam splitting cube can be used to measure the intensities of the σ^+ and σ^- components individually, and by subtracting them the DAVLL signal shown in Figure 3.1 can be obtained. Additional detail about our SA and DAVLL set-ups and the specifics of our side-lock servo circuit can be found in [1].

In principle, if the recapture range of the SA signal was large enough the DAVLL signal would not be necessary to keep a laser on transition. However, since the recapure range of the SA signal is quite small due to locking stability and tuning range the DAVLL signal is required. If instead, the DAVLL signal could be calibrated once and was then stable, the SA signal would not be necessary. However there are long term drifts in the DAVLL signal that require regular recalibration using the

SA signal. Therefore it is important to have the SA signal to determine where each Rb transition frequency is located and the DAVLL signal to provide the needed recapture range. Figure 3.1 shows typical set-ups for both a SA and DAVLL.

3.1.3 Far-Off Resonance Trap Operation Parameters

We used a 125 W 10.64 μm CO_2 laser (Coherent, Inc. GEM-Select 100) to create a Far Off Resonance Trap (FORT). As mentioned in section 1.4.4, the advantage of using the FORT is that it provides a trap with a significantly higher atom density than a MOT and only requires one beam to create a three dimensional trap. Additionally, it provides a way to work in the absence of a magnetic field, which can be quite useful. Finally, the spontaneous scattering rate is very low with spontaneous scattering rates predicted to be less than one photon per 1000 seconds for our FORT parameters. The laser light for the FORT is controlled via a water cooled Acousto-Optical Modulator (AOM), Intraaction model AGM-40, that is used as a very fast switch to turn the trapping beam on and off. The power in the diffracted beam of the AOM available for use in creating the FORT was 75 W. A simple schematic of the CO_2 setup is shown in Figure 3.2. As mentioned, most of the experimental sequences consisted of loading the FORT from a MOT and then performing experiments on the atoms while they are in the FORT. Details about the physics of FORT trapping in general and for our FORT in particular can be found in [1, 2]

A FORT has two characteristic trap frequencies, the radial and axial frequencies, that are important specifications of the confining potential. Near the center of the optical trap the potential is approximately harmonic, justifying the assignment of these trapping frequencies. The radial frequency of the trap was generally between 700 Hz and 900 Hz depending on the beam size and beam power. This frequency was measured using a parametric heating technique [7–9] with typical results shown in Figure 3.3. The parametric heating was accomplished by modulating the signal that controls the CO_2 AOM. If the signal amplitude that drives the AOM is made to oscillate, the trap power will also oscillate. This will cause heating in the atom cloud. In fact, when the oscillation frequency is twice the trap frequency the atoms can be heated substantially through resonant parametric driving of the atoms' motion in the approximately harmonic potential. This is how the trap frequency is identified. As you can see for the data shown in Figure 3.3, the maximum heating occurs at about 1400 Hz indicating a trap frequency of 700 Hz.
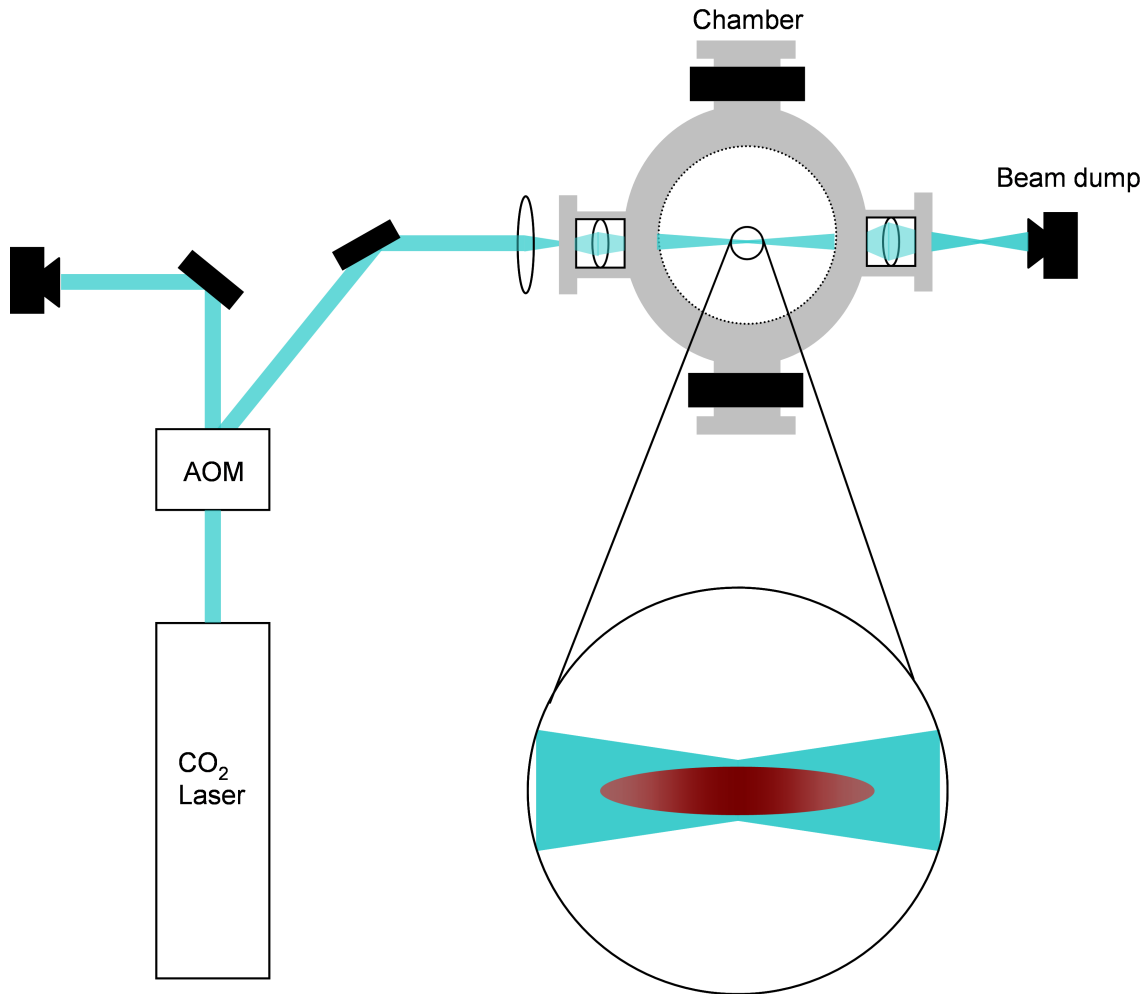
Figure 3.2: A simple cartoon of the system is shown. The path of the CO_2 laser is shown and in the center of the trap, shown in the inset, is the FORT. Due to the high intensity of the CO_2, the AOM shown is water cooled. All of the CO_2 optics shown are made from ZnSe. (figure from [1])

The axial frequency of the trap was found to be 20(2) Hz. The axial trap frequency was not measured via parametric heating. The reason for this is the much lower trap frequency. Applying the same number of cycles as in the radial case would take about 50 times as much time, and in that time the atom cloud temperature has time to adjust via evaporation, making the parametric heating signal difficult to detect. This frequency was instead measured by selectively optically pumping and imaging a small group of atoms as they oscillated from one side of the trap to the other over about three quarters of a cycle. These results are shown in Figure 3.4. While ideally this would correspond exactly to the frequency for the harmonic part of the axial potential near the center of the trap, the optical trapping potential is more anharmonic in the axial direction. The 20 Hz is essentially an average oscillation frequency associated with trapped atom temperatures of about 40 μK, which is typical for our experiments.

3.1.4 Absorption Imaging

The vast majority of data that we collected for all of our measurements was through the technique of absorption imaging. Each absorption image of the gas produced a measurement of the atom number and through the measured spatial extent after ballistic expansion, a measurement of the temperature of the atoms. Absorption imaging is a common technique used in many ultracold atom experiments that consists of sending a pulse of resonant or near-resonant light through the cloud of atoms and then imaging the resulting shadow on a CCD camera. Auxiliary pulses are also applied to normalize the intensity. This is a destructive measurement technique, so a new cloud of atoms is needed each time a measurement is to be taken.

This technique is discussed in great detail in [1]. The atoms are first released from the trap and allowed to expand for a chosen amount of time, and then illuminated. From the resulting image, the radial frequency, and the known expansion time the atoms' density and temperature can be determined. The measured size of the cloud is used to determine the atoms' rms velocity using $\sigma_{final} = \sqrt{\sigma_0^2 + (vt)^2}$ where σ_0 is the initial radial rms size of the atom cloud, t is the expansion time, σ_{final} is the measured rms size of the cloud in the radial direction, and v is the rms velocity of the atoms in that direction, assuming a Maxwell-Boltzmann distribution. $\sigma_0 = \frac{1}{\omega_r \sqrt{(kT/m)}}$ and for our expansion times (2-3 ms) and trap frequencies (700-900 Hz) the σ_0 term can be ignored at
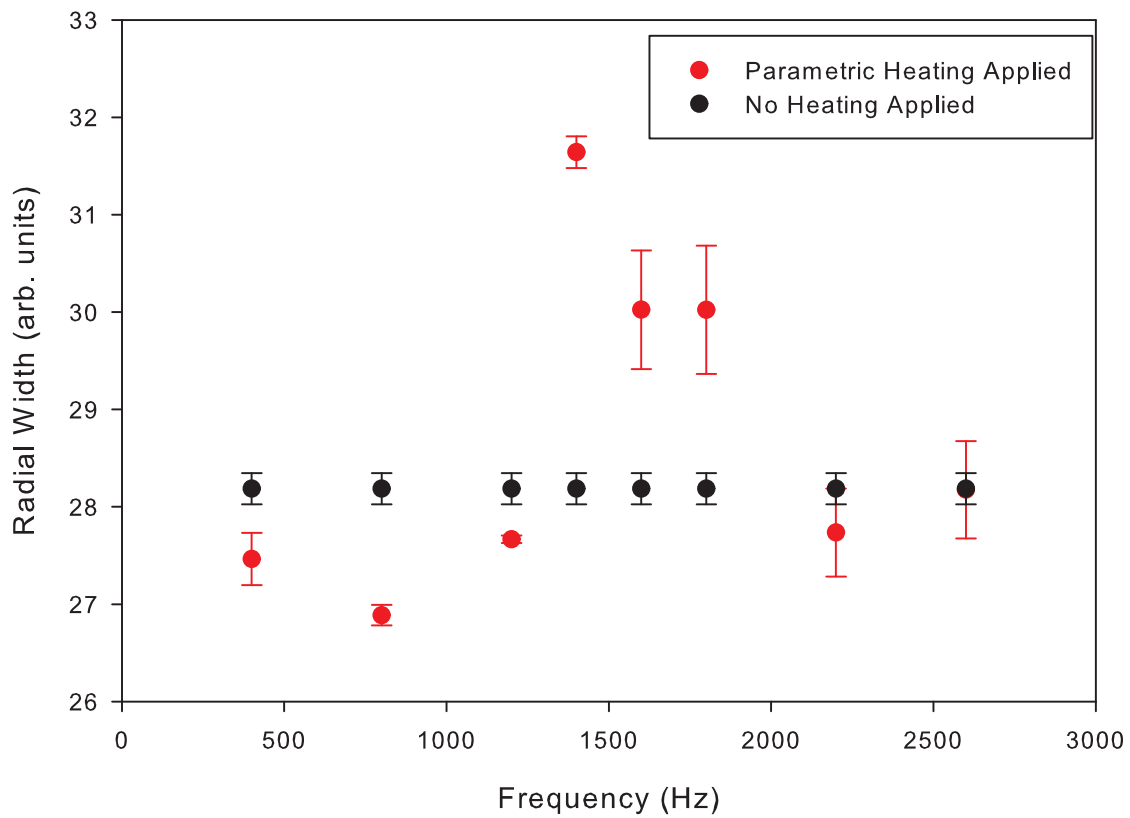
Figure 3.3: A typical example of the results of a parametric heating test are shown. The data in black is the average radial width of the atoms when no heating is applied and the data in red is the radial width when the heating is applied. The radial width is directly related to the temperature of the atoms, so a maximum in radial width corresponds to a maximum in temperature.
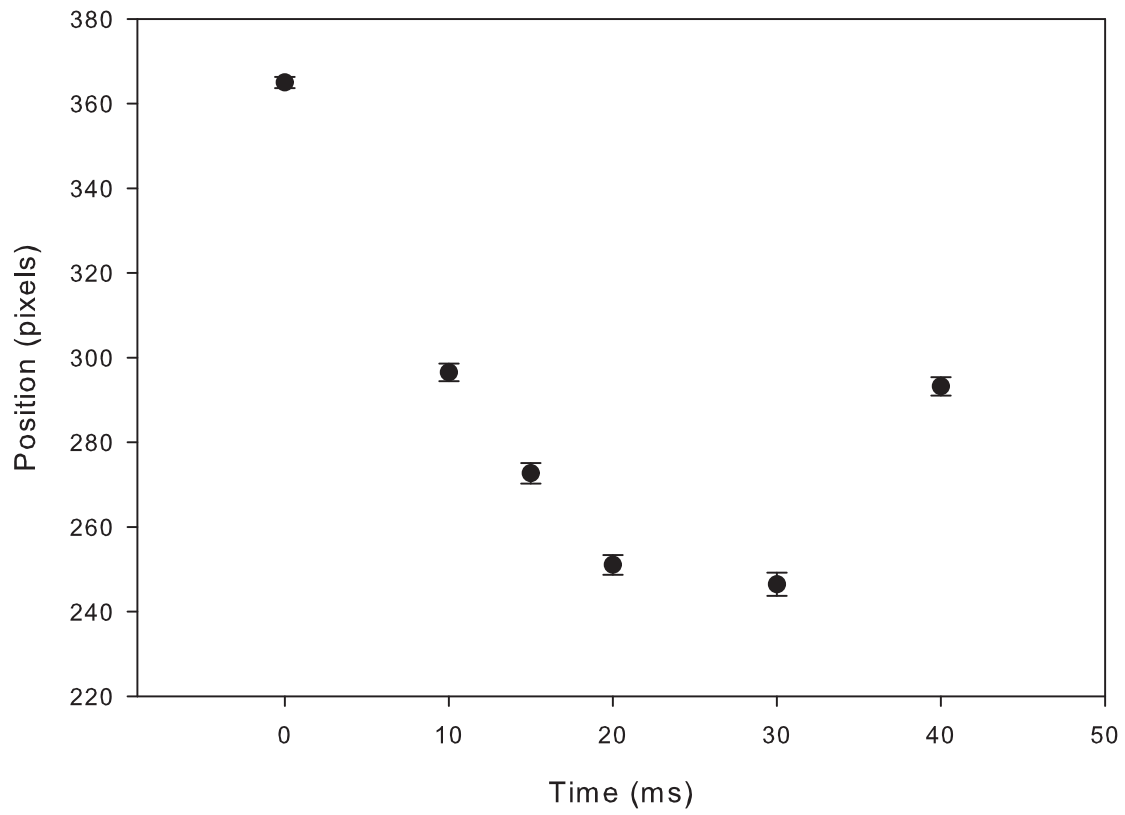
Figure 3.4: This figure shows the results of the axial trap oscillation experiment. The position of the atom cloud is shown by the black circles. The atom cloud began on one edge of the cloud and then slowly traveled towards the center of the trap.

the 1% level and σ_{final} approximated as vt. This leads to the direct radial temperature calculation of $T_{rad} = \frac{\sigma_{final}^2}{t_{expansion}^2} \frac{m}{k}$.

To extract density information about the atoms we first consider a below saturation resonant laser shinning on a cloud of atoms. The intensity of the beam as it travels through the cloud is given by

$$\frac{dI}{dz} = -n\sigma I \tag{3.1}$$

where n is the density of the atoms, σ is the absorption cross section and I is the intensity of the laser. The optical depth is defined as $OD = ln(I/I_0)$. Given the measured optical depth, the column density of the cloud along the direction of the imaging laser pulse is then known. If a particular form of the density spatial distribution is assumed, then the column density can be used to determine the three-dimensional density of the cloud. In all of our experiments, we assumed that the clouds had Gaussian density distributions, which is the expected distribution for clouds undergoing ballistic expansion from a Maxwell-Boltzmann thermal equilibrium. The optical depth is proportional to the atom number so measuring the optical depth spatial profile of the atoms can give us the atom number

$$N = \frac{2\pi \sigma_x \sigma_y}{\sigma_0} OD_{peak} \tag{3.2}$$

where σ_x and σ_y are the rms sizes for the two spatial dimensions orthogonal to the imaging beam direction, $\sigma_0 = 3\lambda^2/2\pi$ and OD_{peak} is the peak optical depth. All of these parameters, except σ_0 are extracted from the absorption imaging method. σ_0 is used to relate the amount of absorption to the number.

To extract the atom number and temperature of the atoms in the FORT, the FORT was turned off rapidly and the atoms were allowed to expand for 2-3 ms. The cloud was then imaged onto a CCD camera using absorption imaging on the atoms' cycling transition. A simple diagram of the probe laser and imaging set up is shown in Figure 3.5.

We also performed an experiment to check our magnification calibration. This was done by allowing the atoms to fall and then imaging them at various times during their fall. This allowed us to calibrate by using the measured acceleration as a function of time. The data for that experiment is shown in Figure 3.6. We found that our magnification was such that each pixel in the image corresponded to 6.39 microns.
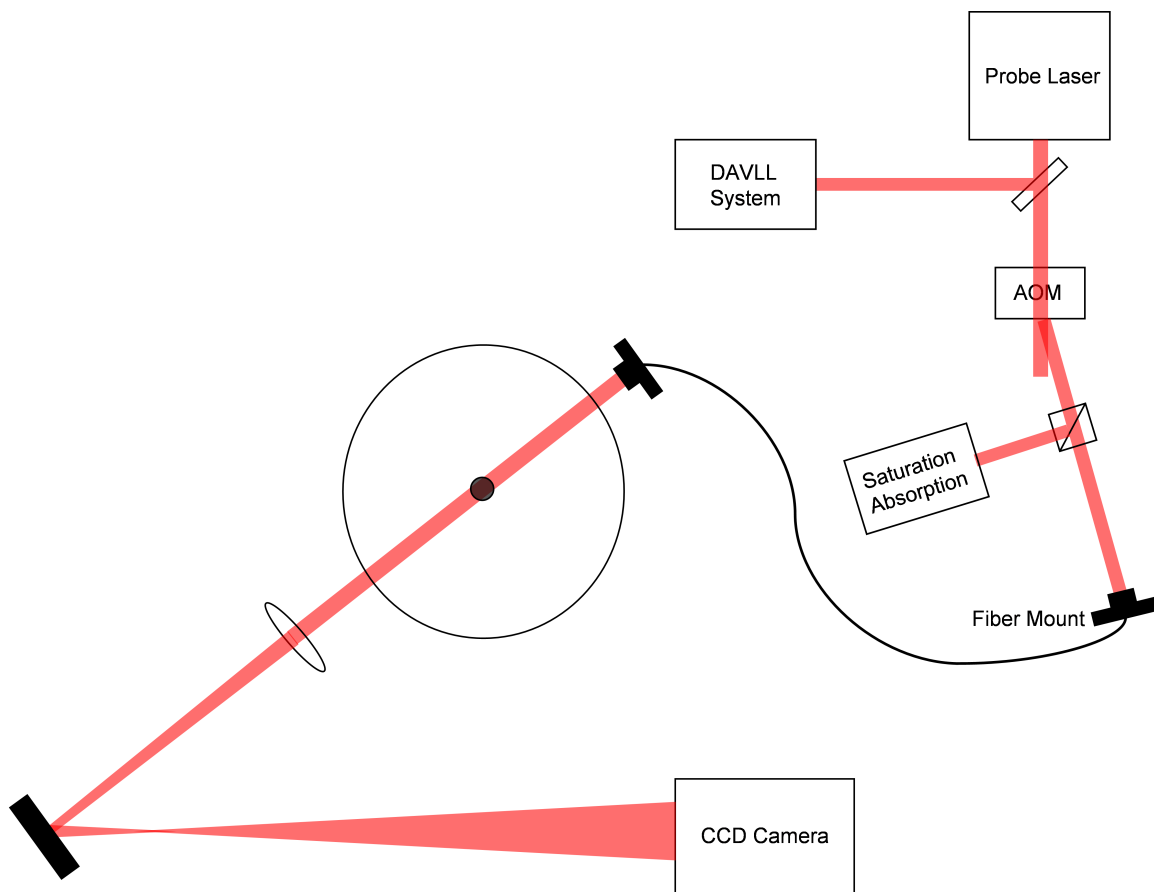
Figure 3.5: A simple diagram of the probe laser system is shown. The probe laser was fiber coupled into the chamber and was turned on and off via an Acousto-Optic Modulator (AOM) (figure from [1]).
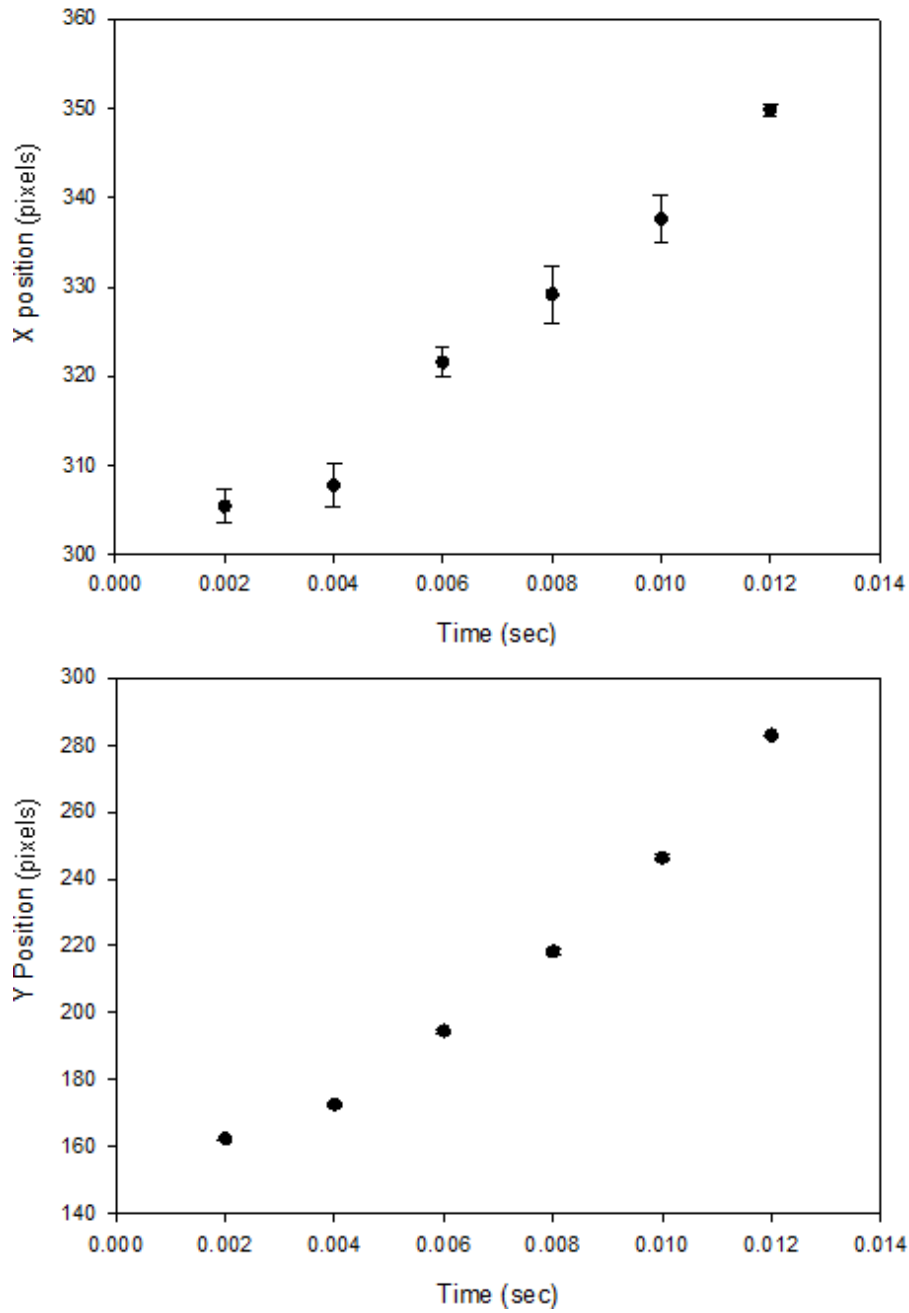
Figure 3.6: The data from the magnification calibration experiment is shown. Both the x and y components of the atoms position are needed since the probe images the atoms at an angle. The two data sets shown were fit with a parabola and the coefficients, modified by the probe angle, were compared to the known value for the acceleration due to gravity.

3.1.5   Basic Experimental Sequence

We began both the STOP and 2-CAZ experiments by loading ^{87}Rb and/or ^{85}Rb from a Magneto-Optic Trap (MOT) into a Far-Off Resonance Trap (FORT). The atoms were loaded from the MOT into the FORT using a compressed MOT stage by reducing the hyperfine repump power and detuning the main trapping laser further to the red of the cycling transition. This increased the density of the atoms in the MOT by almost two orders of magnitude by reducing the radiation pressure in the MOT [10]. Once the atoms were loaded into the FORT we began to perform the various experiments with them. The final step in any of the experiments described here is to image the atoms using absorption imaging.

3.2   Characterizing the FORT Potential for the STOP Experiment

Our optical trap confining potential was anharmonic. This anharmonicity was present for both the 2-CAZ and the STOP cooling experiments. Due to the way that the STOP cooling had to be measured, it was important to characterize this anharmonicity for the STOP cooling experiment. Due to the presence of optical aberrations in the FORT beam path, the anharmonicity could not be calculated from measured beam parameters (or at least could not be calculated straightforwardly). To determine the potential energy variation versus position along the axis of the optical trap, we loaded ^{87}Rb atoms into the trap and then waited a fixed amount of time during which the cloud was calculated to have time to come into thermal equilibrium.. We then imaged the atoms and performed an average over the radial direction in order to extract a linear density. By reducing the two dimensional array of information contained in a FORT image to a one dimensional linear density, we were able to better characterize the axial potential energy as a function of distance from the center of the trap.

To transfer the two dimensional absorption image information into the desired one dimensional linear density data, we used an averaging program to bin the data appropriately. This program began by first fitting a line to the center of the long direction of the optical trap. This main line was then divided up into segments of two pixels per segment. From here, lines were created perpendicular to this main line. The atoms that fell into each two pixel segment were then summed along each of the perpendicular lines essentially creating a bin for each two pixel segment of the
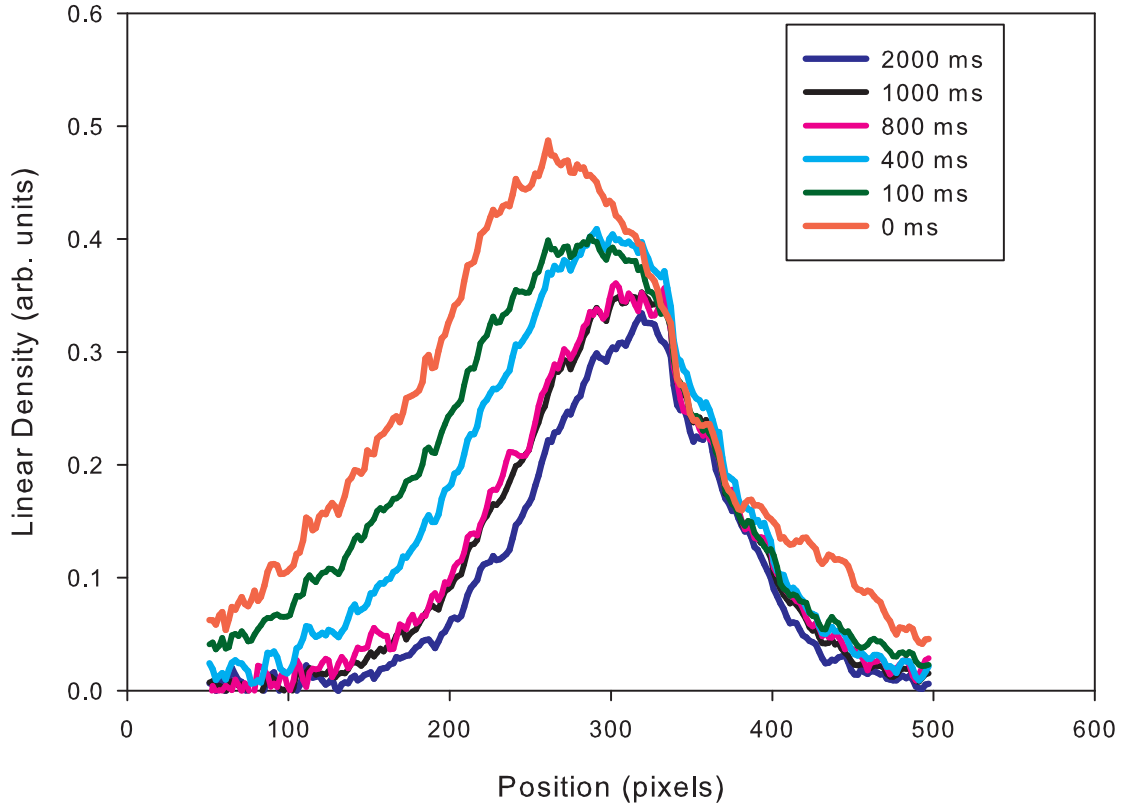
Figure 3.7: The linear FORT density is shown for various hold times. At the initial time of 0 ms the atom density is quite anharmonic, but as time goes on it becomes more harmonic (although never perfectly so).

line. Once we had the atom number in each bin we could use that number in addition to the known position of each bin to create a linear density profile for any given atom cloud. This average for several hold times can be seen in Figure 3.7.

We performed this measurement for a variety of delay times in order to get a sense of the trap evolution over time. It is clear from Figure 3.7 that the atom density distribution in the trap changes quite significantly over time. Its initial shape is significantly more anharmonic than its final shape in the data shown. The evolution in the atom distribution in the trap is due in part to the large evaporation rate in the FORT, which will be discussed in more detail later.

Although it was helpful to know the linear density of the trap at any given time, we were also quite interested in the axial optical trap potential at these times. It turns out that it is fairly

51

straightforward to extract a potential from a measured density distribution, since the density is expected to be proportional to $\exp(-U/k_BT)$. We were able to extract an effective 1-D potential from the linear density by simply taking the natural log of the linear density. Thus we could determine the axial potential energy variation with position. Finally, we fit this resulting axial potential using a fourth-order polynomial that had different coefficients on either side of the trap minimum potential energy point. We also ensured that the derivative and the value of the potential were continuous across any boundary. This allowed us to have an explicit, if approximate, equation for the potential energy which was useful when modeling the trap or analyzing data. The derived potential for the various delay times between optical trap loading and subsequent imaging is shown in Figure 3.8. The potential for times before 400 ms are not expected to be fully accurate because the atom cloud is predicted not to have reached thermal equilibrium. This means the relationship between the linear density and the potential is not as simple as $\exp(-U/k_BT)$. But this analysis still gives us an idea of how the potential evolves over time. For our calculations we used the potential from the 400 ms hold time, since this is the time closest to the time our data was taken and the atoms have thermalized at this point.

Part of the reason that we decided to take our measurements after waiting for several hundred milliseconds was to ensure that the atoms would have had time to thermalize. It is fairly straight forward to make a simple calculation of the thermalization time for a cloud of Rb atoms. In general, the elastic scattering cross section for atoms in distinguishable internal states is $4\pi a^2$. For ^{87}Rb, most collisions will be between atoms in different m_F states, so this is a reasonable scattering cross section to use. The s-wave scattering length is about $100 \cdot 5.29 \cdot 10^{-9}$ cm [11]. On average it takes about 2.5 elastic collisions to thermalize [12]. Additionally, a typical density of atoms in our FORT is $5 \cdot 10^{11}$ cm^{-3}. We can combine these values, along with a average collision velocity of 14 cm/s for the 40 μK cloud, to find an elastic collision rate of 24 collisions/sec. If we then divide this by the 2.5 collisions it takes to thermalize, we find a thermalization time of approximately 100 ms. Given this result, we conducted many of our measurements after waiting several hundred milliseconds to ensure the atoms had reached thermal equilibrium.
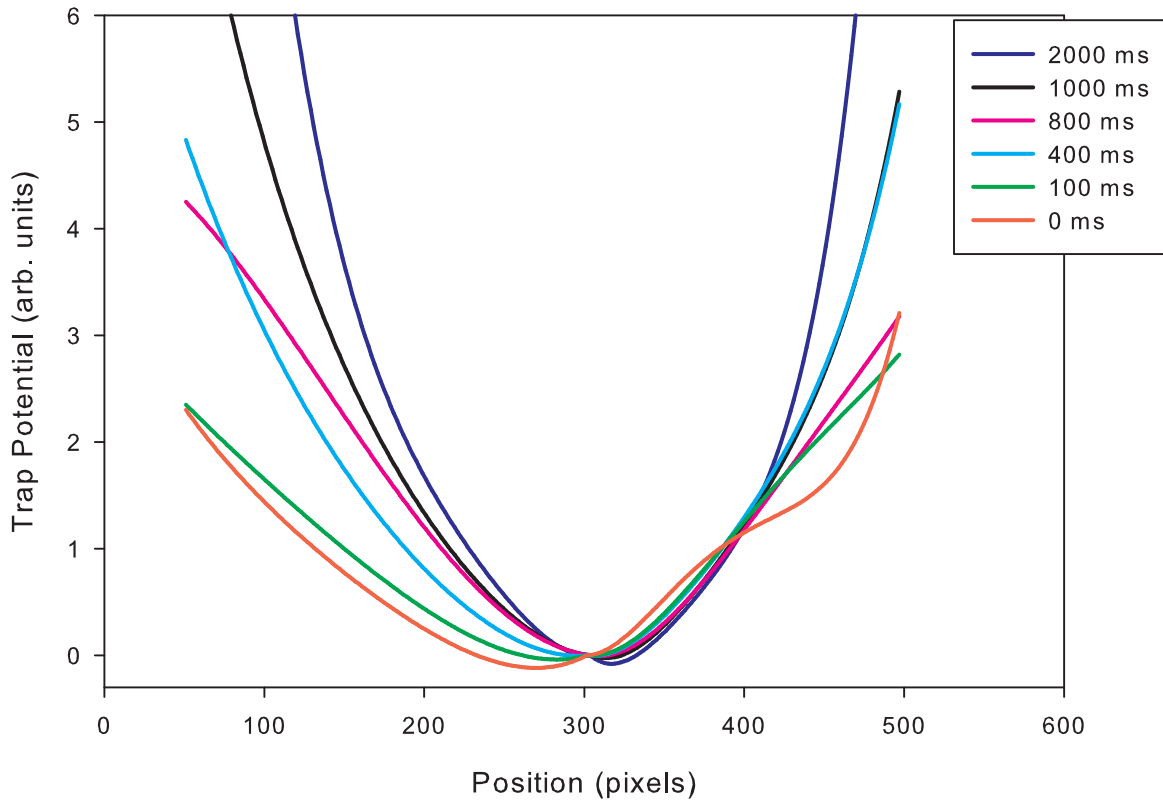
Figure 3.8: This figure shows the FORT potential extracted from the linear density data shown in Figure 3.7. Again it is clear that the potential changes quite a bit over the range of times that we measured.

3.2.1 Challenges encountered with the FORT

We encountered several challenges while working with our FORT. One issue is that the evaporation rate of atoms out of our FORT is too large relative to the cooling measurements that we want to make. The most critical parameter with respect to the evaporation rate in the FORT is the trap depth to atom temperature ratio. Due to the FORT loading process [1], the initial density of atoms loaded into the FORT is approximately fixed. In the summer of 2011 we switched from a 50 W GEM Select CO_2 laser to the 100 W GEM Select model (Coherent, Inc.). While this switch did improve our initial loading by making the loading process more robust as the deeper optical trap put less demands on the laser cooling into the trap, we found that the initial temperature of the atoms was much larger than we naively expected and that proved to be a problem. In retrospect, this can be seen through a simple calculation to examine the trade off between laser power and initial temperature. This calculation shows that the additional optical trap power was not beneficial in suppressing evaporation for the parameters that we used, even though it led to better robustness in the FORT loading process.

The first place to start when examining the FORT potential is to consider the case of a TEM_{00} beam. A standard laser textbook will tell you that the spot size as a function of distance can be written as

$$w = w_0\sqrt{1 + \frac{z^2\lambda^2}{\pi^2 w_0^4}} \tag{3.3}$$

where w_0 is the minimum spotsize and λ is the wavelength of the laser. From here we can determine the trapping potential to be

$$U = \frac{-U_0 w_0^2}{w^2}\exp(-2r^2/w^2) \tag{3.4}$$

where U_0 is proportional to the laser power. We can solve for the radial and axial trapping frequencies by setting the second derivative of the potential, evaluated at $r = 0$ and $z = 0$, equal to $\frac{m\omega^2}{2}$. The resulting trapping frequencies are

$$\omega_r = \frac{2\sqrt{U_0}}{m^{1/2}w_0}, \omega_z = \frac{\sqrt{2U_0}\lambda}{m^{1/2}w_0^2\pi} \tag{3.5}$$

We can see that doubling the intensity increases the frequency by $\sqrt{2}$ and halving w_0 increased the radial frequency by 2 and the axial frequency by 4. Using the density relationship, $n =$

$exp(-U/k_BT)$, we can also model the density of the atoms approximately by

$$n = \frac{N\omega_r^2\omega_z}{8(kT/m)^{3/2}\pi^{3/2}} \qquad (3.6)$$

It is reasonable to consider a case where the density is held fixed. We have experimentally observed that there is a relationship between the loading rate and the density dependent loss rate that tends to keep the density fixed for various experimental parameters [1]. In the case of constant density, we see that if the FORT laser power is increased by 2 then the temperature also increases by 2. This indicates that if the density is held constant there is no way to improve the trap depth to atom temperature ratio by increasing the laser power. If we also look at reducing w_0 by 2, equivalent to increasing the trap depth by 4, we see that the temperature needs to go up by about 6.3 to keep the density constant. Again this shows that there in no real benefit to increasing the trap confinement in terms of the trap depth to atom temperature ratio. Any benefits due to the larger trap depth or tighter confinement are negated by the increase in the initial temperature. Having a higher initial temperature led to a larger initial evaporation rate which made the types of measurements we wanted to take harder. In the future, the optical trap parameters will be changed so that the trap depth to atom temperature ratio will be improved. This will be accomplished by using a larger focal spot size for the FORT. For a fixed FORT laser power and the assumption of a constant density after loading, the atom temperature in the trap scales as $1/w_0^7$, where w_0 is the FORT minimum spot size. The trap depth to atom temperature ratio thus scales as $1/w_0^5$. A drop of trap depth by a factor of 1.5 will improve the trap depth to atom temperature ratio by 2.8, which should result in a significant reduction in the evaporation rate.

Additionally there are spherical aberrations and thermal lensing that occur in our system. The primary source of thermal lensing in our system is the AOM used to turn the CO_2 light on and off. Thermal lensing occurs when a gain medium is heated unevenly, specifically when the medium is heated more at the center of the laser beam than on the edges causing a gradient in the refractive index. This effect is of course worsened by a higher power laser, so our 125 W CO_2 laser causes more thermal lensing than the previous 50 W CO_2 laser. Our AOM is rated for a 100 W laser and was originally purchased to work with our previous 50 W CO_2 laser. When the system was upgraded to a 125 W CO_2 laser we found that the AOM still worked with the higher power laser,

but we noticed that as we held atoms longer in the trap there was a general relaxation of the trap, contributing to a larger evaporation rate. Spherical aberrations are evident in the two lenses used to create the focus of the CO_2 beam used to create our FORT [1]. The spherical aberrations cause our trap to be more anharmonic and the thermal lensing leads to a general relaxation of our trap over time. Initially this evaporation didn't seem to be a large problem, but as we will see with both the STOP and the 2-CAZ experiment, the evaporation rate ended up limiting both experiments. This problem was only fully diagnosed late in the work presented in this thesis, however. A full discussion of the effects of this evaporation rate on STOP cooling is included in the following section. Additionally, potential solutions to this problem will be discussed in Section 4.4.3 during the discussion of the planned future work designed to more fully explore STOP cooling.

3.2.2 Understanding How the Evaporation Rate in the FORT Effects STOP Cooling Measurements

I have mentioned several times that the evaporation rate in the FORT prevented me from easily measuring the cooling from both 2-CAZ and STOP cooling. The following calculation provides a description of how this evaporation can effect the cooling measurement in the case of STOP cooling. Details of the direct effect of the evaporation rate on 2-CAZ cooling are described in Chapter 6.

For the case of STOP cooling, the ideal way to measure the cooling rate would have been to apply a cooling pulse and then look at the the resulting temperature decrease. Unfortunately this cannot be done in a straightforward way quantitatively. The reason that we cannot just measure the temperature of the atoms after one cooling pulse is that they have not had any time to thermalize. So although we have reduced the energy, and therefore temperature, of a large group of atoms this temperature decrease is not yet reflected in the total atom temperature. One might wonder why we don't just wait for the atoms to thermalize and then measure the temperature decrease. This would be a great method to measure the cooling if we did not have the large evaporation rate in our FORT. This rate ends up masking the cooling if we wait the length of time needed for the atoms to thermalize.

The best way to understand how this masking occurs is to consider the evaporation rate for a three dimensional and a two dimensional cloud of atoms. The evaporation rate can be expressed

as the rate of atom loss per unit time via evaporation (η):

$$\eta_{3-D} = \frac{d}{T}\alpha \exp(-\frac{d}{T})$$ (3.7)

$$\eta_{2-D} = \sqrt{\frac{d}{T}}\alpha \exp(-\frac{d}{T})$$ (3.8)

where α is the collision rate and d is the trap depth in temperature units. These evaporation rates are derived in detail in [13].

We can now consider how these rates apply to our experiment. When the atoms are simply being held in the trap the 3-D evaporation equation best describes the evaporation that is occurring. But if we were to apply a STOP pulse and remove 20% of the energy in the axial direction, the evaporation in the axial direction would be almost completely cut off. This means that until the atoms rethermalize the evaporation would be best described by the 2-D evaporation rate.

To demonstrate how this change from 3-D to 2-D evaporation masks the cooling, I have plotted a comparison of the 20% cooling case and subsequent 2-D evaporation and the uncooled 3-D evaporation case in Figure 3.9. We can see that after only 500 ms what started as a clear 2 μK temperature difference is down to a less then 0.5 μK temperature difference. Since our experiment generally cannot accurately measure the temperature to better than 0.5 μK, the two conditions become indistinguishable. This is why we were not able to measure the temperature reduction from the cooling in any sort of traditional way. A discussion of the actual cooling measurement technique will be discussed in Section 3.3.4.

3.3 STOP Experiment

After loading our ultracold atoms into the FORT, we implemented the STOP cooling scheme in order to further reduce the temperature of the trapped atoms. As mentioned in the previous chapter, this technique relies on three distinct steps; applying a spatially selective beam to pump the atoms up to the upper hyperfine ground state, applying a pulse to oppose the atoms' velocity once at the center of the trap and slow them down, and finally applying a pulse to pump the atoms back to their original hyperfine ground state and remove the entropy from the system. For the STOP experiment the FORT had a trap depth of 195(39)μK and trap frequencies of 735(12)Hz
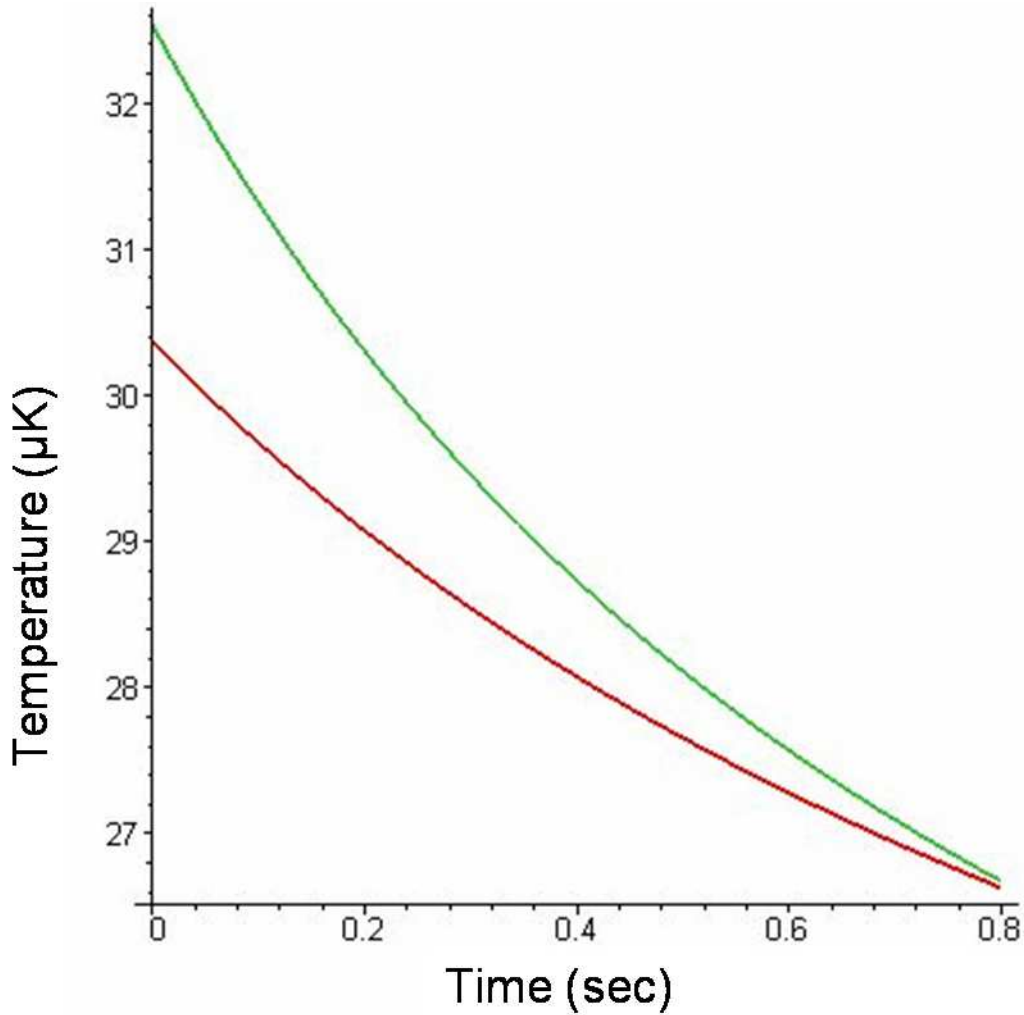
Figure 3.9: Right after the initial axial temperature reduction of 20% the cooled cloud, represented by the red line, has a much lower temperature, but since the cloud is now experiencing 2-D evaporation the temperature of the uncooled cloud, represented by the green line, quickly catches up since it is evaporating at the much faster 3-D rate.
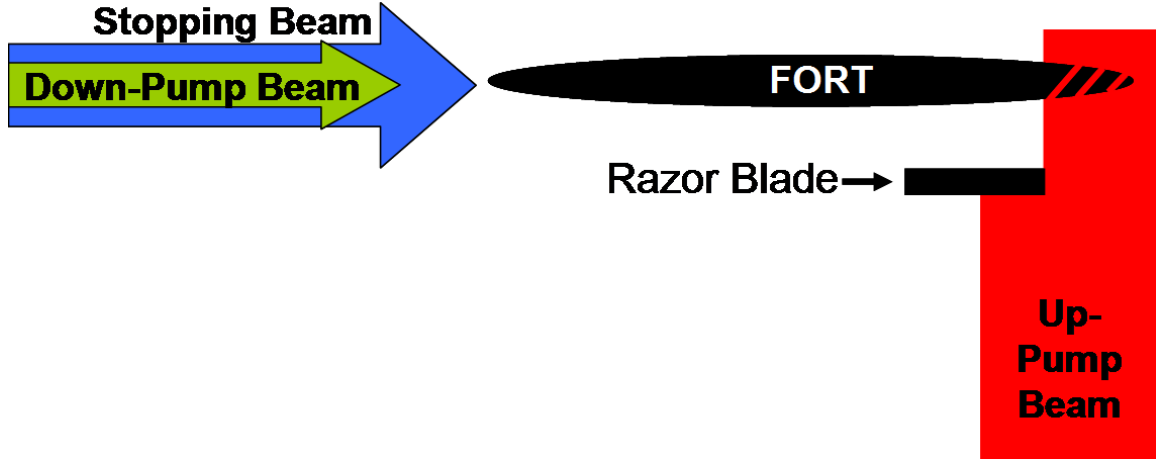
Figure 3.10: A simple schematic of our experimental set up is shown. The black elongated oval represents the extent of the ^{87}Rb atoms in the FORT. The black rectangle represents the razor blade used to truncate the up-pump beam to control the up-pumped atom fraction. The rest of the objects represent the laser beams used in the implementation of the cooling as described in the main text.

in the radial direction and 20(2)Hz in the axial direction. I will begin by discussing each of the required steps in more detail and then will discuss the way that we measured the cooling.

3.3.1 Up-Pump Laser

To repump only the atoms with the highest energy in the FORT, a beam that can move atoms from the $5S_{1/2}$ $F=1$ state to the $5S_{1/2}$ $F=2$ state is aligned with the edge of the FORT. To do this, we picked-off a beam from our repump laser, tuned to the $5S_{1/2}$ $F=1$ to $5P_{3/2}$ $F'=2$ transition, to apply a 1 ms pulse. This up-pump beam was sent through a spatial filter to ensure the highest beam quality. This beam was then aligned with the edge of the trapping region as shown in Figure 3.10. In order to control how much of the trap was illuminated by this beam, we inserted a razor blade into the up-pump beam right before the trapping region. This allowed us to easily adjust what percentage of atoms were up-pumped. This beam was coupled into the chamber through one of the MOT mirrors using the small but finite transmission of the mirror (2%) to allow it to pass through. The pulse time is relatively long, but it is necessary because of the low intensity that is being used. This low intensity was used in an attempt to mitigate any possible problems with reabsorption [1, 14].
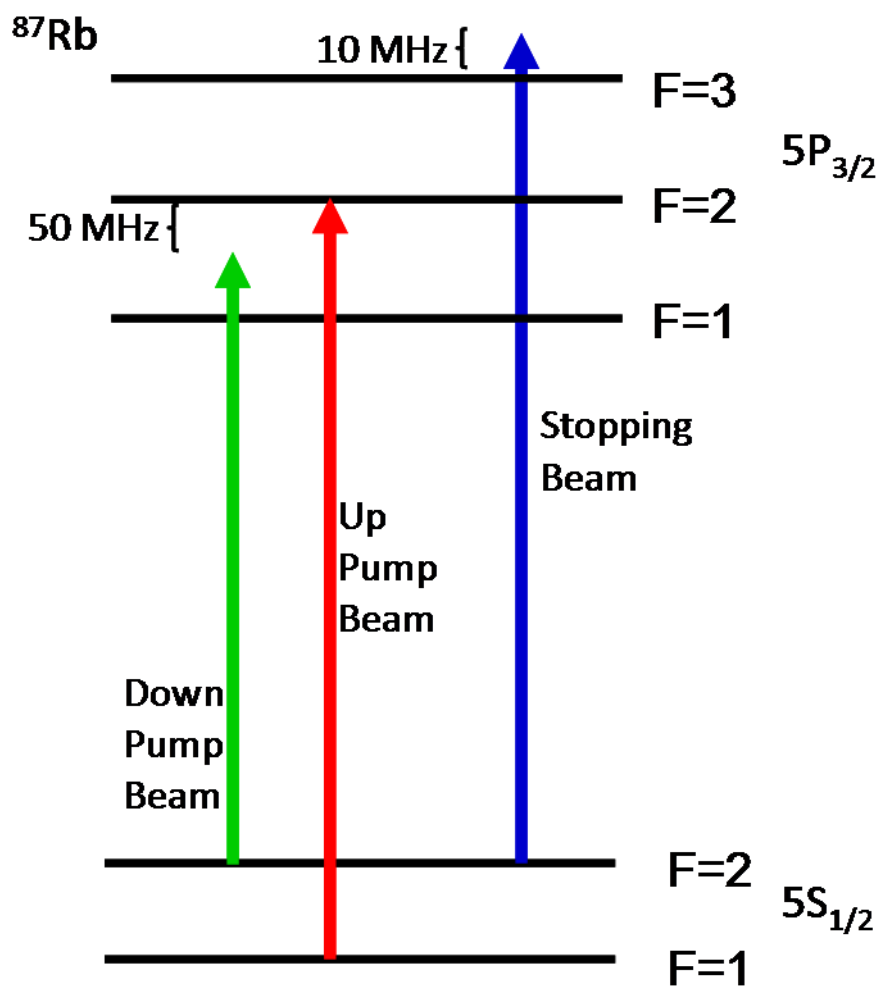
Figure 3.11: The transitions for all of the beams used in STOP cooing are shown. The Up-Pump beam was simply a pick off from the repump laser and its detuning was not changed from the standard repump frequency. The Stopping beam was detuned blue of the $F=3$ excited state as shown and the Down-Pump beam was tuned between the $F=1$ and $F=2$ exited states.
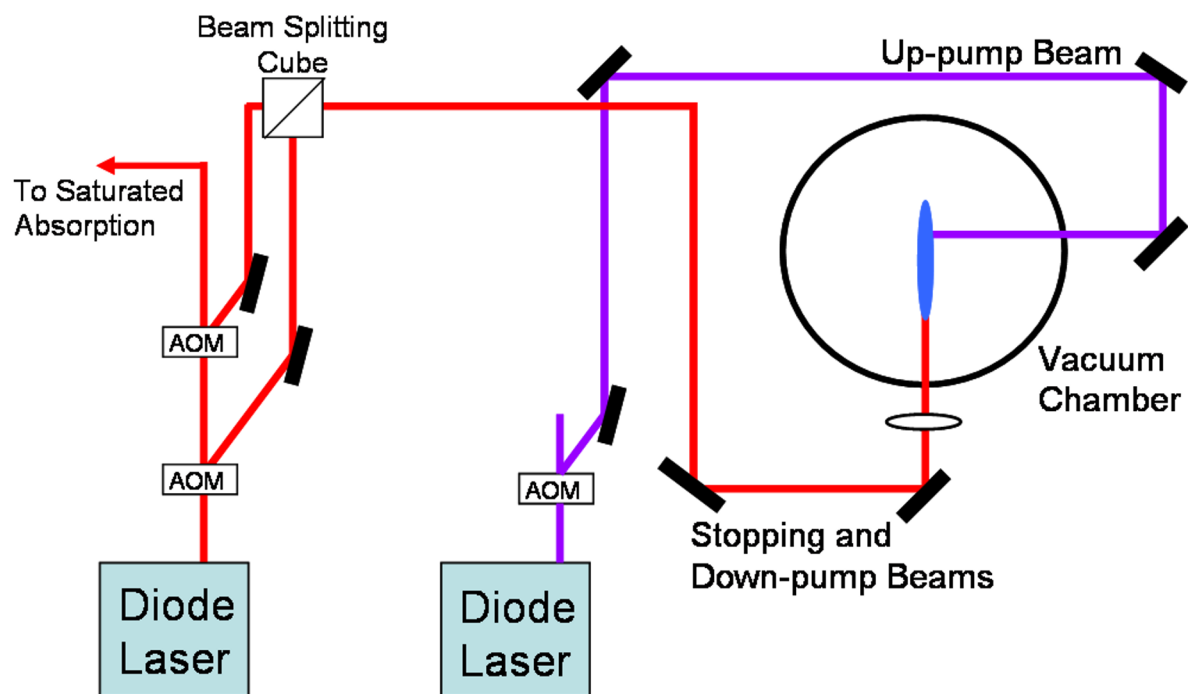
Figure 3.12: A simple diagram of the laser setup for the STOP cooling experiment is shown. The Up-Pump beam is shown in purple and the Stopping and Down-Pump beams are shown in red. The red beams were coupled into the chamber through the output port for the CO_2 beam and a lens was required to compensate for the lens inside the vacuum chamber. The FORT is represented by the blue oval in the center of the vacuum chamber.

3.3.2 Stopping Laser

After applying the up-pump pulse, we waited 12.5 ms until the atoms were in the center of the trap to apply the stopping pulse. At this point, a 0.2 ms pulse from the stopping beam and a 1 ms pulse from the down-pump beam were applied. Both beams were pulsed using Acousto-Optic Modulators (AOM). The stopping beam was detuned 10 MHz blue of the $5S_{1/2}$ F=2 to $5P_{3/2}$ F'=3 main trapping transition. The transitions for all three of the lasers are shown in Figure 3.11.

3.3.3 Down-Pump Laser

The down-pump beam used to pump the atoms from the $5S_{1/2}$ F=2 state to the $5S_{1/2}$ F=1 state was detuned 50 MHz red of the F=2 to F'=2 state, which is 107 MHz to the blue of the $5S_{1/2}$ F=2 to $5P_{3/2}$ F'=1 transition. This ensured that the atoms would be pumped back to the lower hyperfine state which is necessary to complete the cooling cycle.

The stopping beam and down-pump beam were both aligned to be counter-propagating to the CO_2 trapping beam. In order to do this we inserted a mirror that reflected 780 nm light and passed 10.64 μm light. We aligned these stopping and down-pump beams along the trap as shown in Figure 3.12. In order to ensure that these beams were hitting the atoms, they were aligned into the chamber and then one of the beams was tuned to the correct frequency to pump the atoms into the upper hyperfine state from the lower hyperfine state. These upper hyperfine state atoms were imaged using absorption imaging without a hyperfine repump laser. In this configuration, atoms remaining in the lower hyperfine state would not be detected. By adjusting the alignment of these beams into the chamber, the number of atoms seen by the probe laser could be maximized.

As discussed in the model considerations, it is important that the atoms all scatter about the same number of photons from each of these beams to ensure efficient cooling. In Figure 3.13, I have shown the square of the various Clebsch-Gordon coefficients for all of the necessary transitions. As you can see the variation in the square of the CG coefficients is smallest for pure linear polarization. The best way to ensure an even number of scatters per atom was to have both the stopping and down pump beams have linear polarization. This polarization was aligned along a small magnetic field produced by current flowing through coils external to the vacuum chamber.
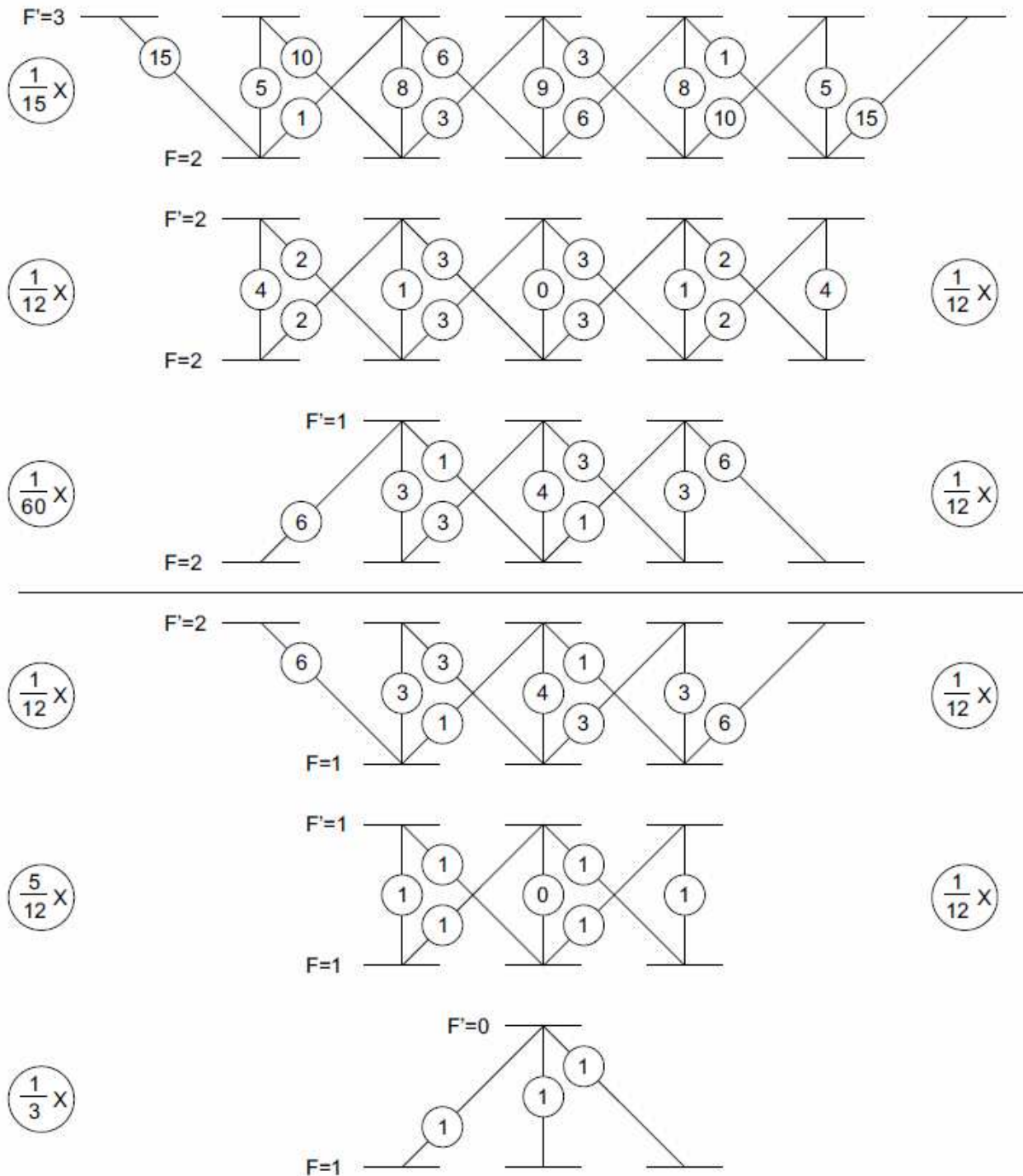
Figure 3.13: A table of branching ratios (proportional to the square of the Clebsch-Gordon coefficients) for ^{87}Rb is shown. As you can see there is much less variation between just the linear transition than between the $\sigma+$, $\sigma-$ and linear transitions. This was why it was important for only linear transitions to be used. Multiplying by the number in the circle will give the branching ratio for the D2 or D1 line. [15]

By using this setup, we were able to ensure the most even scattering of photons. Of course, the photon scattering rate from both beams will still have a distribution best described by a Poission distribution. Given the random nature of the photon scattering, there was nothing we could do about this. As mentioned in the model section, if we had used a method that precisely controlled the number of photon scatters that each atom experienced, we could have increased the cooling somewhat. But techniques of that sort are much more complicated, and for the initial atom temperatures we were working at we would only have expected a few percent improvement in the cooling rate.

3.3.4 Extracting Information About the Cooling

To determine the energy removed from the gas during a cooling cycle we measured the axial size reduction of the gas one quarter cycle after one cooling pulse was applied. The best way to understand this method is to consider one atom in a harmonic trap as shown in Figure 3.14. If we begin with the atom near one edge of the trap, it will have mostly potential energy. We can then wait until the atom is in the center of the trap and has converted all of its energy into kinetic energy. From that point we consider two possible cases: we can either allow the atom to continue to travel in the trap until it is at the far side of the trap, again converting its energy to all potential energy, or we can apply a cooling pulse to the atom and then allow it to travel in the trap. If we look at this atom in both cases at the time that it would normally be at the far side of the trap without STOP cooling applied we will be able to see a difference between the atom that has been cooled and the atoms that was left alone. The atom that has been cooled will not have traveled nearly as far towards the edge of the trap, since it had its velocity at the center of the trap reduced by the cooling pulse. If we were to compare the positions of the two atoms, the one we cooled and the one we left alone, we will be able to extract information about how much cooling occurred. This is the general idea behind the technique we use to determine the cooling from one cycle of STOP cooling.

The first step in extracting the cooling data was to convert the information from a two dimensional image, like the two shown in Figure 3.15, to a one dimensional line. To do this we performed a radial average of the images to obtain the atom linear density vs. axial direction in the optical trap. This was done in just the same way as was described in Section 3.2. Figure 3.16 shows the
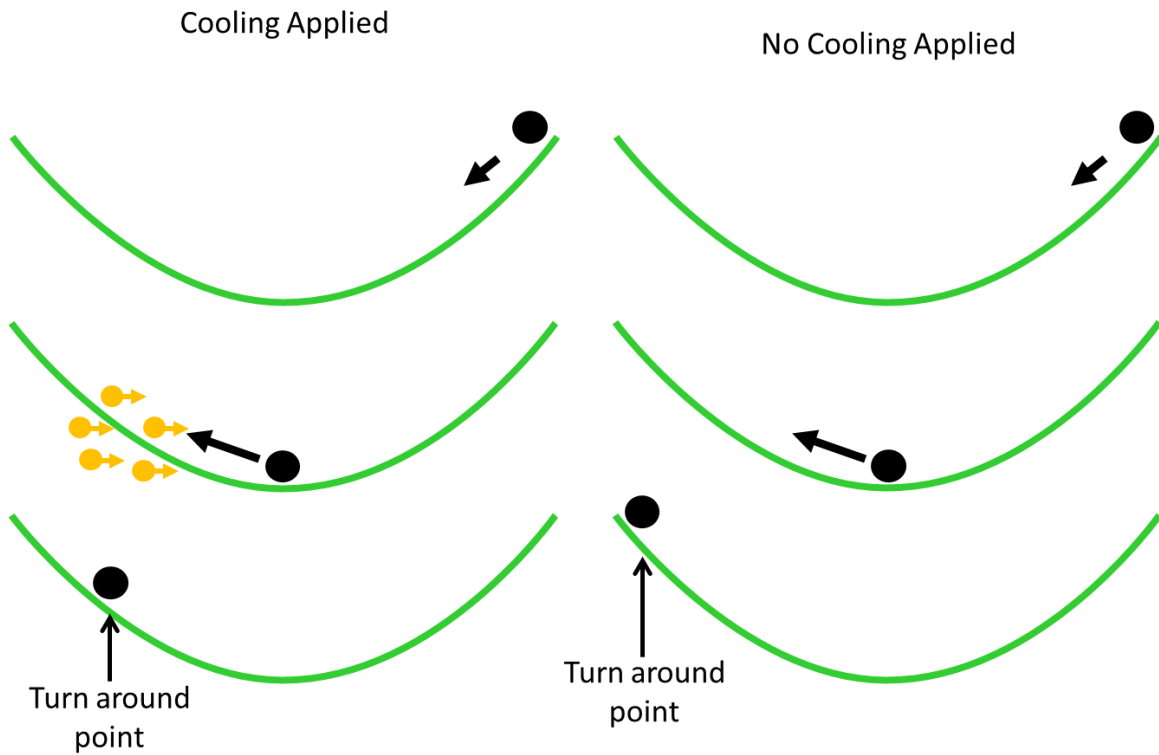
Figure 3.14: A simple diagram of cooling for one atom is shown. The final position of the atom after it travels a half cycle is quite different depending on whether or not it was cooled. This difference in final position was exploited to determine the cooling from one cycle of STOP cooling.
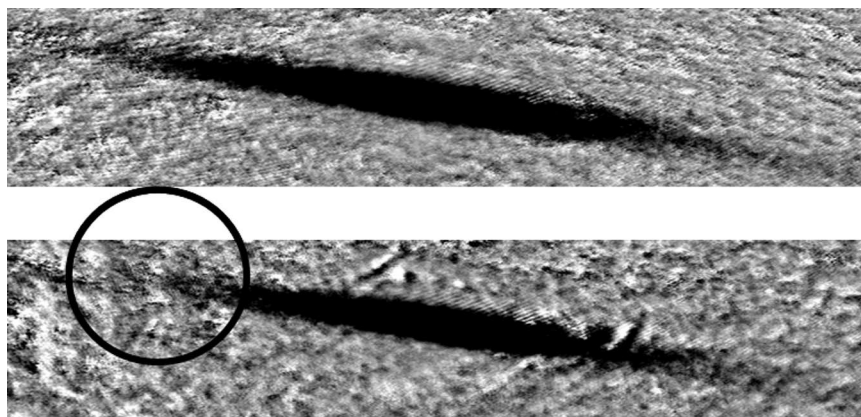
Figure 3.15: This figure shows the large axial size reduction that occurs after one cycle of cooling. By characterizing this axial reduction we can calculate a potential energy reduction and thereby extract an axial energy reduction.
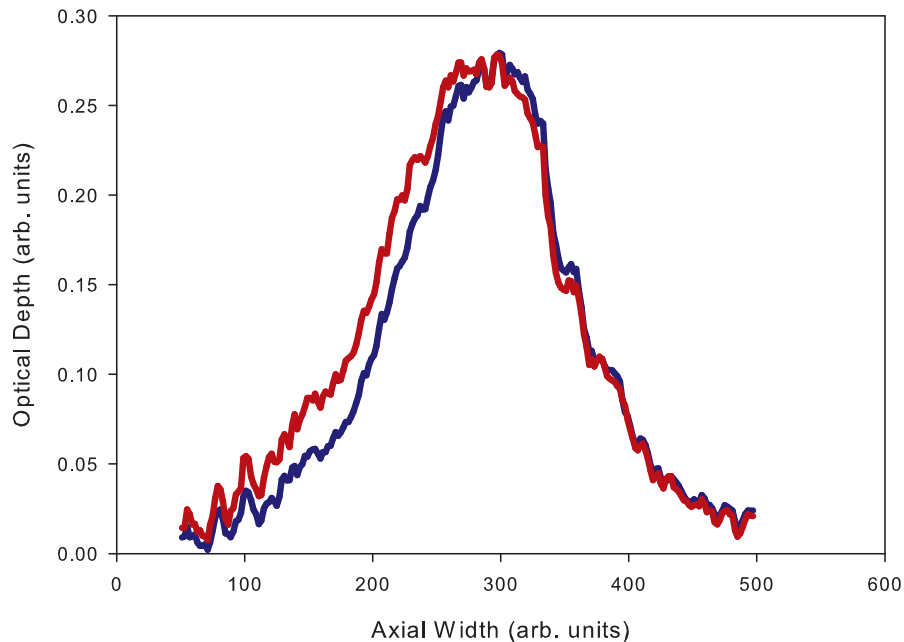
Figure 3.16: This figure shows the linear density extracted from images like those in Figure 3.15. The large axial reduction is still quite clear in these images.

curves created from data like that in Figure 3.15. You can clearly see the axial size reduction for a set of this averaged data. Once we had a linear density we could use the potential that we extracted from our earlier measurement, discussed in Section 3.2.

By then using the experimentally-determined potential energy and the atom linear density, we determined the total axial potential energy of the atoms in the trap to be

$$\text{Potential Energy} = \frac{\int U_{400\text{ms}} n(z) dz}{\int n(z) dz} \tag{3.9}$$

where $n(z)$ is the linear density and $U_{400\text{ms}}$ is the previously determined potential associated with the time our data was taken.

Once we had the ability to extract a potential energy value for a given data set, we then compared the potential energy with and without an applied cooling pulse to calculate a percentage decrease in potential energy in the axial direction. This percentage reduction can then be compared to the predicted reduction produced by the model calculation.

From this reduction in energy we were able to evaluate the cooling from one pulse cycle. We were also able to look at the results of several applied pulses to evaluate the loss produced by this technique. These measurements will be discussed in detail in the next chapter.

3.4   Conclusion

The experimental equipment described in this chapter was built and modified over the course of many years. The original vacuum chamber and MOT set up was built in 2004. Since that time, several diode lasers were added to the system and a large amount of maintenance and repair was done to keep the system running. We were also forced to develop an unusual technique for extracting cooling information due to the large evaporation rate in our optical trap. The results of this measurement will be discussed in the next chapter. Additional information about the experimental apparatus will be included in Chapter 6 when the 2-CAZ experiment is discussed.

References for Chapter 3

[1] Anthony Gorges, Ph. D. Thesis, Colorado State University (2010).

[2] Mathew Hamilton, Ph. D. Thesis, Colorado State University (2013).

[3] K. B. MacAdam, A. Steinbach and C. Wieman Am. J. Phys. 60, 1098 (1992)

[4] L. Ricci et. al., Opt. Commun. 117, 541 (1995)

[5] Kristan L. Corwin et. at., Appl. Opt. 37, 3295 (1998).

[6] D. W. Preston, Am. J. Phys. 64, 1432 (1996).

[7] Wu J, Newell R, Hausmann M, Vieira D J, and Zhao X 2006 J. Appl. Phys. 100 054903

[8] Roati G, Jastrzebski W, Simoni A, Modugno G and Inguscio M 2001 Phys. Rev. A 60 052709

[9] Friebel S, Dandrea C, Walz J, Weitz M and Hansch T W 1998 Phys. Rev. A 57 R20-R23

[10] Petrich W, Anderson M H, Ensher J R and Cornell E A 1994 J. Opt. Soc. Am. B 11 1332-1335

[11] E. G. M. van Kempen, S. J. J. M. F. Kokkelmans, D. J. Heinzen, and B. J. Verhaar Phys. Rev. Lett. 88, 093201 (2002)

[12] Jacob Roberts, Ph. D. Thesis, University of Colorado (2001).

[13] W. Ketterle, and N.J. van Druten, Advances in Atomic, Molecular, and Optical Physics 37, 181 (1996).

[14] Y. Castin, J. Cirac, and M. Lewenstein, Phys. Rev. Lett. 80, 5305 (1999).

[15] Heather Lewandowski, Ph. D. Thesis, University of Colorado (2001).

Chapter 4

Spatially-selecTive Optical Pumping (STOP) Cooling Results

Now that the experimental techniques have been discussed, the results of our STOP cooling measurements will be presented. In this chapter, I will first discuss a few optimization procedures that were performed and then I will discuss the measured cooling rates. After that, I will briefly discuss the simple model that I used to confirm that our results were reasonable and calculate the total net cooling rate. Finally, I will discuss the future of the STOP cooling experiment.

4.1 Optimization Procedures

The goal of the STOP cooling experiment that I performed was to determine how much of the maximum predicted cooling rate could be achieved for our optimum signal to noise conditions. In order to do this, several optimization procedures were performed. The first step was optimizing the length of the stopping pulse. For instance, a change in the pulse length from 0.20 ms to 0.30 ms reduced the observed cooling by as much as 34%. Typical optimization data can be seen in Figure 4.1. Ensuring that this pulse was the ideal length was a crucial step towards observing the maximum predicted cooling rate. Additionally, the initial up-pump percentage was selected to be 25%, the predicted optimum value, although the predicted cooling rate was fairly insensitive to this percentage. After these optimizations were complete, we were able to extract a one-cycle cooling rate. At the same time, these measurements were able to also determine the extent to which losses were associated with the STOP cooling technique.

4.2 Cooling Results

Averaging over a total of 40 measurements of one cycle cooling for our best signal-to-noise conditions we observed a fractional reduction in the axial potential energy of 0.088 ± 0.008(statistical) $\pm$ 0.004(systematic) per cycle for a $42.1\mu K \pm 0.7$(statistical)± 8.3(systematic) initial cloud temperature and a total cycle time of 15 ms, including the time required for the optical pumping pulses. The systematic uncertainty is primarily due to uncertainties in the determination of the axial potential.
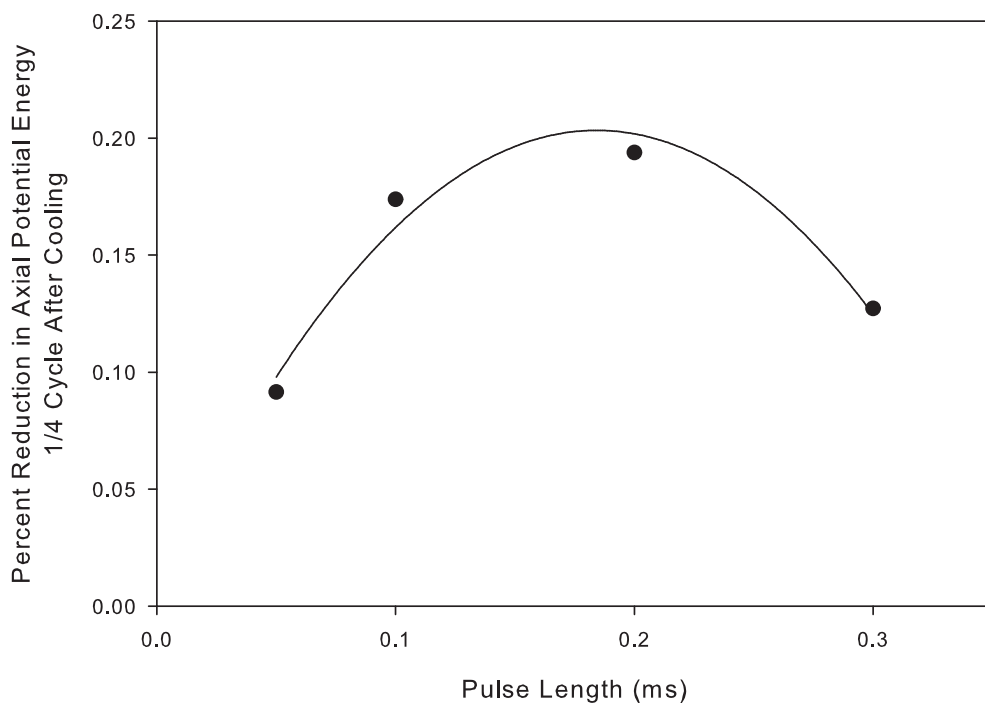
Figure 4.1: Typical Pulse length optimization data is shown in this figure. Several cooling pulse lengths were used to determine the optimum time.

From this data, a cooling rate in μK/sec can be extracted, but, in order to get the total cooling rate, additional analysis is necessary.

4.3 Net Cooling Rate Extraction via Modeling the Measured Anharmonic Potential

This one-cycle energy reduction reported in the previous section did not match the predictions from the harmonic model and was significantly lower. This was not necessarily surprising for a first attempt at the technique especially since some part of this discrepancy between expected and measured energy reduction is due the fact that our optical trap is significantly more anharmonic than even the ideal optical trap case.. We needed to develop a model that would give us an idea of what the total energy reduction was for our optical trap potential. While the anhamonic model in Chapter 2 was developed for an ideal optical trap potential from a focused laser beam, the aberrations in our optical system produced an optical trap that was distorted significantly from the ideal. This required the measurement of the optical potential as described in Section 3.2 and the development of an entirely different model.

This model began by using the 1-D trap potential extracted from experimental measurements, as described in Section 3.2. Due to the 1-D nature of the trap potential, the anharmonic calculation was 1-D as well. If we were to attempt to extend this model to 3-D, the increase in the dimensionality of the calculation of the cooling would lead to significantly longer calculation times. Although a longer calculation time is not necessarily prohibitive, in this case we also discovered that the uncertainties in several of the parameters involved in the calculation were large enough that extending this model beyond a straightforward 1-D calculation did not make sense. Any improvements in precision gained by performing a 3-D model, would be largely negated by the large uncertainties in these model parameters. Another issue in extending the model to 3-D occurs when inferring the radial atom extent from the 1-D data collected to determine the axial potential. This can be done by making assumptions about the optical trap radial variation and the thermal distribution of the atoms, but at the cost of a considerable complication of the analysis and some question about the validity of the assumptions (i.e. how to treat the cutoff in the thermal potential due to the finite

depth of the optical trap). These factors lead us to perform the following 1-D calculation using the experimentally derived potential.

As mentioned in Chapter 3, the cooling was measured as a potential energy reduction, not as a reduction in the temperature. So, to determine the STOP cooling rate from this measured potential energy reduction, it was necessary to model the atoms' motion in the anharmonic optical trapping potential. This is because unlike in a harmonic potential where kinetic and potential energy are exchanged every $\frac{1}{4}$ cycle for every atom in the potential, in an anharmonic potential the exchange between kinetic and potential energy occurs at different times for different atoms. So, the total energy reduction is greater than any observed potential energy reduction. The nature of this energy exchange is one of the differences between atom behavior in a harmonic trap versus atom behavior in an anharmonic trap as discussed in Section 2.5.

Using a Maxwell-Boltzmann distribution modified by a sharp cutoff at the optical trap depth in a 1-D calculation, we specified an initial distribution of atoms. We began with 40 velocity classes for each point in the distribution. In addition to the velocity classes, we used 200 points that spanned the full range of the spatial distribution of atoms. Each atom was then assigned a state, either in the upper hyperfine state or the lower hyperfine state. Ideally, the boundary between atoms in the upper hyperfine state and atoms in the lower hyperfine state would be infinitely sharp, but in our current apparatus that boundary was blurred. This blurring was largely due to reabsorption effects and will be discussed in more detail shortly. The initial distribution of up-pumped atoms can be measured via absorption imaging by only imaging atoms in the upper hyperfine state just after the application of the up-pumping pulse. This spatial distribution of atoms can be compared to the total distribution of all of the atoms in the trap. A measurement of the atom radially-averaged linear density distribution is shown in Figure 4.2 along with a fit of this data in Figure 4.3. The distribution of atoms into either the upper or lower hyperfine state was initially determined by this measured distribution. However, given that the data obtained in Figure 4.2 were taken after the atoms had expanded from the trap after release and that the data does not have infinite signal to noise, there is some uncertainty in the initial up-pumping distribution.

The atoms' motion was then modeled using the ordinary differential equations associated with the trap potential. When the atoms reached a point in the potential corresponding to the experimental delay time used, a theoretical stopping pulse could be applied in the direction generally

72

opposite the motion of any atoms in the upper hyperfine state. The atoms then continued to propagate for an amount of time corresponding to the experimental delay time before imaging. At this point the potential energy and the total energy of the gas was calculated for all of the atoms. These energies were calculated as a function of photon scatters. We once again used a Poisson distribution and assumed each photon contributed $(1/3)\hbar^2 k^2/(2m)$ of axial direction energy per scatter. For each condition, the average number of photon scatters was optimized to produce the largest energy reduction. These results could be compared to the experimental results. When these results were compared to the measured cooling, it became clear that the uncertainty in the initial up-pump distribution produced cooling results that spanned a wide range of values due to a somewhat unexpected sensitivity to the initial up-pumped distribution. The precision of the experimental results was much greater than that of the model due to the uncertainty in the initial up-pump distribution.

This uncertainty did reduce the usefulness of the model as a check on the degree to which the observed cooling matched a predicted maximum cooling rate. However, we were still able to use it to extract the total energy removed given the measured potential energy removed. We adjusted the distribution of the initial atoms, within the measured uncertainty, until the predicted potential energy reduction obtained from the model calculation matched the experimental value. The model then allowed the determination of the total energy reduction (which is greater than just the measured potential energy reduction). Our model indicated that the total energy reduction was about twice that of the measured potential energy reduction. There were two primary reasons for this. First, as mentioned the anharmonic potential means that the conversion of reduced kinetic energy to reduced potential energy does not occur at the same time for all atoms. Secondly, the model indicated that we were not using optimal delay times to observe the greatest amount of potential energy reduction. We relied too much on approximating the potential as a harmonic one in setting the experimental delays. Rather than retake this data with different timings in the hope of slightly improving our results, we decided to wait until the other major experimental modification were completed.

Using this analysis technique, the measured potential energy reduction was found to correspond to a total *one-dimensional* total cooling rate of $236\mu K/s\pm21$(statistical)±32(systematic). Naturally, we would expect the overall (i.e. three-dimensional cooling rate) to be $\frac{1}{3}$ of this value. Our modeling
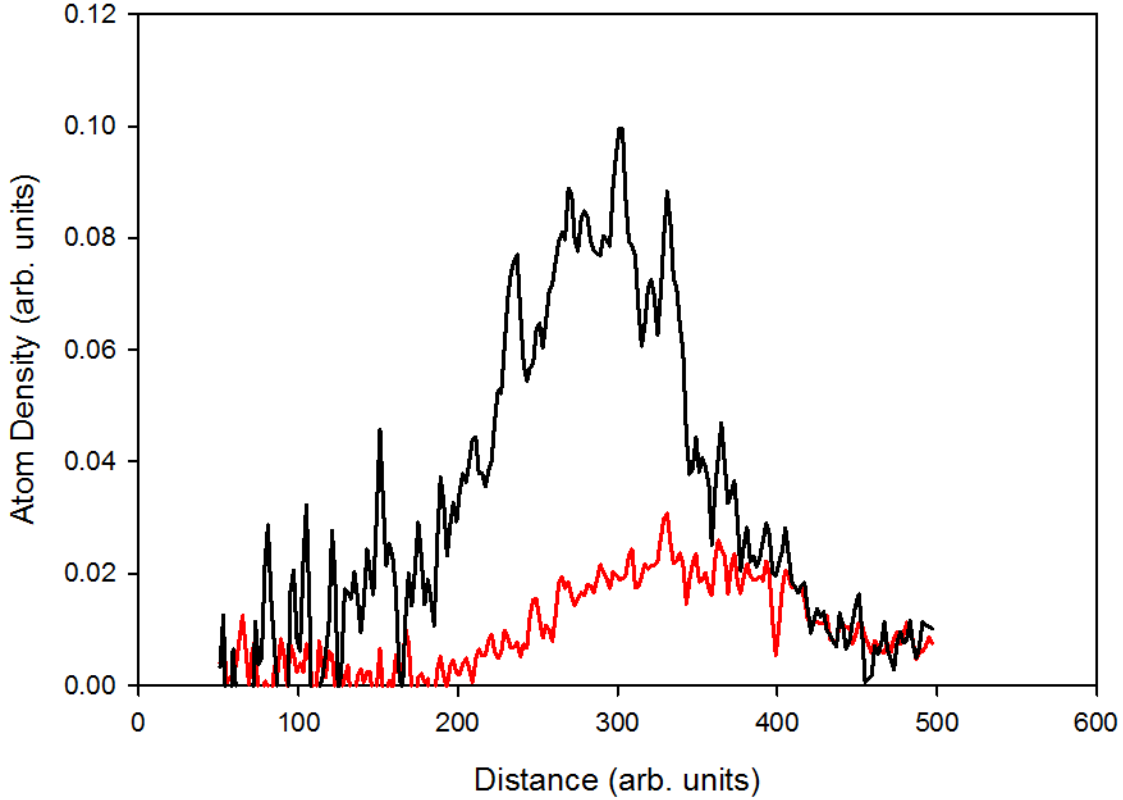
Figure 4.2: The red trace shows clearly that the up pumped atoms have a Gaussian distribution, not sharp cutoff as hoped. The black trace shows the standard atom distribution of our FORT. For reference, the razor blade was located at about 350 on the x-axis.

also indicated that this cooling rate could be improved by 37% by improving the sharpness of the up-pumped atom boundary, which is part of the planned upgrades to the apparatus.

4.3.1   Atom Loss per Cooling Cycle

Ideally, we would not have observed any loss of atoms as part of the cooling cycle because the cooling does not intrinsically require any loss. However, we did observe a density-dependent loss of atoms that was consistent with light-assisted collisional losses. The loss rate varied as a function of laser detuning, with for instance 6(3)% loss per cycle when the stopping beam was detuned to be 30 MHz to the blue of the cycling transition. At a 10 MHz detuning from the blue, 1(1)% loss per cycle was seen. This variation with detuning is consistent with expectations about the scaling of the light-assisted collisional losses in an optical trap [1]. For sufficiently small detuning, the
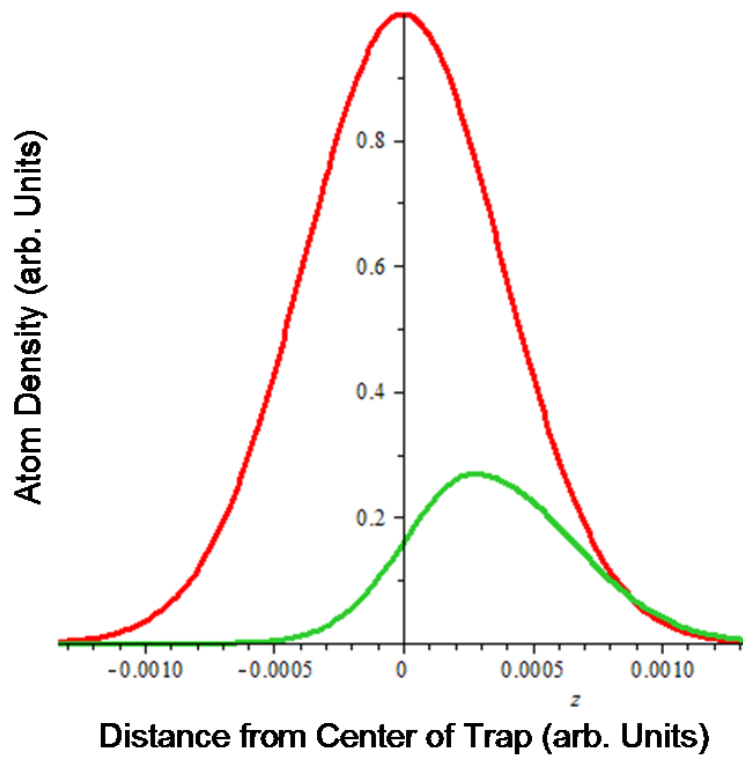
Figure 4.3: A fit to the data of Figure 4.2 is shown. This up pump distribution is shown in green and the full atom distribution is shown in red.

resonant excitation of atom pairs to the excited state molecular potential occurs at such a large atom separation that the molecular potential is relatively shallow, leading to small accelerations and thus reduced losses.

Future measurements are expected to improve the determination of the loss rate per cycle through the ability to apply many STOP cooling cycles sequentially in a way that each effectively cools the gas. Just blindly applying multiple pulses does not really test the true loss rate, as later cooling cycles will not likely be effective without proper evaluation of the amount of thermal equilibration in the gas. In the presence of the relatively large evaporation rate, such a cooling cycle extension would have been difficult and likely would not have yielded very useful information. While it would have been good to try to resolve the loss rate with respect to its possibly being zero, it is difficult to collect number data efficiently with our apparatus. There are 20-30% shot-to-shot variations in the measured number, and so the 1% loss determination already represents a significant data collection effort. The loss rate will become clearer in the next set of experiments with this cooling technique.

4.4 Future Modifications

This chapter and the previous two have discussed the techniques and results of a single cycle of STOP cooling. Ideally we would have liked to have been able to push this technique much further than just a single cycle measurement. Unfortunately, we were unable to do that without several major modifications to the experimental apparatus. I will discuss the planned modifications in this section, beginning with the plans for an adjustment to the up-pump beam and then a discussion of the plan to reduce the evaporation in the optical trap

4.4.1 Up-Pump Beam

Ideally, the sharp cutoff on one edge of the beam would have resulted in an equally sharp cutoff in the up-pumped atom distribution. However, the beam that was used as the up-pump beam was directed into the chamber through the back of one of the MOT mirrors. This mirror had a transmission of about 2%. This meant the intensity of the beam was on the order of μWs. Due to this intensity limitation, it was necessary to operate the laser close to resonance and that led to

a blurring of the atom selection through optical thickness and rescattering. Instead of the hoped for sharp cutoff, the atom distribution was instead Gaussian in shape with a width of 0.64 mm centered at a location controlled through the position of the razor blade, as seen in Figure 4.2. The original up-pumping tests were done earlier in the FORT sequence with lower density atoms. In that case, the cutoff was reasonably sharp and so we were initially satisfied with the system. But, once we learned that anharmonicities in that configuration were a more serious an issue than initially expected, we switched to parameters that resulted in optically thicker clouds and that is where we observed this problem.

We were fairly confident that the need to run the up-pump laser on resonance due to the intensity limitation was a large part of the reason that our initial up-pump distribution was not very sharp. But, we wanted to confirm that this assumption was reasonable with an auxiliary experiment. The goal of this auxiliary experiment was to confirm that when a high intensity beam is directed at atoms in the FORT, reabsorption effects can be observed if the beam is on resonance. This was demonstrated by confirming that the scattering rate did not scale as it should have if reabsorption was not present. From this result we would be able to confirm that the on resonance nature of the up-pump beam was most likely the cause of the blurred nature of the initial atom distribution.

For this auxiliary experiment, we used a much more intense beam than the up-pump beam. This beam was tuned to the $5S_{1/2}$ F=1 to $5P_{3/2}$ F'=2 transition and was directed into the chamber through the main MOT beam path. Unlike in STOP cooling, this test beam was much larger than the atom spatial extent and so interacted with all of the atoms in the gas. This path did not reduce the intensity like the path for the up-pump beam did. This beam was then pulsed, using an AOM, and the fraction of atoms that were pumped into the upper hyperfine state was measured as a function of time. This fraction was measured for the beam on resonance and for the beam detuned to the blue and the red by 11 MHz. The results of this measurement are shown in Figure 4.4.

In the absence of rescattering and reabsorption problems, the expectation is that the time it takes for a beam to up pump a number of atoms should scale directly with the predicted scattering rate. This scattering rate was given in Equation 1.1. Using this rate one can predict how much the scattering rate should change as a function of the detuning. For a detuning of 11 MHz, the time it takes for 30% of the atoms to be up-pumped is expected to increase by a factor of 8 over the
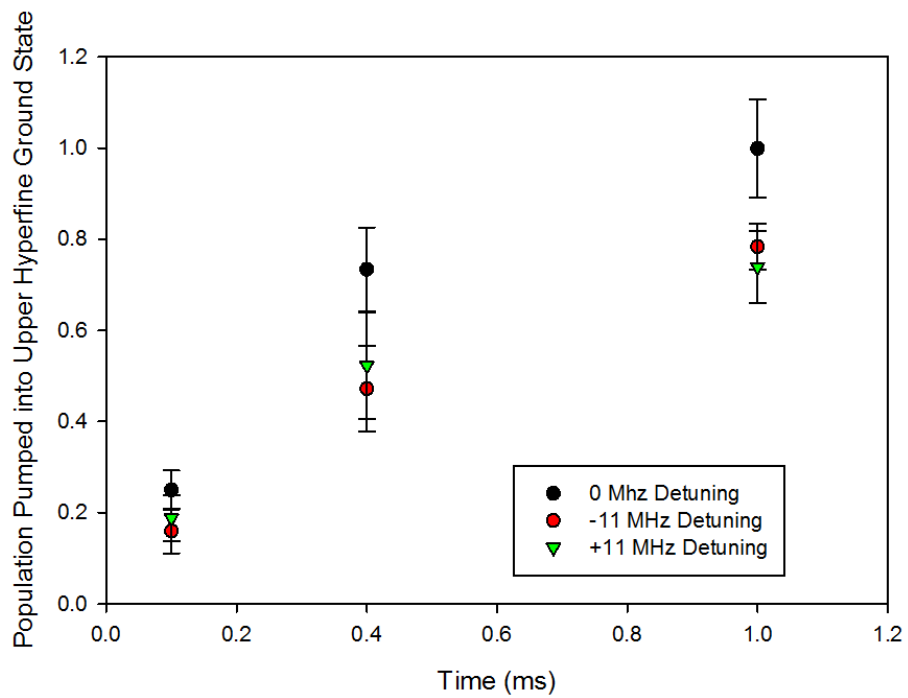
Figure 4.4: The black circles show the up pump time for an on resonance beam. As you can see from the green triangles and red circles, detuning by 11 MHz did not decrease the up-pump time as much as predicted, indicating reabsorption is playing a role this close to resonance.

on resonance time. As you can see in Figure 4.4, this time only increased by about a factor of 2. This indicates that the reabsorption and rescattering are indeed present when working so close to resonance.

The above analysis ignores the effects of saturation. In this case, we are simply looking to see if reabsorption has a significant effect, since the effect of saturation is not enough to change our conclusions. However, it is still useful to do additional analysis to confirm that our conclusions are correct even with saturation effects included. When I refer to 'saturation effects' I simply mean that even for a very slow pumping speed, the atoms will all eventually be pumped up into the upper hyperfine state. This means that it becomes very important at which point in the up-pump curves you decide to compare the data. We can avoid the issue of what point on the curves it is safe to compare by writing a simple differential equation that describes the up pump time.

$$\frac{d(f(t))}{dt} = R * (1 - f(t));$$
(4.1)

This has a trivial rising exponential solution, assuming $f(0) = 0$

$$f(t) = 1 - \exp(-Rt)$$
(4.2)

It is then possible to compare two predicted up-pump curves that differ in detuning by a factor of 11 to correspond to the experimental condition. We can graph these two equations ($f_1 = 1 - \exp(-t)$, $f_2 = 1 - \exp(-t/11)$) to see what the expected up pump data should have looked like in the absence of reabsorption. This is shown in Figure 4.5 (note that t is arbitrary here). As you can see, this looks nothing like that observed data shown in Figure 4.4. This result confirms our previous conclusion that reabsorption is indeed present in our system at these intensities and detunings.

The results of this experiment demonstrated that we were very likely limited by reabsorption effects. This confirmed that the problems we encountered by working on resonance will most likely be solved by simply increasing the intensity and detuning slightly. This is a fairly straightforward but time-consuming modification to make in our system, but it was important to confirm that the reabsorption effects were occurring as expected.
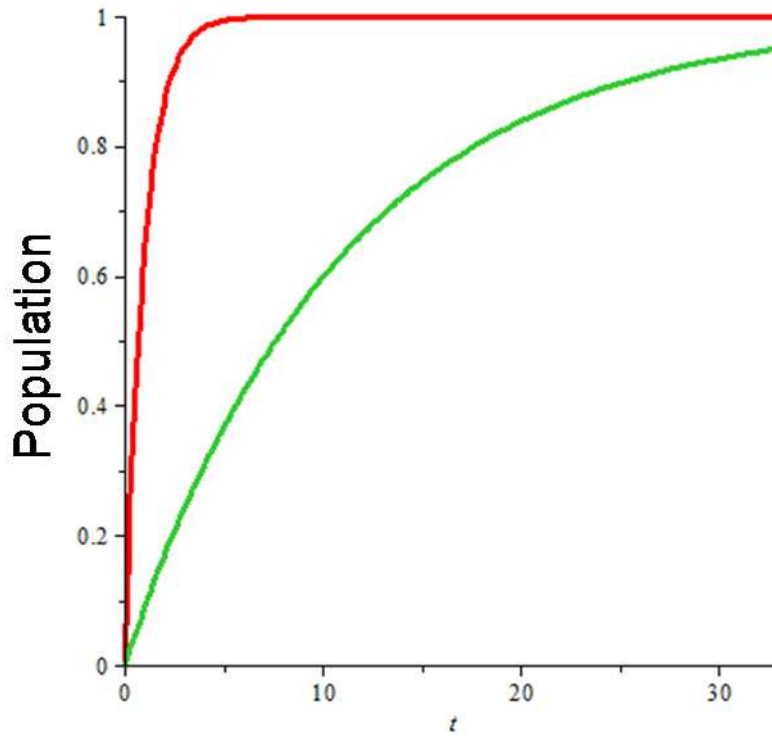
Figure 4.5: This graph shows the expected shape of an up-pump curve for the case of on resonance light (red) and off resonance light (green). The off resonance light has a decrease in up-pump rate of 11 to match the expected results for the auxiliary experiment.

4.4.2 Razor Blade on a Controllable Translation Stage

An additional modification that will need to be made if the cooling is to be extended to multiple cycles is to adjust the section of the atom cloud that is illuminated by the up-pump beam. The current configuration does not allow for the adjustment of the up-pump beam location during the cooling process. This did not cause a problem for the experiments I performed since I only looked at the cooling from one STOP cooling pulse. If, however, multiple STOP cooling pulses were applied, the axial extent of the atoms would be quickly reduced, and the highest energy atoms would no longer be illuminated by the up-pump beam. A simple solution to this problem is to have the razor blade that is used to control the portion of the cloud that is illuminated be adjustable during the time of the experiment. One simple way to do this is to place the razor blade on a motorized translation stage that is controled by the LabView code. This simple modification will allow the axial cutoff location to be moved closer and closer to the center of the atom cloud as the atoms cool and the axial extent shrinks.

4.4.3 Optical Trap Modifications

As mentioned in Chapter 3, the evaporation rate in our FORT prevented us from making any multiple cooling pulse measurements. The next step for this experiment is to modify the FORT to reduce this evaporation rate significantly. There are several things that can be done to reduce the evaporation rate in the FORT.

Increase the FORT Focus Spatial Extent

One of the major things that can be done is to increase the spot size of the CO_2 beam at the focus of the FORT. A larger spot size will decrease the trap depth, but it should increase the trap depth to atom temperature ratio. This should reduce the FORT evaporation rate. The spot size increase will be done by resizing the beam through the optical trap optics. We have experience operating with smaller trap depths in the past, and so do not anticipate problems in doing so in the future.

Realigning the beam

An additional adjustment that will improve the FORT evaporation rate is to realign the FORT beam. The current method for aligning the CO_2 trap with the atoms results in the largest possible atom number loaded into the trap, but it does not result in the lowest possible temperature for those loaded atoms. Instead the initial atom load number tends to be maximized when the CO_2 trap is aligned off center with the MOT resulting in higher than average energy atoms being loaded into the FORT. Additionally, increasing the focal spot size will reduce the size of the CO_2 beam on the focusing lens, reducing the amount of spherical aberration. Substantial spherical aberration was observed in our recent implementations of the FORT. These aberrations lead to a distortion of the optical trap that tends to allow more atoms to be loaded into the edges of the CO_2 trap than would be ideal. This excess atom number on the edges of the distribution leads to an initial increase of the trap evaporation rate as the atoms attempt to come into equilibrium.

Cooling in Three Dimensions

So far, STOP cooling has been discussed in terms of one-dimensional cooling. In the end, however, it is three-dimensional cooling that will be relevant for most applications of this technique. In future implementations of the cooling technique, elastic collisions will be used to thermalize the different directions in the optical trap. A standard set for cooling cycles will then consist of (for 25% of the atoms selected for up-pumping) four cycles of STOP cooling spaced to affect all of the atoms in the gas, followed by 150 ms of delay time to allow some thermalization, and then repeating the four pulse cycle. Eleven such cycles should reduce the temperature of gas by an order of magnitude in under three seconds, assuming initial cloud temperatures of 40 μK.

4.5 Molecules

In this thesis, I describes the results primarily in terms of atoms, but the potentially more interesting application is to extend this technique to molecular cooling. There has been a great deal of recent interest in cold and ultracold molecules due to the predicted usefulness of molecules in investigating many-body physics studies in the presence of long-range interactions[2, 3], fundamental physics studies such as parity violation and electron dipole measurement searches[4–7], and

potential applications in quantum information and quantum simulation[8–10]. Many of these lines of investigation benefit from either cold temperatures and/or high phase-space density, and so a widely applicable cooling technique would be useful in these studies. An outline of how STOP cooling would be applied to a gas of ultracold molecules is detailed below. A more detailed analysis of the application of STOP cooling to an actual molecular system including a specific optical pumping scheme and particular transitions is under way, but beyond the scope of this thesis.

Optical pumping of molecules has been demonstrated with femtosecond laser pulses, both for vibrational and rotational degrees of freedom. Using a technique outlined in references [11–13] it should be possible to create a dark state or set of dark states (as defined by the target state of the optical pumping) for a particular molecule. For instance, consider the molecule NH discussed in reference [14]. One can define the lowest or lowest few vibrational energy states as discussed in reference [14] as the dark state(s). The molecules can then all be pumped into that state or states using the techniques in reference [14]. Pumping the atoms into higher vibrational states would then be the means to select them. Once a dark state has been identified, this cooling technique can be applied as described for ^{87}Rb. High-energy molecules can be selectively excited out of the dark state or states as part of the cooling process, and then pumped back into them at the end of the cooling process just as would be done for an atom.

4.6 Conclusion

In this thesis I have discussed the wide applicability of STOP cooling to both atoms and molecules. I have also discussed in detail the model we created to extract cooling rates and have seen that the spatial distribution of up-pumped atoms has a moderate effect on the achievable cooling rates. I have also been able to demonstrate successful one-cycle cooling of ^{87}Rb. Finally, the planned modifications for this experiment have been discussed. In the remaining chapters I will discuss the details of the 2-CAZ cooling experiment.

References for Chapter 4

[1] A. R. Gorges, N. S. Bingham, M. K. DeAngelo, M. S. Hamilton, and J. L. Roberts, Phys. Rev. A **78**, 033420 (2008)

[2] M. Cavagnero and C. Newell, New J. Phys. **11**, 055040 (2009)

[3] J. L. Bohn, M. Cavagnero, C. Ticknor, **11**, New J. Phys. 055039 (2009)

[4] D. DeMille, F. Bay, S. Bickman, D. Kawall, D. Krause, S. E. Maxwell, and L. R. Hunter, Phys. Rev. A **61**, 052507 (2000)

[5] E. R. Meyer and J. L. Bohn, Phys. Rev. A **78**, 010502 (2008)

[6] D. Cho, K. Sangster, and E. A. Hinds, Phys. Rev. A **44**, 2783 (1991)

[7] M.G. Kozlov, L.N. Labzovskii, and A.O. Mitrushchenkov, Sov. Phys. JETP **73**, 415, (1991)

[8] A. Pe'er, E. A. Shapiro, M. C. Stowe, M. Shapiro, and J. Ye, Phys. Rev. Lett. **98**, 113004 (2007)

[9] E. A. Shapiro, A. Peer, J. Ye, and M. Shapiro, Phys. Rev. Lett. **101**, 023601 (2008)

[10] M. Ortner, A. Micheli, G. Pupillo, and P. Zoller, New J. Phys. **11**, 055045 (2009)

[11] C. Lien, S. Williams and B. Odom. Phy. Chem. Chem. Phys. **13**, 18825-18829 (2011)

[12] D. Sofikitis, S. Weber, A. Fioretti, R. Horchani, M. Allegrini, B. Chatel, D. Comparat, and P. Pillet, New J. Phys. **11**, 055037 (2009)

[13] I. Manai, R. Horchani, H. Lignier, P. Pillet, D. Comparat, A. Fioretti, and M. Allegrini, Phys. Rev. Lett. **109**, 183001 (2012)

[14] J. Riedel, S. Hoekstra, W. Jager, J.J. Gilijamse, S.Y.T. van de Meerakker, and G. Meijer, Eur. Phys. J. D **65**, 161-166 (2011)

Chapter 5

Collision Assisted Zeeman Cooling Theory

The second major experiment that I am going to address in this thesis is Two Isotope Collision-Assisted Zeeman (2-CAZ) Cooling. The general concept of 2-CAZ cooling was discussed in Chapter 1. In this chapter, I will begin by discussing the one-isotope CAZ cooling technique that was proposed in 2000, including its advantages and disadvantages[1]. I will then discuss the modification made to this cooling scheme to use two isotopes of Rb rather than just one. I will discuss the details of the two isotope cooling scheme including advantages, disadvantages and the expected cooling rates. Just to be clear, the experiments conducted in this thesis were for 2-CAZ cooling, and the single type of atom cooling is included just as a description of the technique. Once a full description of the theory of CAZ and 2-CAZ cooling has been completed in this chapter, the next two chapters will discuss our experimental techniques and results. Throughout this thesis I will discuss 2-CAZ cooling in terms of two isotopes of Rb, but 2-CAZ cooling could just as easily be used with two different atoms.

5.1 Single Isotope Collision Assisted Zeeman (CAZ) Cooling

Collision-Assisted Zeeman (CAZ) Cooling was first proposed for a single atom in reference [1]. The idea is relatively simple. First, spin-exchange collisions are used to convert kinetic energy to magnetic energy in a trapped ultracold gas. Then, the atoms are optically pumped to reset the atoms spin and remove the Zeeman energy from the system. As was done in reference [1], CAZ cooling is described here by considering ^{87}Rb as an example system. ^{87}Rb has one valence electron with spin $S=1/2$ and a nuclear spin $I=3/2$. The cooling takes place with the atoms (ideally) always in the lower $F=1$ hyperfine state. I will begin by discussing the importance of a magnetic field to this cooling scheme and then discuss the details of the cooling process.

5.1.1 Magnetic Field

A critical aspect of CAZ cooling is the application of a magnetic field. The magnetic field must be large enough that the second order Zeeman shift, as defined in Chapter 1, is on the order of

the thermal energy in the trapped gas (i.e. $k_B T$). Figure 5.1 shows the relative energy differences between the states that arise through the first and second order Zeeman shifts for a general $F{=}1$ atom. As is shown in Figure 5.1, the shift between the $m_F{=}0$ and $m_F{=}$-1 states is not the same as the shift between the $m_F{=}0$ and $m_F{=}{+}1$ states. This difference is crucial to the success of CAZ cooling.

5.1.2   CAZ Cooling Process

To describe the cooling via example I first consider two atoms optically pumped into the $m_F{=}0$ state with a magnetic field present, as shown in Figure 5.1. If the atoms undergo a spin-exchange collision (described in Chapter 1) one atom will move to the $m_F{=}{+}1$ state and the other to the $m_F{=}$-1 state. Because of the contribution from the second order Zeeman shifts the $m_{F1}{=}0{+}m_{F2}{=}0$ state has lower magnetic energy than the $m_{F1}{=}$-1 $+ m_{F2}{=}1$ state. This increase in Zeeman energy comes at the expense of the pair's average kinetic energy, meaning the atoms are slowed. The final step in the cooling process is to optically pump the two atoms back into the $m_F{=}0$ state. This final step creates a closed cycle that results in the net removal of energy from the gas, resulting in a cooling of the gas.

5.1.3   Advantages of CAZ Cooling

There are several potential advantages of this technique over other non-evaporative laser cooling methods [2–7]. First of all, it makes use of spin-exchange collisions that occur spontaneously in many systems, making this technique less experimentally complex than many other systems [8]. It also only relies on one main adjustable parameter, namely the externally applied magnetic field, again reducing the complexity of the experimental realization of this cooling. Also the cooling is intrinsically three-dimensional, which is always advantageous for effective cooling. Finally, more energy is removed in a cooling cycle per photon scattered than all-laser based cooling techniques like Raman cooling [2]. Most non-evaporative cooling schemes, like Raman cooling, are limited by photon reabsorption in optically thick gases [9], and so by increasing the energy each photon carries away the limitation from photon reabsorption is lessened for the CAZ technique. All of these things make CAZ cooling an intriguing cooling technique.
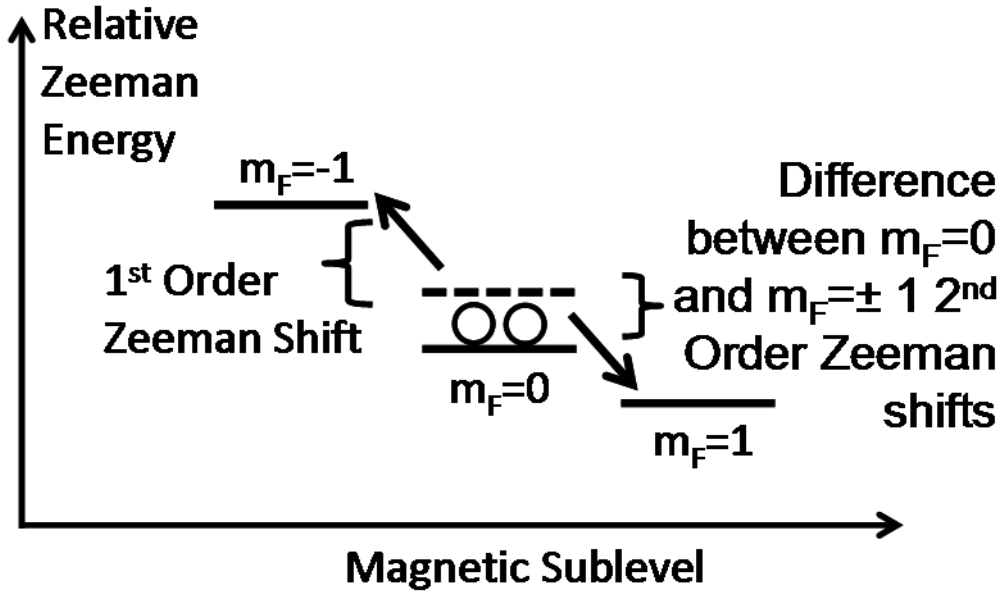
Figure 5.1: The relevant states for single atom CAZ cooling as described in reference [1] are shown. The solid lines depict Zeeman shifted m_F states while the dotted line indicates the average energy of the $m_F = +1$ and -1 states. The circles are meant to represent the states of two atoms at the start of the cooling cycle and the arrows indicate the change in state due to spin-exchange collisions.

5.1.4 Disadvantages of CAZ Cooling

There are, of course, some challenges associated with this cooling technique. One experimental challenge is the inconveniently large ($\sim$100 G) magnetic field that is required for cooling typical systems such as alkali atoms. Creating the large magnetic field is fairly straightforward, in fact, 100 G fields are routinely produced in ultracold atom experiments, but they require water cooling the magnetic coils and large current sources and so are experimentally inconvenient. The real challenge with these large magnetic fields is that they greatly complicate the optical pumping required as part of the cooling cycle. Due to the splitting between the m_F quantum states at such magnetic fields, either a large number of different laser frequencies are required for optical pumping due to variable Zeeman shifts in the required optical pumping transitions, or relatively intense laser light needs to be used, making it difficult to drive desired transitions without driving undesired ones. This problem could in principle be avoided by ramping the magnetic field down during the application of optical pumping light in order to perform the optical pumping at a lower field. While in principle rapid ramps could allow for such a cycling on a sub-ms time-scale, in practice eddy currents in the

vacuum system will limit the magnetic field ramp times to about 1 ms both for ramping down and ramping back. For sufficiently high densities and spin-exchange collision rates, heating can occur during this time such that this can be a significant factor in the ultimate cooling rate that can be achieved.

For the required magnetic field size, there are problems besides those associated with optical pumping. One of those problems is dipole relaxation collisions [10]. These are collisions that result from the presence of magnetic dipoles in the atom. The m_F quantum number of one or both of the atoms in the colliding pair changes in these collisions, with the resulting change in spin angular momentum being compensated for by a change in orbital angular momentum between the incoming and outgoing pair. These collisions occur at a higher rate and release more energy in a high magnetic field [10].

A last potential limitation of CAZ considered here is reabsorption [9]. As mentioned in Chapter 1, a large number of all optical cooling methods are limited by reabsorption so it is not surprising that this one could be as well. Any light-based cooling technique relies on entropy being carried away by photons in some way, and so any process that inhibits photons escaping from the gas will reduce the achievable cooling rate. All of the disadvantages that I have listed in this section can be addressed to some extent in a system with two different types of atoms rather than just one. This type of system will be discussed in the next section.

5.2   Two Isotope Collision Assisted Zeeman (2-CAZ) Cooling

Now that a detailed discussion of single atom CAZ cooling has been completed, I will discuss the details of CAZ cooling using two isotopes (2-CAZ). I will start by explaining the 2-CAZ cooling process and then I will discuss some of the advantages of 2-CAZ cooling as compared to single atom CAZ cooling.

5.2.1   2-CAZ Cooling Process

Extending CAZ cooling to two different types of atoms or two isotopes of the same atom is reasonably straightforward. The general cooling method is the same, except that now the spin-exchange collisions occur between the two different types of atoms or isotopes. Optical pumping is still used

in 2-CAZ to close the cooling cycle, but only one of the two types of atoms (or isotopes) needs to be optically pumped irreversibly. The other atoms' spin state just needs to be periodically reoriented.

A diagram of generic 2-CAZ cooling is shown in Figure 5.2. Again a magnetic field is required, but this time the field only needs to be large enough to create a 1st order Zeeman shift, as long as the two atoms have different g_F factors. The figure depicts only the magnetic sublevels of the two atoms that are relevant to the cooling. As shown in the figure, a spin-exchange collision changes the atoms' magnetic sublevels and since the energy splitting is different for each atom, the net change in energy from a spin-exchange collision can increase the Zeeman energy of the system, again at the expense of the system's kinetic energy. Finally, one of the atoms is optically pumped back into its original state, removing energy from the system and completing the cycle.

For the sake of illustration, I consider 2-CAZ with ^{85}Rb (nuclear spin I=5/2) and ^{87}Rb (I=3/2) in their lower hyperfine states (F=2 and 1, respectively). Further, I consider the main spin-exchange collision channel to be represented by a collision between an ^{85}Rb atoms in the F=2, m_F=-2 state and an ^{87}Rb atom in the F=1, m_F=0 state. As a result of such a collision, the ^{85}Rb and ^{87}Rb atoms would be scattered from their initial states into m_F=-1 states. Because for ^{85}Rb E$_{Zeeman}$=-1/3μ_BB m_F and for ^{87}Rb E$_{Zeeman}$=-1/2μ_BBm_F (i.e. their g_F [11] factors are different), the total Zeeman energy increases by μ_BB/6 as a result of this collision. As defined earlier, μ_B is the Bohr magneton and B is the magnitude of the applied magnetic field. To close the cooling cycle, the ^{85}Rb atoms are optically pumped back to the m_F=-2 state. For ^{87}Rb, RF fields are used to drive transitions between ^{87}Rb m_F states to "scramble" their populations periodically to make sure that there are always ^{87}Rb atoms available for kinetic-energy-reducing collisions with the spin-polarized ^{85}Rb atoms.

5.2.2   2-CAZ Advantages as compared to 1-CAZ

There are several additional potential advantages of 2-CAZ cooling in addition to all of the previously listed advantages it shares with CAZ cooling. Once again the main adjustable parameter in the experiment is still the magnetic field. As mentioned earlier this reduces the experimental complexity since magnetic fields are generally straightforward to produce and adjust. In the case of 2-CAZ cooling, the magnetic field does not need to be nearly as large as in CAZ cooling since 1st-order rather than 2nd-order Zeeman shifts are relevant. For effective cooling, the magnetic field
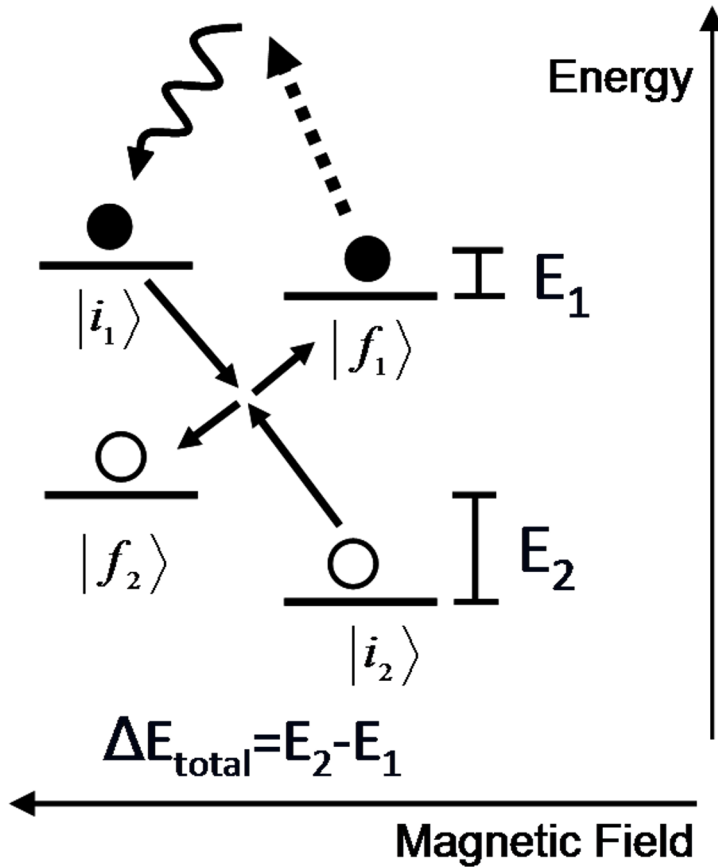
Figure 5.2: 2-CAZ cooling is shown in this figure. Only the magnetic sub-levels between the two atoms that are relevant to a cooling cycle are shown. A magnetic field separates the otherwise degenerate energy levels. Atom 1 (Black circles) has a smaller Zeeman energy difference between initial ($|i>$) and final ($|f>$) states than atom 2 (white circles). An inelastic collision between atoms (solid arrows) changes atom spin states, requiring ΔE collision of kinetic energy. An optical pump (dashed arrow) returns atom 1 to the initial state, with the spontaneous photon removing energy and entropy. It is assumed in the case being depicted that the g_F factors associated with each atom are different.

magnitude should produce Zeeman shift energy differences between the entrance and exit states of a spin-exchange collision on the order of $k_B T$. For a 50 μK cloud of an $^{85/87}$Rb mixture, this is about 2 G, as compared to the $\sim$100 G field required for CAZ cooling in a pure ^{85}Rb or ^{87}Rb gas. The ability to work at a lower field is a significant advantage for 2-CAZ as compared to single-atom CAZ cooling due to the reduction in experimental complexity and because lower magnetic fields imply much lower dipole relaxation rates and so less loss and heating from those types of collisions.

The other main advantage of 2-CAZ cooling is the potential for reabsorption mitigation. Since there are two different atoms involved in the cooling process it is possible to reduce the optical thickness of just one of the atoms. This would mitigate reabsorption if it was done on the atom that is optically pumped. This atom could be made optically thin without changing the density of the other atom. This density decrease does reduce the net cooling rate by reducing the spin-exchange rate, but calculations have shown that the reduction in spin-exchange rate due to lower density of one of the two atoms is more than compensated by the reduction of reabsorption[11]. This preserves the ability of this technique to cool an atom to very low temperature and density while still avoiding reabsorption problems. More detail can be found in [11].

5.2.3   2-CAZ Disadvantages as compared to 1-CAZ

One of the major disadvantages of this technique over single atom CAZ cooling is the increase in experimental complexity. Adding a second atom to the experiment requires the addition of at least two more lasers, one for trapping and one for repumping the new atom. In our system this meant the addition of two more diode lasers, but for some elements the required lasers are more complicated to acquire and implement experimentally. Even in our system, the addition of two diode lasers increased the maintenance required on our system and the addition of the second type of atom doubled the amount of data that needed to be collected. But we considered the increase in experimental complexity to be worth the effort given the predicted potential for cooling and reabsorption mitigation inherent in the 2-CAZ cooling technique.

5.2.4   Predicted Cooling

It is helpful to have a sense of what kind of cooling we can expect from the 2-CAZ technique. To do this we need to examine the predicted cooling rate. A previous graduate student [11] spent a
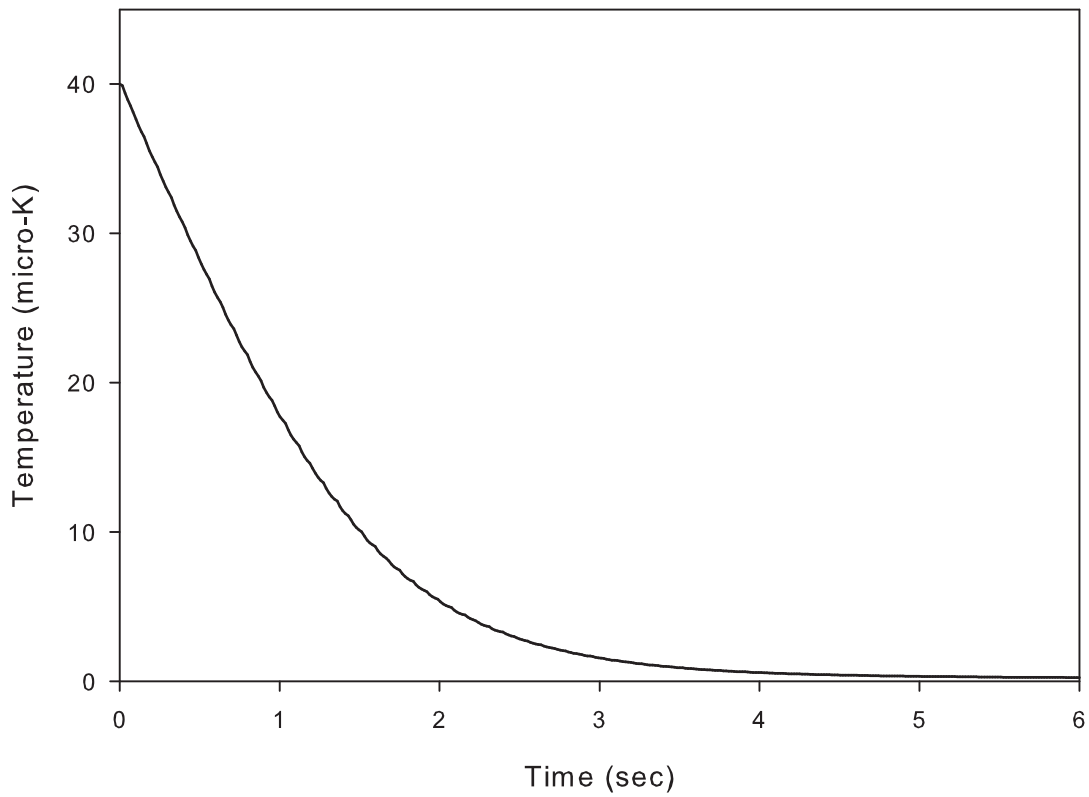
Figure 5.3: The predicted cooling is shown for the ideal case. The cloud is assumed to start at 40μK. After 1 second the cloud temperature has reduced by more than half.

considerable amount of time detailing the cooling rate model associated with 2-CAZ cooling, so I will only briefly review some of the details.

The 2-CAZ cooling rate can be described by [11]

$$\frac{dT}{dt} = -\frac{1}{\tau_{SE}} \frac{exp(-\Delta/k_B T)N_2}{3k_B(N_1 + N_2)}(\Delta - \kappa)\frac{1}{1 + \frac{\tau_{OP}}{\tau_{SE}}(1 + \exp(-\Delta/k_B T))} \tag{5.1}$$

where N_1 and N_2 are the total number of atoms for each atom, τ_{SE} is the spin-exchange time constant defined as $1/\tau_{SE}=k_s n_1$ where a spin-exchange rate of $k_s=2.4\cdot10^{-11}$ cm^3/sec was used and n_1 is the non-optically pumped atom density, τ_{OP} is the optical pumping time constant, Δ is the change in Zeeman energy in a spin-exchange collision where $|\Delta m_F| = 1$ and κ is the average energy imparted per successful optical pumping driven population transfer. Ideally, κ would be zero, but inevitably some energy is imparted during the optical pumping process since random photon scatters occur, leading to random momentum kicks due to photon recoils.

To generate a rough estimate for the expected cooling rate given our experimental parameters, a few simplifying assumptions can be made. The first is that the optical pumping is infinitely fast so $\tau_{OP}=0$. Additionally we can set Δ to its optimum value of $\Delta = k_B T + \kappa$. If we do both of these things we find the optimum cooling rate is

$$\frac{dT_{opt}}{dt} = -\frac{1}{\tau_{SE}} \frac{\exp(-1 - \kappa/k_B T)N_2}{3(N_1 + N_2)}T \tag{5.2}$$

where everything is defined the same as above. The results of this equation are plotted in figure 5.3 showing the predicted temperature as a function of time. We see that in just one second the cloud temperature has reduced by more than half. This compares favorably to evaporative cooling for the same experimental parameters, without intrinsically requiring any loss from the gas. A value of 1 μK was used for κ. This comes from the limit set by the fact that about 4 photons are needed to close the cooling cycle so rounding up from 4(0.18 μK(the heat imparted per photon $(\hbar k)^2/(2m)$)) gives us 1 μK.

5.3 Conclusion

In this chapter, I have discussed in detail the techniques of both CAZ and 2-CAZ cooling. I have also discussed the potential advantaged and disadvantages of both techniques. In the following two chapters, I will build upon the theory discussions in this chapter to explain how the 2-CAZ cooling scheme was actually used. In the next chapter I will discuss the details of the 2-CAZ cooling experiment and in Chapter 7 I will discuss the results of that experiment.

References for Chapter 5

[1] G. Ferrari, Eur. Phys. J. D 13, 67-70 (2001).

[2] H. Lee, C. Adams, M. Kasevich, and S. Chu, Phys. Rev. Lett. 76, 2658 (1996).

[3] V. Vuletic et al., Phys. Rev. Lett. 81, 5768-5771 (1998).

[4] A. Aspect et al., Phys. Rev. Lett. 61, 826-829 (1998).

[5] H. Perrin et al., Euro. Phys. Lett. 46, 141-147 (1999).

[6] D. Boiron et al., Phys Rev. A 52, R3425 (1995).

[7] M. Kasevich, S. Chu, Phys. Rev. Lett. 69, 1741 (1992).

[8] W. Happer, Rev. Mod. Phys. 44, 169-250 (1972).

[9] Y. Castin, J. Cirac, and M. Lewenstein, Phys. Rev. Lett. 80, 5305 (1999).

[10] James Patrick Burke, Jr., Ph. D. Thesis, University of Colorado (1999).

[11] Mathew Hamilton, Ph. D. Thesis, Colorado State University (2013).

Chapter 6

Collision Assisted Zeeman Cooling Experiment

I began this experiment with two main goals. First, I wanted to directly measure a 2-CAZ cooling rate and confirm that it matched predicted values for our experimental parameters. I had planned to do this by comparing measurements of the temperature of ultracold optically trapped ^{85}Rb and ^{87}Rb atoms with and without the 2-CAZ cooling technique applied. Second, I planned to investigate the performance and limitations to the 2-CAZ technique at lower temperatures, ideally at the few μK levels. Unfortunately, there were several unexpected challenges, which I will discuss in more detail shortly, that forced these goals to be modified. The first adjustment that was made involved changing the way the 2-CAZ cooling rate was measured. Due to unexpected initial loading inefficiencies and an unfavorably large evaporation rate I was unable to quantitatively measure 2-CAZ cooling through direct comparison of the atom temperature with and without 2-CAZ cooling applied for experimental conditions where the fastest cooling rates were expected. I instead had to measure all of the components that would contribute to a net cooling rate individually to extract the net cooling rate. The same factors that led me to modify the plans for measuring the cooling rate also meant that I was not able to push to sub-10 μK temperatures to investigate low temperature performance of 2-CAZ. However, I was able to use the information obtained through measuring the components of the net cooling rate to extract information about the lowest possible temperatures that could be expected to be achieved in this system even with more ideal loading behavior and in the absence of evaporation. In this chapter, I will begin by discussing several challenges that were encountered during this experiment. I will then proceed to discuss the experimental apparatus, especially the 2-CAZ specific techniques that were not mentioned in the previous experiment chapter (Chapter 3).

6.1 Challenges Encountered with the FORT

Before discussing the experimental measurements that I conducted, I want to explain in more detail some of the challenges encountered when attempting to directly measure the 2-CAZ cooling rate. Clearly, the most straightforward way to measure the cooling rate would have been to eliminate

any other significant heating and/or cooling of the trapped gas, apply 2-CAZ, and measure the resulting gas temperature as a function of time. This straightforward measurement was precluded, however, by unfavorable initial conditions resulting from the interference of the two Rb isotopes during FORT loading, as reported in Ref [1]. The initial density was not sufficient for a rapid 2-CAZ cooling rate as compared to the background gas-limited 5 second lifetime of the FORT. This will be discussed in more detail in the following section. Additionally, the gas temperature after initial loading was too large compared to the trap depth to avoid a substantial amount of evaporative cooling.

6.1.1 Simultaneous loading physics

One of the first experiments that was performed to prepare for the full 2-CAZ experiment was to load both ^{85}Rb and ^{87}Rb into the FORT at the same time. This was a crucial experiment since the 2-CAZ cooling experiment requires a trapped mixture of two Rb isotopes. During this initial experimentation, it was discovered that loading ^{85}Rb and ^{87}Rb simultaneously produced significantly fewer atoms in the trap than was originally predicted. This result was published in [1] and was detailed even further in [2, 3]. I will give a brief overview of the results especially as it pertains to the effect it had on the success of 2-CAZ cooling. All of these optical trap loading experiments were performed before I arrived in the lab.

The general expectation when loading two isotopes into the same trap is that if there is no interaction between the two you would simply get the sum of the individual load numbers. Unfortunately, this is not the case. Light-assisted collisional loss was predicted to reduce the overall load number by about 17% [3]. However when the dual loading experiment was performed the overall number of atoms was reduced by 36%[3]. This result indicated that there is some sort of loss mechanism that was not predicted by only considering the heteronuclear light-assisted collisional loss. The result of one of the loading experiments from Ref. [3] is shown in Figure 6.1. The open circles show the number of ^{87}Rb (top) and ^{85}Rb (bottom) loaded alone. The results for the simultaneous FORT load are indicated with the solid circles. Clearly, the number reduction is significant for the simultaneous loading case.

From similar measurements and others it was concluded that the decrease in load number was due to a decrease in the laser cooling efficiency that was needed for effective loading. There have
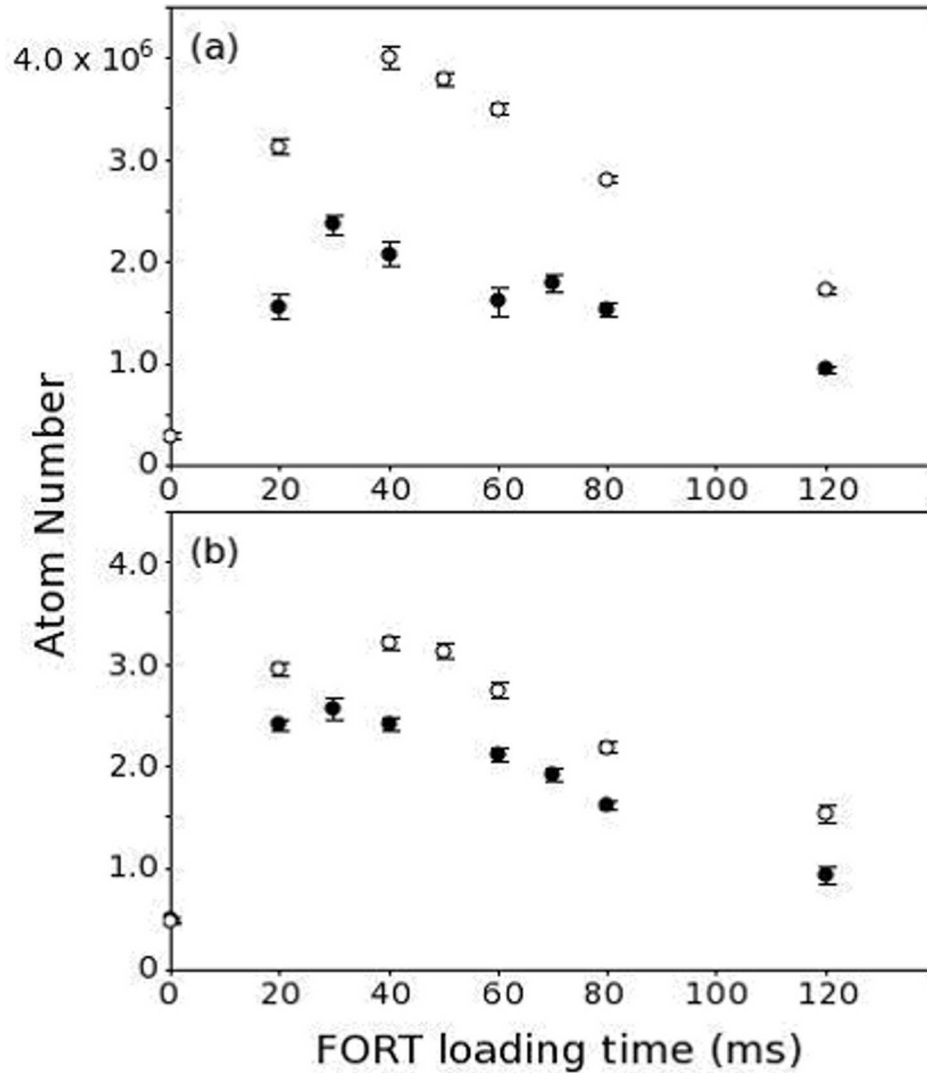
Figure 6.1: This figure shows simultaneous loading data. Graph (a) shows the results for ^{87}Rb and graph (b) shows the results for ^{85}Rb. The data collected with only one isotope present is indicated by the open circles and the dual isotope data is indicated by the solid circles. This figure was taken from [3]

been previous observations of dynamics that disrupt loading efficiency due to atom density, but this type of cross-isotope effect was not expected given that the detuning between the transitions for ^{87}Rb and ^{85}Rb are on the order of several hundred natural linewidths. Several other possible losses, including collisions between the two isotopes in the absence of laser light and light assisted collisional losses, were investigated as possible sourced of the load number reduction, but both were ruled out. The conclusion was that the presence of the laser light altered the collision rates and thereby affected the overall cooling efficiency of the trapping laser resulting in a reduced load number for both ^{87}Rb and ^{85}Rb.

The unfortunate results of this experiment indicated that it was going to be harder than anticipated to achieve the initial atom numbers that we had been hoping for for 2-CAZ cooling. Our initial hope had been to achieve several million of each isotope of Rb, but in the end we were not able to routinely load more than about one million of each isotope with our experimental conditions. It is important to note, however, that the predicted cooling rate scales with density, not atom number, and the density of the atoms in our trap was slightly greater than the less tightly-confining trap associated with the data shown in Figure 6.1. Thus, while the number reduction was disappointing and not expected in the absence of the inter-isotope interference in loading, in terms of the expected cooling rate it was not as severe. There were experimental changes, including the replacement of the FORT laser, between the data shown in Figure 6.1 and the experimental parameters used in the present measurement.

6.1.2 Evaporation Rate in the FORT

As mentioned, the gas temperature after initial loading was too large compared to the trap depth to avoid a substantial amount of evaporative cooling regardless of the initial loading conditions. It is important to note that the evaporation rate decreases exponentially with increases in the trap-depth-to-atom temperature ratio. The presence of this evaporative cooling masked the cooling due to 2-CAZ, just as it did in the STOP experiment, although to a somewhat lesser extent since the dimensionality of evaporation was not reduced during 2-CAZ cooling (Section 3.2.2). For the experimental parameters used, any 2-CAZ cooling largely just reduced the evaporative cooling rate and so the temperature evolution as a function of time changed only modestly. Figure 6.2 shows the results of a model calculation based on the experimental parameters corresponding to

the standard conditions for which these measurements were conducted. This model calculation was performed by numerically solving a set of first-order differential equations that tracked ^{87}Rb and ^{85}Rb m_F state populations as well as the total energy in the gas as a function of time. This calculation was very similar to the calculation done by Ref. [2]. Effects such as evaporative cooling, spin-exchange collisions, optical pumping, periodic ^{87}Rb m_F state scrambling, three-body recombination, and background gas trap loss were included in the model. As shown in Figure 6.2, the model confirmed the observed insensitivity of the temperature evolution to 2-CAZ cooling in the presence of evaporation. This competition between cooling rates observed in the model and in the experimental measurements required a different set of techniques to measure the 2-CAZ cooling rate with any amount of precision. In principle, reducing evaporation could also reduce the net loss rate, but this is certain only if new losses channels are not introduced and that is discussed below, too.

We attempted several things to try to reduce the influence of evaporation, but none of these attempts were successful. For instance, I tried loading atoms into a very shallow FORT and then ramping up the trap depth in an attempt to cut off the evaporation. The idea was that the temperature of the atoms loaded into the shallow trap would necessarily have to be relatively cold in order to be trapped, and so subsequently ramping up the trap (adiabatically with respect to the radial and axial trap frequencies) would increase the trap depth to atom temperature significantly. This loading sequence did reduce the amount of evaporation that was observed, but the reduction in initial number for both ^{85}Rb and ^{87}Rb in conjunction with the losses already caused by the cross isotope interference left too few atoms to perform the experiment. Other possible ways to mitigate the evaporation rate had a similar problem in that the atom number loaded was reduced as part of the mitigation technique. For instance, the optimal number of atoms was loaded in a configuration where the MOT was not centered on the center of the optical trap. While this improved the number in the trap by 30% or more, it meant that the energy of the atoms in the trap was higher than for loading right at the center of the trap, contributing to evaporation through a lower trap-depth to atom temperature ratio. I concluded that it was not feasible to easily modify the current experiment in a way that would get rid of the large evaporation rate without significantly reducing the number of atoms to a level where poor 2-CAZ cooling would be predicted (Note that conditions are different for the STOP cooling work, and improvements are expected there). This conclusion
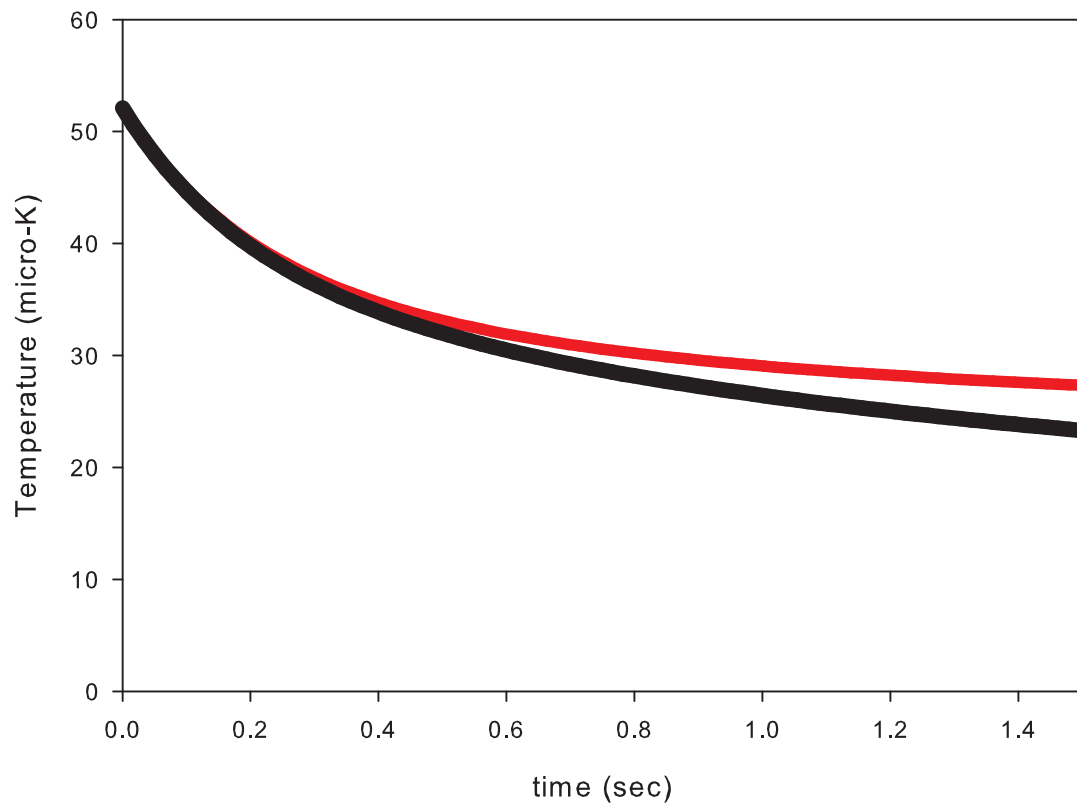
Figure 6.2: 2-CAZ cooling in the presence of significant evaporation is shown above. The figure shows predicted temperature vs. time for the experimental conditions with (red) and without (black) 2-CAZ cooling. The cooling in the no-2-CAZ case is due to evaporation.

does come with the caveat that the parameter space for optical trap loading is large since the power, beam size, and beam quality can in principle all be changed. There could in principle be a much better configuration for this system, but I did not see any indications that would be the case. Changing the CO_2 beam significantly misaligned the optical trap with respect to the MOT, and restoring the alignment was a multi-day procedure, complicating a search through optical trap parameter space.

A more drastic solution to this problem would be to use an entirely different trap, such as a hybrid magnetic/optical trap [4]. Although this in all likelihood would effectively address the evaporation problem, it would be very challenging to implement in the current experimental setup and add significantly to the experimental complexity of the system. For instance, given the large size of the vacuum chamber the magnetic coils would need to be very large to fit around the chamber. This leads to cooling concerns when considering the amount of current that would need to be run though them in order to confine the atoms in a magnetic trap, such as an anti-Helmholtz trap [5]. The coils could instead be placed inside the vacuum chamber, but given the need for water cooling the coils, this leads to concerns as well.

A less drastic solution may simply be to use a precooling technique, such as Raman cooling [6] or Polarization Gradient Cooling [7] that would cool the atoms significantly in a short time. This would improve the trap depth to atom temperature ratio right after loading thus reducing the effects of evaporation and allowing us to then apply the 2-CAZ cooling and measure its effect on the atom temperature in a straightforward way. This was a much more reasonable solution and I actually began investigating the STOP cooling technique in the hopes that it may be the precooling method needed. As I've already discussed it turned out to be a technique with applications beyond simply precooling.

6.2 Experimental Techniques used in the Measurement of the 2-CAZ Cooling Rate

Now that I have discussed some of the challenges encountered in this experiment I will now discuss how the experiments were conducted. The CAZ experiment used the same vacuum chamber and standard MOT-to-FORT loading described in the STOP cooling experimental section, with the
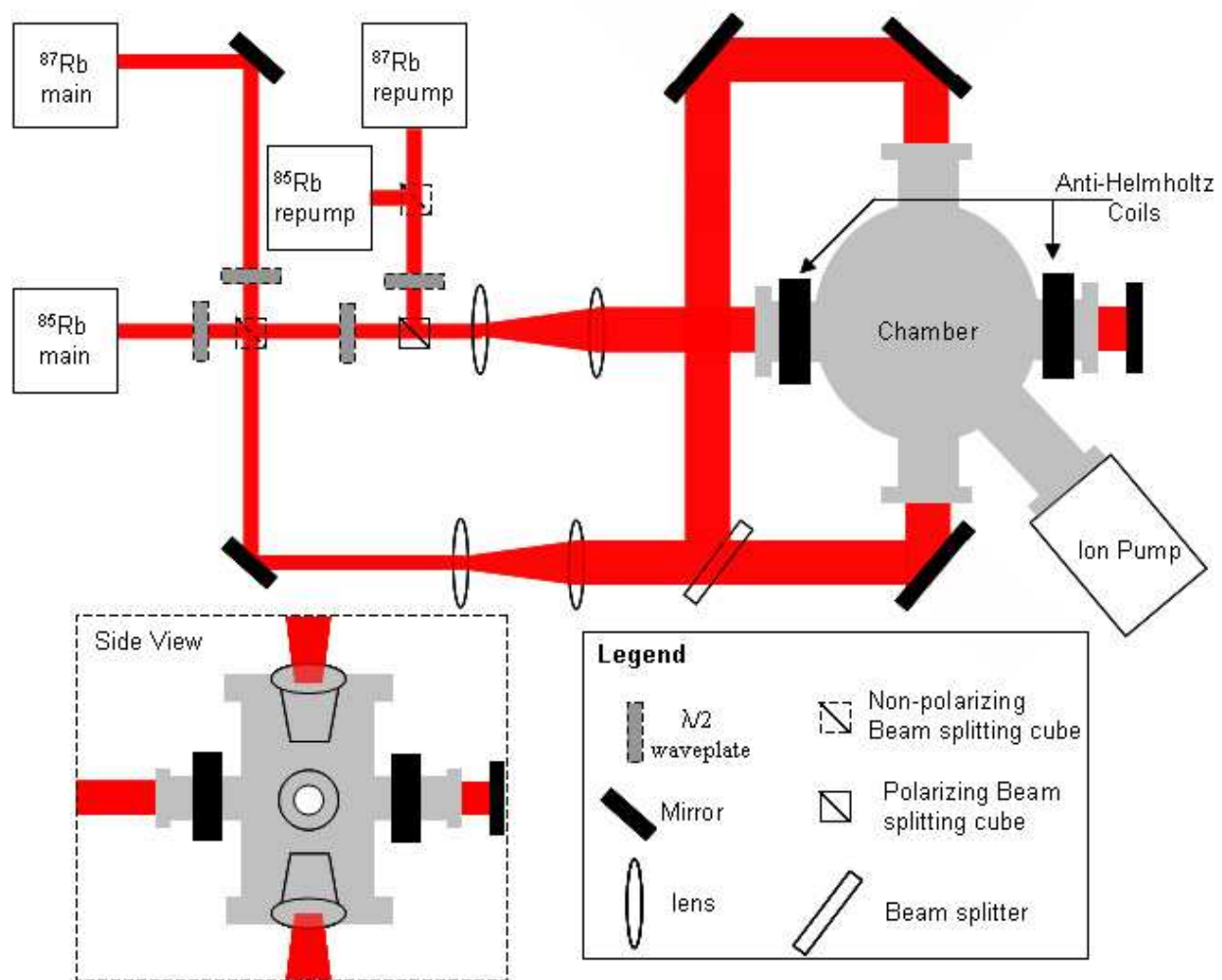
Figure 6.3: A cartoon of the experimental system is shown including the beam paths from the four lasers used. This figure comes from [3]

only difference being that the STOP experiment only used ^{87}Rb while the 2-CAZ experiment used both ^{85}Rb and ^{87}Rb. A simple schematic of the four trapping lasers and vacuum chamber is shown in Figure 6.3.

The CAZ experimental sequence started with loading ^{85}Rb and ^{87}Rb atoms simultaneously into overlapping magneto-optical traps (MOTs). From the MOTs, they were then loaded into the FORT. Once in the FORT, a uniform magnetic field of 2.0 G was applied. From this point a variety of measurements were performed : characterization of the evaporation rate in the optical trap, effects of 2-CAZ cooling on the atom temperature, m_F population changes due to spin-exchange collisions, optical pumping efficiency and effectiveness, and loss and heating rates due to the light applied during optical pumping. Below I describe each of the components that were built into the apparatus in order to complete the measurements needed for evaluating 2-CAZ cooling.

6.2.1 MOT/FORT

Given that the details of the FORT loading and the dual-Rb-isotope MOT have been covered in detail in [2, 3], only an overview of the dual-isotope loading will be given here. The ^{85}Rb and ^{87}Rb MOTs were created using standard techniques [2, 3, 8]. The atoms were loaded from the MOTs into the FORT using a compressed MOT stage implemented by reducing the hyperfine repump power and detuning the main trapping laser further to the red of the cycling transition [9]. The FORT was created using an AOM-controlled 75 W 10.64 μm CO_2 laser focused to a spot that results in a FORT with a trap depth of 280(56) μK and trap frequencies of 855(30)Hz in the radial direction and approximately 30 Hz in the axial direction. The radial frequency was measured using a parametric heating technique [10–12]. Generally, just over one million atoms total were routinely loaded into the FORT using these techniques, with the ratio between ^{85}Rb and ^{87}Rb being approximately 1.

6.2.2 Imaging

To extract number and temperature information from the atoms, the FORT was turned off rapidly and atoms were allowed to expand for a selected time in the range of 2-3 ms. The cloud was then imaged onto a CCD camera using absorptive imaging on the atoms' cycling transition. Normally hyperfine repump light was applied during the imaging to measure the total atom number. For some measurements, though, I imaged without hyperfine repump light to measure just the atoms in

their upper hyperfine state. With this system, I could only measure the number and temperature of one of the two Rb isotopes per experimental sequence.

6.2.3 AH Coils/2G Field

The Anti-Helmholtz coils used to create the MOTs were reused to create a uniform magnetic field by reversing the current direction in one of the coils using a set of mechanical relay switches. The coils had 36 turns each, with a radius of 3.18 cm and a separation of 20 cm. More detail about this aspect of the experiment can be found in [2]. Magnetic fields of up to 20 G were possible with this configuration, but I typically applied much smaller fields since the optimum cooling field was much lower, near 2.0 G. I also performed measurements at 1.0 G to confirm the 2.0 G results.

The optimum magnetic field for 2-CAZ cooling was predicted to be greater than 2.0 G for our experimental conditions. However, the need to periodically scramble the ^{87}Rb m_F state populations combined with limitations to our scrambling technique limited the magnetic field that could be used. At higher frequencies, the inductance of the scrambler coils and the chamber resulted in insufficient field strength to drive the scrambler transitions, resulting in a magnetic field limitation of about 2.0 G. This limitation will be discussed in more detail in Section 6.3.4.

6.2.4 Calculating the Optimum Value for the Magnetic Field

As I discussed in the previous chapter, the energy removed per spin-exchange collision between ^{85}Rb and ^{87}Rb is dependent on the magnetic field. The spin-exchange collision rate, however, decreases with increasing magnetic field as less atoms in the thermal distribution of velocities in the gas have enough energy to overcome the energy barrier. As one would expect, if the magnetic field is too large, the atoms cannot overcome the barrier height to collide and if the barrier is too low the cooling will not be very efficient since not much energy will be removed per cooling cycle. Therefore it is important to calculate the barrier height for our experimental conditions. I begin a calculation of this optimal magnetic field by considering the spin-exchange rate for a fully spin-polarized sample so that only kinetic energy-reducing collisions occur. This spin-exchange rate can be written in the following general form

$$R = K_2 \exp\left(\frac{-\Delta}{k_B T}\right) n_1 n_2 \tag{6.1}$$

where Δ is the value of the potential energy barrier ($\Delta = 1/6\mu_B B$ for the experiment), T is the gas temperature, K_2 is a constant, and n_1 and n_2 are the densities of the two types of atoms in the proper states to be involved in the spin-exchange collision. Each collision will transfer kinetic energy of an amount equal to the barrier height to the colliding atom pair so the kinetic energy reduction can be written as

$$E_{reduction} = \Delta K_2 \exp\left(\frac{-\Delta}{k_B T}\right) n_1 n_2 \tag{6.2}$$

Ideally, the optical pumping would return the atoms to their original states after the spin-exchange collision with no heat imparted and 100% efficiency. In that case, the net energy reduction for the gas would be equal to the kinetic energy reduction in equation 6.2 above. However, in a real system some heat will be imparted in the optical pumping stage of the cooling cycle. The amount of heat per cooling cycle due to the optical pumping can be represented by the quantity θ. The net cooling reduction, now including heating from the optical pumping process, is

$$E_{reduction+heat} = (\Delta - \theta) K_2 \exp\left(\frac{-\Delta}{k_B T}\right) n_1 n_2 \tag{6.3}$$

In order to find the optimum value of Δ, the first derivative of this quantity is taken and set equal to zero. This equation indeed confirms that if Δ is too low, then the first quantity in parenthesis is too low, and each collision will not transfer much energy. If Δ is too high, then the exponential factor results in a low collision rate. After taking the derivative the optimum value of Δ and the cooling at the optimum value are found to be

$$\Delta_{opt} = k_B T + \theta \tag{6.4}$$

Net cooling at $\Delta = \Delta_{opt}$:

$$E_{reductionopt} = k_B T K_2 \exp\left(-\left(1 + \frac{\theta}{k_B T}\right)\right) n_1 n_2 \tag{6.5}$$

106

From this the optimum barrier height is shown to be about the value of the gas temperature times k_B, in the limit that θ goes to zero. For a standard experimental sequence the atom cloud had a temperature of about $30\mu K$. A magnetic field of 2.7 G is ideal for the cloud temperature of 30 μK according to equation 6.5 with θ set equal to zero. For reasons associated with scrambler operation (Section 6.2.3 above and 6.3.4 below), we could not operate 2-CAZ cooling at 2.7 G, but only at a 2.0 G maximum field. However, with $\theta=0$, this implies a cooling rate that is only 4% less than the optimal value and so the inability to run at 2.7 G should not be a serious limitation to the cooling.

6.2.5 Microwave measurement of ^{85}Rb m_F state distribution

It is very useful to be able to measure the spin state distribution of the atoms. This capability allows one to characterize the optical pumping, perform spin-exchange rate measurements, and characterize the 2-CAZ cooling rate. All of these measurements were necessary to successfully perform the 2-CAZ experiment. A microwave signal was used in conjunction with other experimental components to extract the needed spin state distributions.

The microwave signal was created using a microwave generator (Anritsu MG3691B) and amplifier (Mini-circuits ZHL-16W-43-S) that was connected to a microwave antenna inside of the vacuum chamber. The antenna was placed inside the vacuum system and the microwaves were coupled to it through a feedthrough. The antenna was made with a diameter to provide a 50 Ohm impedance in the chamber with the chamber as the ground, and the antenna terminated in a sharpened point about 7 cm from the location of the atoms.

Although the polarization of this microwave signal could not be controlled, we were still able to measure the population in the individual m_F states in the ^{85}Rb ground state. Figure 6.4 shows a cartoon of the ground states of ^{85}Rb in the presence of a magnetic field. As is clear in the figure, the frequencies associated with each of the $\Delta m_F=0$ transitions are not degenerate. This meant the microwave frequency could be tuned to any of the individual ^{85}Rb ground state $F=2$ to $F=3$ $\Delta m_F=0$ transitions. Once an individual state transition had been selected, any atoms in the chosen $F=2$, m_F state could be driven into the F=3 state. From the F=3 state, the atoms could be imaged using absorption imaging (Section 3.1.4). Using this technique I was able to measure the population in any of the $F=2$ m_F states. This allowed me to characterize the spin state distribution of the atoms or characterize the optical pumping as needed.
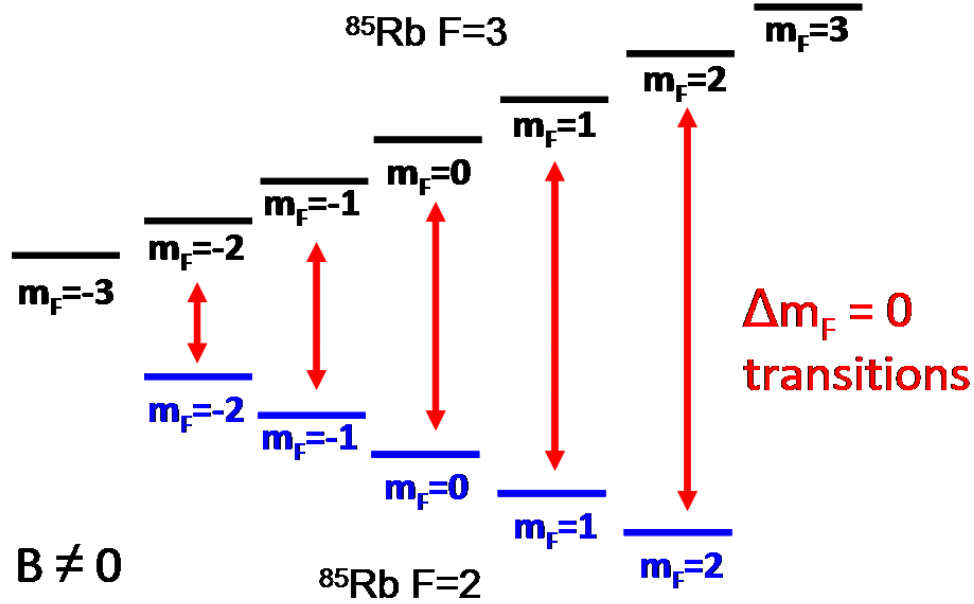
Figure 6.4: This diagram depicts a cartoon of the energy shifts of the two ground states of ^{85}Rb in the presence of a magnetic field. The Δm_F=0 transitions are shown in red. The figure clearly shows that none of these transitions are degenerate, allowing me to measure the population in any of the individual m_F state populations in the F=2 ground state.

In order to successfully identify the individual transition frequencies, the frequency shift associated with all of the states involved were calculated. From those values, the desired Δm_F=0 frequencies could be identified. Most of the frequencies were calculated using the Breit-Rabi equation [13]

$$E_{m_F=m_i+m_s=m_i\pm 1/2} = -\frac{h\nu_{hfs}}{2(2l+1)} + g_I\mu_B m_F B \pm \frac{h\nu_{hfs}}{2}\sqrt{1 + \frac{4m_F x}{2l+1} + x^2} \qquad (6.6)$$

$$x = \frac{(-g_j - g_I)\mu_B B}{h\nu_{hfs}}$$

The exception is with the state with $m_F = \pm 3$. For these states the energy is simply

$$E = g_F\mu_B B m_F \qquad (6.7)$$

The relevant values for ^{87}Rb and ^{85}Rb are listed in Table 1.2 as well as the values for both isotopes listed in Table 1.1.

Table 6.1: A table summarizing the various constants needed to evaluate the energy splitting described in equation 6.6 [14].

Constant	Value
h	6.626E-34 Js
g_J	2.00233
g_I	-0.000293
μ_B	9.274E-28 J/T

Table 6.2: A table summarizing the constants associated with ^{85}Rb and ^{87}Rb needed to evaluate the energy splitting described in equation 6.6 [14].

Constant	^{85}Rb	^{87}Rb
ν_{hfs}	6.834682614 GHz	3.035732439 GHz
I	3/2	5/2
g_F	1/2	1/3

6.3　Spin Polarization Techniques

2-CAZ cooling in this system required optically pumping ^{85}Rb into its F=2; m_F = -2 state from its other m_F states with F=2. The 2-CAZ cooling scheme specific to the experiment is shown in Figure 6.5. Note that it is crucial that the ^{85}Rb atoms begin in the F=2; m_F = -2 state to ensure that spin-exchange collisions that occur reduce the kinetic energy of the colliding pair rather than increase it. It is not possible to move the atoms to the F=2; m_F = -2 state solely through closed transitions, so any useful optical pumping method requires some provision for addressing ^{85}Rb atoms in both the F=2 and F=3 states. I investigated two different methods that met this requirement. The first was a purely optical pumping method. While relatively straightforward to implement, I found that it created too much heat and loss during the course of its operation. I then implemented an optical pumping technique based on a combination of microwave sweeps and optical pumping. I found that the losses from this combination microwave and optical technique were significantly lower than the purely optical case.

6.3.1　Pure Optical Pumping.

The simplest implementation of a pure optical pumping scheme used two lasers (Figure 6.6a). The first, L1, was pulsed and was detuned 12 MHz to the blue of the ^{85}Rb $5S_{1/2}$ F=2 to $5P_{1/2}$ F'=2 transition (i.e. near the D1 line). Near the end of this experiment, L1 was changed from a 795 nm laser to a 780 nm laser, meaning the transition was then 12 MHz to the blue of the ^{85}Rb $5S_{1/2}$ F=2 to $5P_{3/2}$ F'=3 transition. The second laser, L2, was detuned 24 MHz to the blue of the $5S_{1/2}$ F=3 to $5P_{3/2}$ F=3 transition with a polarization 75% σ^-, 23% σ_0 and 2% σ^+ by intensity and was left on continuously. This particular polarization was obtained by sending a circularly polarized beam onto the atoms from a direction that was not along the magnetic field. The combined effect of L1 and L2 was to drive the ^{85}Rb atoms into the F=2, m_F = -2 state after (on average) several photon scattering events. The second laser, L2, needed to have some σ_0 component so that the atoms did not get stuck in the F=3, m_F=-3 state. The optical pumping lasers were pulsed rather than left on continuously. The reason we did this was that to control the number of atoms pumped precisely, it was easiest experimentally to use a particular intensity and tune the pulse length appropriately, as opposed to trying to tune the laser intensity very precisely.
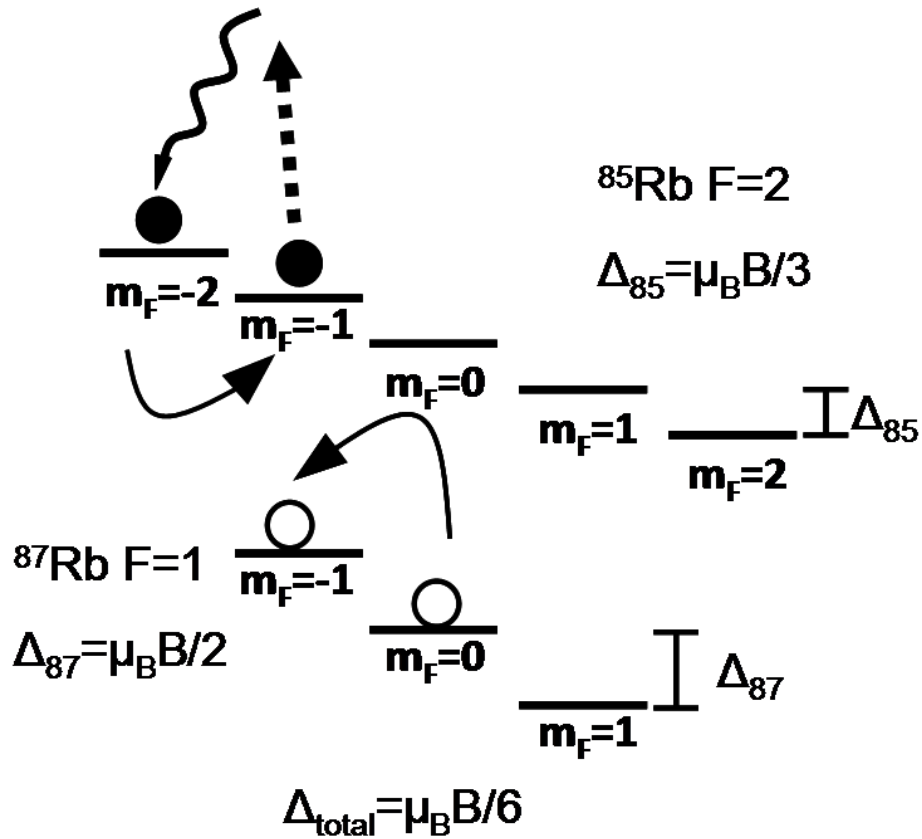
Figure 6.5: Collision-Assisted Zeeman Cooling of ^{85}Rb/^{87}Rb. This diagram depicts CAZ cooling in an ^{85}Rb/^{87}Rb mixture. Spin-exchange collisions cause state changes in ^{85}Rb (F=2, m_F=-2 to F=2, m_F=-1) and in ^{87}Rb (F=1, m_F=0 to F=1, m_F=-1; or F=1, m_F=+1 to F=1, m_F=0). Each collision results in $1/6\mu_B B$ of kinetic energy being removed from the sample. ^{85}Rb is optically pumped back into its initial state, keeping it spin-polarized. This ensures that only cooling collisions take place.
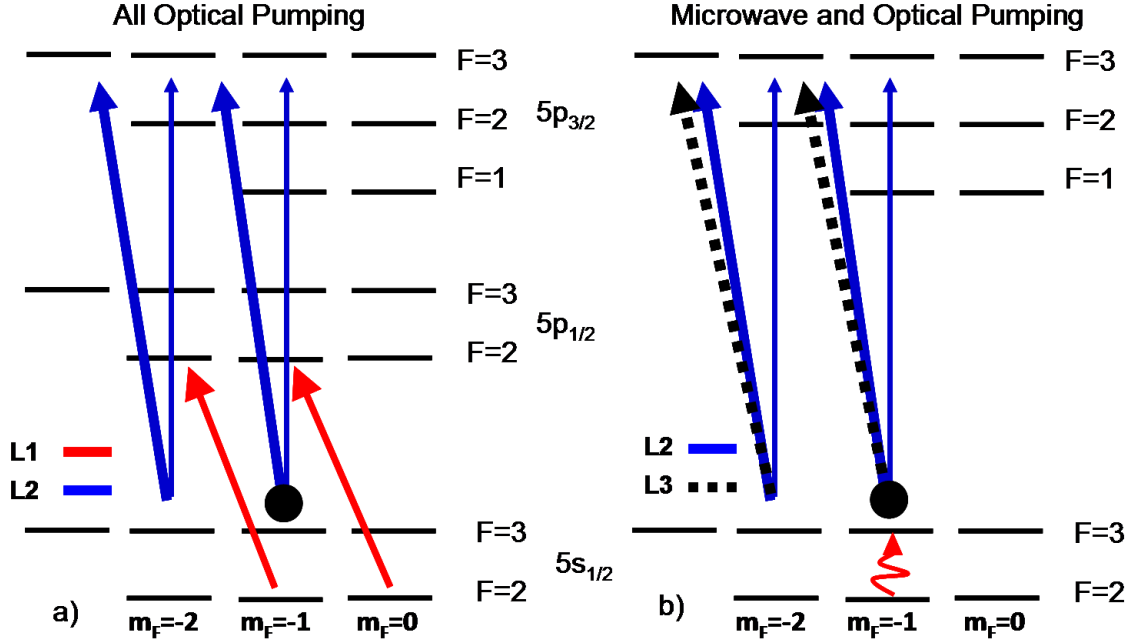
Figure 6.6: Diagram of the two pumping laser transitions used for spin-polarization of ^{85}Rb. All Optical Pumping (a) for Spin-Polarization of ^{85}Rb. Direct optical pumping used purely circular polarized light for the repump beam (red). The initial spin polarization setup used one beam with no σ^+ polarization (solid blue) component. Eventually an additional beam with pure σ^- polarization was added. Microwave and optical pumping (b) uses a microwave transition (red) to move atoms into the upper ground state. For the spin polarization, one beam has pure σ^- polarization(dashed) and the other has no σ^+ polarization (solid black/blue) component. The goal of each pumping method is to put atoms into a state with a high probability to end up in the $F=2$, $m_F=-2$ ground state.

While this pure optical technique was effective in spin-polarizing the atoms, L1 created too much light-assisted collisional loss despite a relatively low intensity. I measured a loss rate of $1.50(75)\times10^{-12}$ cm^3/sec with a 12.1 μW/cm^2 L1 intensity. This loss rate was too large for the system for use during 2-CAZ as it led to an unacceptable increase in the loss rate, and so the combination microwave/optical system was used. I still used the purely optical technique for initializing the ^{85}Rb m_F population distribution, however, as it was more suited to optically pump atoms across the full m_F state distribution in a timely manner.

In addition to the large loss rate for the purely optical configuration I also found that there was a small ($\sim$10% per optical pumping cycle) but constant fraction of the atoms that were traveling the wrong direction in the distribution, namely from the $F=2$, $m_F=-1$ state to the $F=2$, $m_F=0$ state. Any atom in the $m_F=0$ state will not be able to participate in a cooling spin-exchange

collision. Instead, most collisions an atom undergoes in that state will add heat to the cloud. My initial supposition was that most of this population in the m_F=0 state was caused by the small component of σ^+ polarization and σ_0 polarization contained in the L2 laser. That the σ^+ component drives atoms towards positive m_F states is immediately apparent. However, the σ_0 polarization can also drive atoms in this direction. This occurs if the atoms are pumped from the F=2, m_F=-1 state to the F=3, m_F=-1 state, then there will be an excitation to the F'=3, m_F=-1 state via the σ_0 polarization. From the F'=3, m_F=-1 state, decays to the F=3, m_F=0 or F=2, m_F=0 state are possible. To evaluate this initial supposition, I developed a rate equation model that will be discussed in Section 6.3.3. This model confirmed that the mixed polarization of the laser was contributing significantly to the m_F=0 population. To address this problem another beam tuned to the same transition as L2, but with pure σ^- polarization, was added to minimize transitions to the F=3 or F=2 m_F=0 state.

6.3.2 Microwave Assisted Optical Pumping

The microwave pumping scheme was developed as an alternative to the pure optical pumping scheme. One microwave pumping cycle consisted of a 10 ms microwave adiabatic rapid passage sweep [15] spanning 100 kHz centered on the transition from F=2, $m_F = -1$ to the F=3, $m_F = -1$ state followed by a 7 ms pulse from L2 (Figure 6.6b). Additionally, pure σ^- light from L3, at the same detuning as L2, was on continuously during the entire sequence. L3 was added to prevent L2 from driving atoms away from the desired F=2, $m_F = -2$ state as described above. The main advantage of the microwave system over the pure optical system is that it avoids the light assisted collisional losses that were produced in the pure optical scheme since those were associated with light close to the F=2 ground state to upper state transitions.

Although I was able to replace most of the functionality of the all optical technique with this microwave assisted optical technique, I still needed to use the all optical technique to initialize the atoms' spin state. This was because the microwave technique can only address atoms in the F=2, m_F=-1 state. This left a large number of atoms in the other F=2, m_F states that would have caused heating and loss-inducing collisions. In order to avoid this problem I initialized the system using two pulses from L1 to insure that the atoms were all in the m_F=-2 or m_F=-1 state.

6.3.3 Rate Equation Model

I developed this rate equation model to understand the interaction of the optical spin polarization beams, namely L2 and L3, with the atoms. This model was used to determine whether the mixed polarization of the optical pumping laser was contributing to the population in the $m_F=0$ state and give a general idea of how the atoms were expected to move through the distribution as polarizations and intensities were varied. The model looked at the population in the m_F=-2,-1 and 0 states during the application of the optical spin polarization beams. This model assumed the atoms initially started entirely in the $F=3,m_F$=-1 state, in agreement with the microwave assisted optical pulse experimental conditions, and that eventually all of the atoms wind up in the $F=2$ state where they no longer scatter light after the optical pump pulse sequence is completed. Thus, the main utility of the model is determining the final state distribution after the application of the pulses. The first calculation done with this model was purely qualitative and was only intended to confirm that the mixed polarization laser (L2) would leave atoms in the $m_F=0$ state.

This rate equation model contained the $F'=3$, $F'=2$ and $F'=1$ excited states for ^{85}Rb as well as the $F=3$ and $F=2$ ground states and the m_F levels for each of these states. This produced a set of 27 coupled differential equations that were then solved for a given set of laser intensities and polarizations. The equations used for the model were of the form

$$\frac{dN_{gi}}{dt} = \sum_j AC_{ij}^2 N_{ej} - \frac{IA}{I_{sat}}C_{ij}^2 \sigma_{m_j - m_i}^2 [N_{gi} - N_{ej}] \tag{6.8}$$

$$\frac{dN_{ej}}{dt} = -AN_{ej} + \sum_k \frac{IA}{I_{sat}}C_{jk}^2 \sigma_{m_j - m_k}^2 [N_{ej} - N_{gk}] \tag{6.9}$$

where $A = 1/26.5ns$ describes the spontaneous emission, N_{gi} or N_{ei} is the population in a given ground or excited state respectively, C_{ij} is proportional to the Clebsch Gordan coefficients and σ describes the light polarization. Note that the $F'=4$ state was not included because the detuning of L2 from that state was much greater than from the $F'=2$ and $F'=3$ states. The atoms are assumed to all start in the $F=3$, m_F=-1 state. Figure 6.7A shows the model derived population in the $F=2$, m_F=-2, m_F=-1 and $m_F=0$ states when only L2 (the mixed polarization laser) was applied. As you can see, there is a steady state population in the $m_F=0$ state. Figure 6.7B shows the model results when starting with the same initial state distribution, but now applying a pure

114
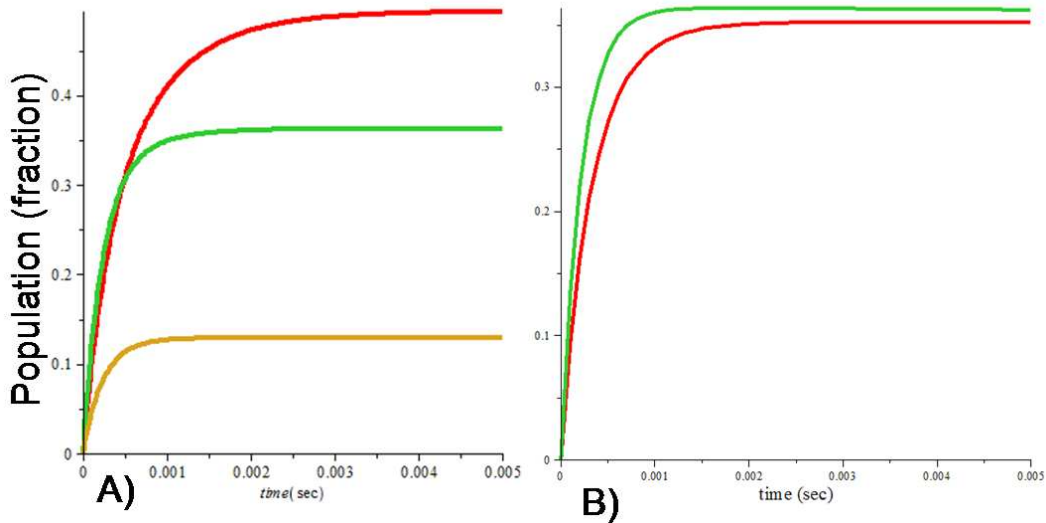
Figure 6.7: Graph A and B show the population in the F=2 m_F=-2,-1, 0 ground states in red, green and yellow respectively. Graph A shows the non-zero population in the m_F=0 state with only the application of the mixed polarization laser. Graph B shows that the m_F=0 state is now zero in the case of a beam with pure σ^- polarization. Note that the two states shown in case B do not add to 1 since some of the population is stuck in the F'=3, m_F=-3 state.

σ^- beam instead of a mixed polarization beam. You can now see that the m_F=0 state has been cleared out as desired. In the case of the pure σ^- beam, the model shows some population is stuck in the F'=3, m_F=-3 state. This model qualitatively confirmed that the mixed polarization of L2 was a problem and a solution was to add an additional pure σ^- beam.

The above discussion explains the advantage of including the pure σ^- beam, but it doesn't really quantitatively address the expected state populations using the combination of the two beams. To model the experiment more accurately, I used the measured intensities from the microwave assisted optical pumping experiment of 0.12 mW/cm^2 for the mixed polarization beam and 0.009 mW/cm^2 for the pure σ^- beam. In the model, the two beams were applied one at a time. I began by applying the pure σ^- laser (L3) for 10 ms, similar to the actual experimental application. I then took the resulting state populations and used those as the initial states. Starting from this initial state distribution, I then applied the mixed polarization laser and looked at the resulting steady state population. The model result using the combination of the two beams is shown in Figure 6.8. As is apparent from Figure 6.8, the addition of the pure σ^- beam has decreased the final population in the m_F=0 state from about 12% (the results using only L2) to about 4%, a significant but not

complete reduction of the $m_F=0$ population. Given the finite time required for the microwave pulses, it was not possible to immediately measure the $m_F=0$ population directly after an optical pumping cycle. However, several ms after the cycle was completed an $m_F=0$ population of about 2% was observed. Given imperfect population transfer via the microwave sweeps, the presence of spin-exchange collisions, and uncertainties in the laser intensities involved in the optical pumping sequence, such a difference is reasonable. In any case, this small population would have minimal impact on the net cooling rate and so a precise agreement between the model and the observations is not required.

This last point can be illustrated with a simple estimate. Any atoms in the $m_F=-2$ state will collide with ^{87}Rb and cool whereas atoms in the $m_F=0$ state will collide with ^{87}Rb and generally heat. To estimate the reduction in cooling from these $m_F=0$ atoms I start by taking the ratio between the fraction of atoms that start in the $F=2$ $m_F=-1$ state and wind up in the $F=2$, $m_F=$ -2 state (55%) and the fraction that wind up in the $F=2$, $m_F=0$ state (4%). This is then weighted by $\exp(\Delta/k_BT)$, where Δ/k_BT is about 0.7. Using these values I find that the 4% population in the $m_F=0$ state reduces the cooling by about 15%. If I were to use the state population from the condition without the pure σ^- beam (i.e. 12% in the $m_F=0$ state) I would see a reduction in cooling of close to 50% so you can see the addition of the pure σ^- beam was calculated to be important. All of these state populations are estimates from the rate equation model. In the actual experiment, I saw $m_F=0$ state population of less than 2%, which would suggest a cooling rate reduction closer to 5%. In reality, due to the distortions in the $m_F=0$ population measurement due to spin-exchange collisions the reduction in cooling rate is likely between this 5% value and the 15% value determined earlier. While non-ideal, this reduction in cooling was not nearly as large as other reductions to the cooling rate (discussed in Chapter 7) and so I did not characterize it more carefully than this estimate. If the cooling had ultimately been limited by this reduction I would have needed to increase the intensity of the pure σ^- beam by at least an order of magnitude, which for this experimental setup was not feasible without major modifications to the system. For the configuration of the apparatus with which these measurements were conducted, I was severely limited in the intensity of the pure σ^- beam that could be used since it was directed through the back of one of the MOT retro mirrors. That mirror is not perfectly reflecting (98% reflection) and so light can be transmitted, but at the expense of a large amount of attenuation.
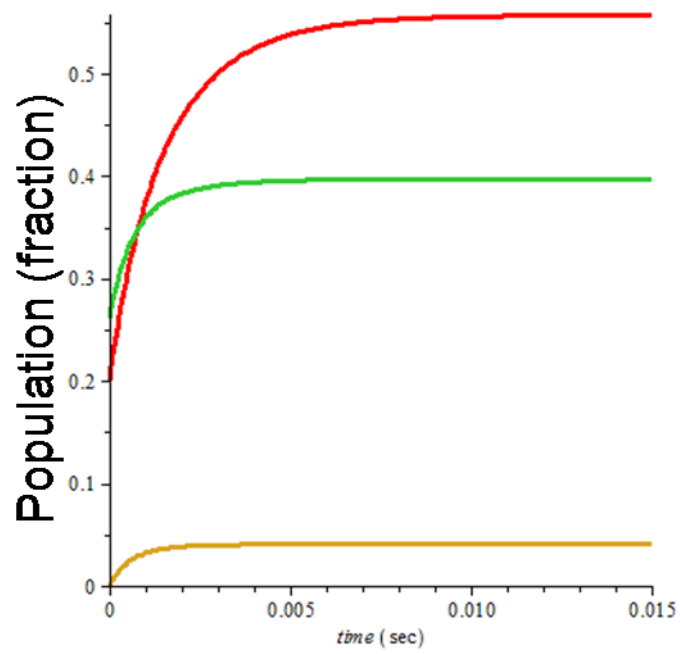
Figure 6.8: The results of a rate equation model, using the actual intensities of the mixed polarization and the pure σ^- beam. The population in the F=2 m_F=-2,-1, 0 ground states are shown in red,green and yellow respectively.

6.3.4 RF Scrambler

A ten turn coil was located inside of the vacuum chamber and was suspended about 10 cm above the trapping region. Every 80 ms an RF sweep was sent to this coil using a function generator. This sweep was centered at 1.4 MHz when a 2.0 G applied magnetic field was used and spanned 200 kHz. This frequency was chosen appropriately so that the sweep scrambles the population of the ^{87}Rb atoms, preventing the accumulation of ^{87}Rb population in any one of the m_F states. As mentioned above, the RF scrambler did not work effectively at frequencies much greater than 1.4 MHz. When I initially began 2-CAZ measurements I started at a magnetic field closer to the optimum value at 2.7 G. After struggling to see any cooling I investigated the efficiency of the Scrambler at several frequencies. I did this by spin polarizing the atoms with several pulses from L1 and then looking at the population in the ^{85}Rb $F=2$, m_F=-2 and m_F=-1 states. From these measurements I was able to see the population in the m_F=-2 state decrease and the population in the m_F=-1 state increase exactly as expected. Using these measurements I confirmed that the scrambler worked well up to 1.4 MHz, but above this its effectiveness dropped rapidly. I believe this is because eddy currents are induced by the coils in the metal chamber that tend to cancel the field at the atoms. This cancellation does not occur with DC currents, and gets worse as the frequency of the applied current increases. In addition, the coils also have a finite inductance that reduces the current for a fixed applied voltage for increasing frequencies as well.

6.4 Conclusion

This concludes the description of the individual elements of the apparatus needed to conduct the measurements relevant to 2-CAZ cooling. These measurements included: characterizing the optical pumping efficiency, measuring heating and loss during optical pumping, measuring evaporation rates, measuring the initial m_F state populations after initial spin polarization, measuring the 2-CAZ cooling rate through monitoring the ^{85}Rb $F=2$, $m_F = -1$ state population, and examining collisional loss rates in the gas. These measurements will be discussed in the following chapter.

References for Chapter 6

[1] Hamilton M S, Gorges A R and Roberts J L 2012 J. Phys. B: At. Mol. Opt. Phys. 45 095302

[2] Mathew Hamilton, Ph. D. Thesis, Colorado State University (2013).

[3] Anthony Gorges, Ph. D. Thesis, Colorado State University (2010).

[4] Y.-J. Lin, A. Perry, R. Compton, I. Spielman, and J. Porto, Phys. Rev. A 79, 063631 (2009).

[5] Jacob Roberts, Ph. D. Thesis, University of Colorado (2001).

[6] H. Lee, C. Adams, M. Kasevich, and S. Chu, Phys. Rev. Lett. 76, 2658 (1996).

[7] J. Dalibard and C. Cohen-Tannoudji, J. Opt. Soc. Am. B 6, 2023 (1989).

[8] Raab E L, Prentiss M, Cable A, Chu S, and Pritchard D E 1987 Phys. Rev. Lett. 59 26312634

[9] Petrich W, Anderson M H, Ensher J R and Cornell E A 1994 J. Opt. Soc. Am. B 11 1332-1335

[10] Wu J, Newell R, Hausmann M, Vieira D J, and Zhao X 2006 J. Appl. Phys. 100 054903

[11] Roati G, Jastrzebski W, Simoni A, Modugno G and Inguscio M 2001 Phys. Rev. A 60 052709

[12] Friebel S, Dandrea C, Walz J, Weitz M and Hansch T W 1998 Phys. Rev. A 57 R20-R23

[13] A. Corney, Atomic and Laser Spectroscopy (Clarendon Press, Oxford, 1977).

[14] E. Arimondo, M. Inguscio, and P. Violino, Rev. Mod. Phys. 49, 31 (1977).

[15] N. V. Vitanov, T. Halfmann, B. W. Shore, and K. Bergmann, Annu. Rev. Phys. Chem. 52, 763 (2001).

Chapter 7

Collision Assisted Zeeman Cooling Results

Now that the experimental techniques used in the 2-CAZ experiment have been presented in Chapter 6, I will discuss the results of out various measurements. As mentioned in Chapter 6, due to experimental limitations, it was not possible to directly measure the cooling from the 2-CAZ cooling technique. The goal of the experiment was adjusted to instead extract the experimentally achievable cooling rate by measuring the components that contribute to that cooling rate individually and then combining them to determine a total net cooling rate. I will begin by discussing several different types of measurements that were performed to characterize the cooling process. Then I will discuss how these measurements were combined to allow the extraction of a 2-CAZ cooling rate. Finally, I will discuss the future outlook for 2-CAZ cooling given the reported measurements.

7.1 Microwave Assisted Optical Pumping Transfer Efficiency Measurement

First we characterized the efficiency of the optical pumping sequence. This efficiency was needed to extract expected cooling rates as described in the following subsections. As discussed in the previous chapter, several circularly polarized lasers and sometimes microwave sweeps were used to move the ^{85}Rb atoms into the $F=2$, m_F=-2 state to insure that the correct spin-exchange collisions would occur. Therefore, it was very important to characterize how efficiently the optical pumping pulses were able to move the atoms to this initial state. Ideally, the microwave/optical pumping cycle would transfer atoms from the $F=2$, $m_F=$ -1 state to the $F=2$, $m_F = $ -2 state with 100% efficiency. In a real system, however, this will not be the case. During the course of several measurements it became clear that the microwave transfer was indeed imperfect. There are several reasons why perfect transfer was not expected in this system. The first was imperfect adiabatic rapid passage, meaning that the microwave transfer used to move the atoms from the $F=2$ ground state to the $F=3$ ground state was imperfect. This is something that was experimentally observed, and is attributed to variations in the microwave amplitude applied to the atoms due to the boundary conditions imposed by the metal chamber. Evidence for this comes from the inability to drive an effective

π pulse due to different Rabi frequencies in the cloud. This then leads to a non-100% adiabatic rapid passage transfer. The actual transfer percentage for our experimental parameters will be characterized by α. A second reason why perfect transfer was not seen is that part of the technique includes putting population in the excited state F'=3, m_F=-2 during the optical pumping process and so with linearly polarized light present there will always be some spontaneous decay back to the m_F= -1 state (this will be characterized by β). The optical pumping cycle efficiency needs to be characterized both to predict the behavior of the gas when 2-CAZ cooling is applied and to successfully interpret measurements of atom populations with the microwaves.

To characterize the microwave assisted optical pumping transfer efficiency out of the ^{85}Rb F = 2; m_F = -1 state an experiment was performed that involved several steps. The first step was to initialize the ^{85}Rb m_F populations using pure optical pumping so that the atoms were in only the m_F = -1 and m_F = -2 states as discussed in Section 6.3. At this point the population in the m_F = -1 state of ^{85}Rb when it was loaded into the optical trap alone (e.g. without ^{87}Rb present) was monitored. Finally, a number of microwave-assisted optical pumping cycles (see Section 6.3.2) were applied and the ^{85}Rb atoms were pumped from the F=2 m_F=-1 state to the F=2 m_F=-2 state. This population transfer was measured as a function of the number of pulses applied. It is important to note, that the population in the F=2, m_F=-1 state was not measured directly, rather, a single microwave pulse was used to excite atoms from the F=2, m_F=-1 state to the F=3, m_F=-1 state. At this point, the population in the F=3 state was measured via absorption imaging. The data is shown in Figure 7.1.

From this data the on-resonant adiabatic rapid passage transfer probability(α) and the off-resonant adiabatic rapid passage excitation probability of the next-nearest frequency transitions(γ) was extracted. Note that all of the other transition probabilities are expected to be negligible. Due to the spin-polarization of the gas, it is assumed that there is no population outside the m_F=-1 state and m_F=-2 state in the F=2 ^{85}Rb ground state at the conclusion of the initial optical pumping pulses. The population fraction in the m_F=-1 state after an optical pumping pulse is related to the population before the optical pumping pulse and is modeled by:

$$n_{-1,new} = (1 - \alpha)n_{-1,old} + \beta\alpha n_{-1,old} + \gamma\beta(1 - n_{-1,old}) \tag{7.1}$$
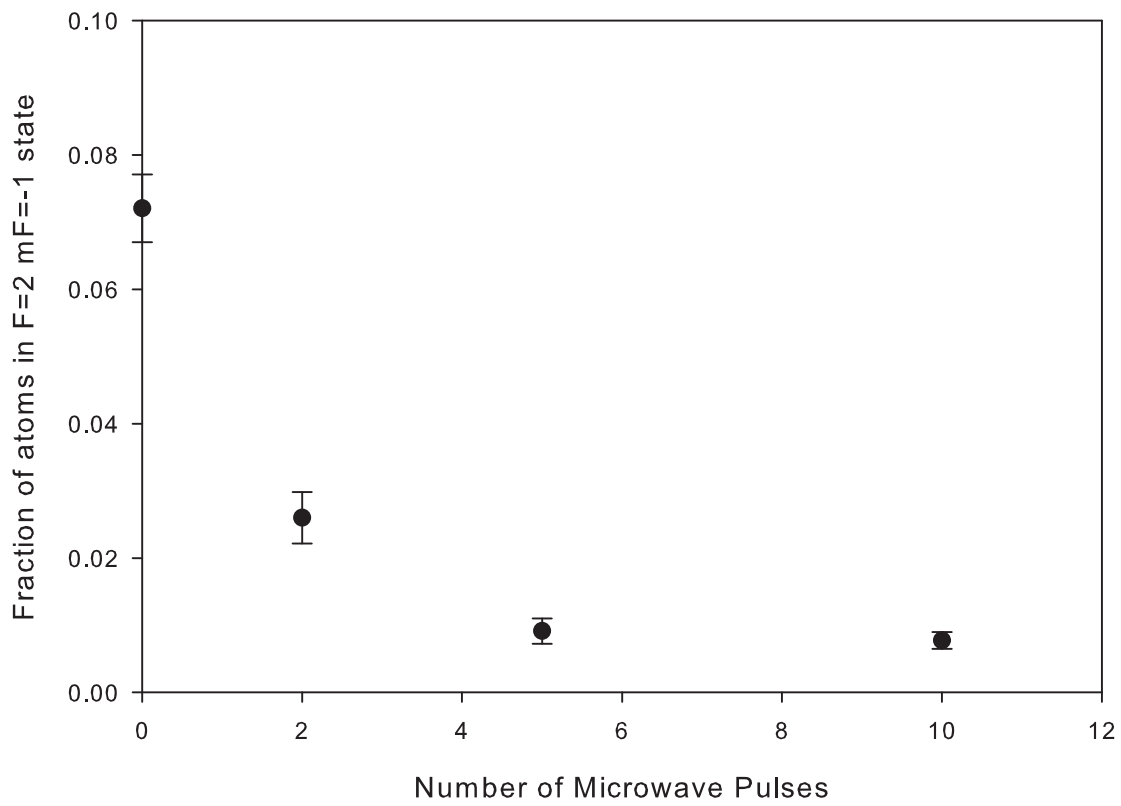
Figure 7.1: The population in the m_F=-1 state is plotted as a function of the applied microwave-assisted optical pumping pulses.

where $n_{-1,new}$ and $n_{-1,old}$ are the fractions of atoms in the m_F=-1 state right after and right before the optical pumping pulse, respectively. $\beta = 0.4$ is a branching ratio that comes from the final population distribution as calculated in the rate equation model of Chapter 6. This branching ratio needed to be modeled since it is not dominated by one particular transition, but is instead a combination of the available transitions. α and γ are fit parameters. As mentioned above, the data collected is not the actual population of the m_F=-1 state but is related to it by

$$n_{F=3} = \alpha n_{-1} + \gamma(1 - n_{-1}) \tag{7.2}$$

where n_{-1} is again the fraction of atoms in the m_F=-1 state and $n_{F=3}$ is the measured fraction of atoms observed in response to the microwave pulse that drives F=2, m_F=-1 atoms to the F=3, m_F=-1 state. α and γ were derived from the data in Figure 7.1 by combining equations 7.1 and 7.2 and then performing a best fit analysis. This analysis yielded an on-resonance microwave excitation probability of α=0.855(78) and an off-resonance excitation probability of γ=0.0054(20).

Additional measurements were performed to confirm the measured value of α. The goal of these additional measurements was to compare the total atom population in the FORT when measured using microwave adiabatic rapid passage for transferring atoms from the F=2 to the F=3 state to the traditional method of optical repumping of the atoms between the same states using laser light. α should be equal to the ratio of the total atom number measured using microwave transfer to the total atom number measured with hyperfine repump light present during absorption imaging. These measurements were done by first using a microwave sweep to move atoms from individual m_F states in the F=2 ground state to the F=3 state. The atoms were then imaged in the F=3 state. This measurement was performed over all of the m_F states in the F=2 ground states, and when these values were summed, a total atom population in the F=2 state was obtained. Using this technique only 85±1% of the atoms were seen as compared to the traditional optical repumping technique from the F=2 to the F=3 state. This value of 85±1% is expected to be approximately equal to α. This measurement confirmed the above value of α and, indirectly, the value of β.

7.2   Steady-State Population Measurement

Part of the analysis of the net cooling rate through summing individual heating and cooling processes is the determination of the energy removal rate. The energy removed per optical pumping cycle is determined in the absence of heating solely by the value of Δ and the number of spin-exchange collisions that occur. Measuring the steady-state population combined with the optical pumping transfer efficiency allows the determination of the number of ^{85}Rb atoms that are transferred from the m_F=-2 state to the m_F=-1 state per optical pumping cycle. For each atom transferred, a spin-exchange collision occurred, and for each spin-exchange collision, an amount of energy equal to Δ is removed. Thus, the steady-state fraction of atoms in the m_F=-1 state combined with the measured optical pumping transfer efficiency can be used to determine the energy extracted per optical pumping cycle.

Once the optical pumping transfer efficiency was determined, the steady-state (i.e. after many 2-CAZ cooling cycles) population in the $m_F = $ -1 state was measured via microwave sweep during 2-CAZ cooling. To ensure the system had reached steady-state, this measurement was performed after 30 optical pumping cooling cycles of 17 ms duration (described in Section 6.3.2). At the time this measurement was performed the full ^{85}Rb number was $1.54(6) \times 10^6$ with a density of $4.8(2) \times 10^{11} \text{cm}^{-3}$ and the full ^{87}Rb number was $1.11(6) \times 10^6$ with a density of $3.4(2) \times 10^{11} \text{cm}^{-3}$, where all of these quoted uncertainties reflect only statistical uncertainty. Systematic uncertainties in the number, temperature and density are about 20% for the system. The temperature of the atoms was $36.8(5)\mu$K. The fraction was measured by comparing the number of atoms in the F=3 state after one microwave sweep resonant with the F=2 m_F= -1 to F=3 m_F= -1 transition to the total number of atoms. That ratio was 0.073(5). Using the determination of α and γ this indicated that the F=2, m_F= -1 population at the start of the microwave sweep was 0.080(9). It is important to note that this is not the average population in the m_F= -1 state, but rather the population that is present right before the start of an optical pumping pulse (i.e. at the end of the previous optical pumping pulse).

7.3 Cooling Rate

Once the steady-state population has been measured, the energy removal rate (not including any heating mechanisms) due to spin-exchange collisions and optical pumping can be determined. The maximum ideal cooling rate, $\frac{dT}{dt}$, is calculated using

$$R_{maxcooling} = \frac{dT}{dt} = \frac{f_{tran}B\mu_B}{6k_B t_{cycle}3(1 + \chi_{87})} \tag{7.3}$$

where f_{tran}=0.0438 (the transfer fraction to the m_F=-2 state) is calculated using the appropriate m_F=-1 state population fraction that is transferred by a microwave sweep at the end of an optical pumping cycle of 0.073(5) times the transfer probability from the F=3, m_F=-1 state from the rate equation model of (1-β), where β=0.4. For this experiment, B=2 G, t_{cycle}= 17 ms and χ_{87}=0.72, the ratio of ^{87}Rb atoms to ^{85}Rb atoms. Note that the 3 in the denominator comes from the fact that the energy in the gas is related to the temperature as $E = 3Nk_BT$. Also note that the 6 in the denominator comes from the definition of Δ for the $^{85/87}$Rb system. The results described above imply a maximum cooling rate of 11.2(9) μK/sec.

In order to compare this result to a theoretical prediction, an equation for the expected 2-CAZ cooling rate needs to be derived. This has been done in great detail in [1]. This result was discussed in some detail in Chapter 5 and is also shown below.

$$\frac{dT}{dt} = \frac{\exp(-\Delta/k_BT)N_2(\Delta - \kappa)}{\tau_{SE}3k_B(N_1 + N_2)} \frac{1}{1 + \tau_{OP}/\tau_{SE}(1 + \exp(-\Delta/k_BT))} \tag{7.4}$$

κ is the average energy imparted per successful optical-pumping driven population transfer, N_1 and N_2 are the total number of atoms of the non-optically-pumped and optically-pumped isotopes, respectively, τ_{SE} is the spin-exchange time-constant and τ_{OP} is the optical pumping time constant. The maximum cooling rate can be compared to the prediction of equation 7.4 with κ set to be 0. From the experimental measurements τ_{OP}/τ_{SE} was estimated to be 7.5 based on measured light intensities and the spin-exchange collision rate used. In order to avoid systematic uncertainties in the determination of the density, an experimentally determined value for the weighted spin-exchange rate $(2.4(4)\times10^{11}$ cm^3/s) was used, which is consistent with theoretical predictions [2]. The corresponding maximum cooling rate from equation 7.4 is 10.9$\pm$3.0 μK/sec including system-

atic uncertainties from the number uncertainty, uncertainty in atom temperature, and uncertainty in spin-exchange rate. Thus, the measured maximum cooling rate and equation 7.4 are in agreement within the systematic uncertainty of the predicted cooling rate. Note that since the magnetic field and optical pumping cycle length can be measured to a high precision and the fractional atom population is a relative measurement free of most systematics, the measured maximum cooling rate is far more precise than the one predicted from equation 7.4.

7.3.1 Heating Considerations

The maximum cooling rate is not the experimentally realized cooling rate. Inevitably, in addition to cooling during an optical pumping cycle there is also heating from a variety of sources. After determining the maximum cooling rate, auxiliary measurements and estimates to account for heating during the optical pumping cycle were performed to determine a net cooling rate.

An auxiliary experiment to measure the heat and loss associated with the microwave optical pumping technique itself was performed. 12 microwave-optical pumping cycles were applied to a gas of ^{85}Rb alone. To ensure the atoms were optically pumped in a closed cycle, I changed the microwave frequency to be resonant with the degenerate ^{85}Rb $F=2$ $m_F = -1$ to $F=3$ $m_F = -2/F=2$ $m_F = -2$ to $F=3$ $m_F = -1$ transitions. By applying a single microwave sweep at the end of this sequence and measuring the fraction of the atoms transferred to the F=3 state, 28% of the atoms were transferred. Given $\alpha=0.855$ this is equivalent to 33% of the atoms being in the F=2, $m_F=-1$ state in our usual microwave/optical pumping cycle. These 12 cycles increased the gas temperature by 4.89(56) μK. During these 12 cycles 16(3)% of the atoms were lost, which was experimentally observed to be density-dependent but not dependent on the intensity of the optical pumping light. By using the optical pumping rate equation model, pulse timings, and predicted hyperfine-changing collision rate, The observed loss was calculated to be consistent with loss expected from hyperfine-changing collisions for the atom density using $(28\%)(5*10^{11}cm^{-3})(4*10^{-12}cm^3/sec)(12)(17ms) = 11.4\%$ within the systematic uncertainties of our measurement and the expected variation of the hyperfine-changing collision rate over the m_F states. The predicted hyperfine-changing collision loss rate is $4*10^{-12}cm^3/sec$ [3, 4], the density is $5*10^{11}cm^{-3}$ and each of the 12 pulses is 17 ms long. We assumed that part of the 4.89(56) μK temperature increase was due to anti-evaporation from two-body collisions in a harmonic trapping potential. The energy loss, in this case, is highest among

126

atoms with lower energy at the dense center of the gas. The average energy of the atoms lost from the cloud can be described by

$$\overline{E}_{2-body} = \frac{1}{N^2} \int f(\vec{x}, \vec{\nu})^2 \left\{ \frac{m\omega_r^2 r^2}{2} + \frac{m\omega_z^2 z^2}{2} + \frac{mv^2}{2} \right\} d^3x d^3\nu = \frac{9}{4} k_B T \qquad (7.5)$$

where $f(\mathbf{x}, \nu)$ is the thermal equilibrium distribution function. Since the average energy lost is less than $3k_B$T, the average energy of an atom in the cloud, we see that heating results due to the two-body losses. I determined the density-dependent portion of the heating to be $1.90(57)\mu$K. This was calculated using

$$H_{density} = T((3k_B T - f_{Ltotal}(2.25)k_B T)\frac{1}{3k_B T(1 - f_{Ltotal})} - 1) \qquad (7.6)$$

where $T=40\mu$K, consistent with the temperature measured in this auxiliary experiment. f_{Ltotal} is the total fraction of atoms lost, namely 16% for this experiment. The atoms lost have an average energy of $2.25k_B$T. To calculate a heating rate I can convert between the density and temperature conditions for this auxiliary experiment and the 2-CAZ experimental parameters to determine a heating rate of 1.19(8) μK/sec. This was calculated using

$$R_{heating-density} = \frac{T}{t_{cycle}}(\frac{3(1 + \chi_{87})k_B T - f_L(2.25)k_B T}{3k_B T(1 + \chi_{87} - f_L)} - 1) \qquad (7.7)$$

where χ_{87} =0.72 and f_L=0.16/12*0.073/0.28=0.003476 is the fractional loss per cycle. f_L is the loss in one cycle of optical pumping adjusted for the fraction of atoms eligible for an optical pumping cycle. This implicitly assumes that the hyperfine changing collision rates between $^{85/85}$Rb and $^{85/87}$Rb are the same, but this is a reasonable assumption for this estimate.

The remaining 2.99 μK of heating observed in the auxiliary experiment is owing to random momentum recoils from the photon scattering required for optical pumping. This recoil heating was consistent with the calculated number of photons required in the optical pumping cycle after taking into account the direction of the optical pumping beam. A redesign of the apparatus to align L3 to be exactly perpendicular (rather than 45°) to the optical trap axis would reduce this heating by a predicted factor of 2. This photon-scattering-induced heating rate was converted from

the auxiliary experiment to the relevant rate for 2-CAZ cooling by adjusting for the fraction of ^{85}Rb atoms that cycle through the $F=3$ state to be $2.22(12)\mu K$/sec using

$$R_{heating-photon} = \frac{T_{Heat}f}{12(0.28)t_{cycle}(1+\chi_{87})} \tag{7.8}$$

where $T_{Heat}=2.99$ μK and t_{cycle} and χ_{87} are the same as previously defined and $f=0.073$ is the fraction of ^{85}Rb atoms in the $F=3$ state.

I did not observe any statistically significant heating due to off-resonant light-assisted collisions caused by the optical pumping light. This off-resonant heating was measured by applying the optical pumping light to the cloud, but not the microwaves. I did expect heating during the optical pumping cycle due to ^{85}Rb atoms in $F=3$ state undergoing spin-exchange collisions. Since the ^{85}Rb $F=3$ state has a g_F factor opposite in sign from the $F=2$ state these collisions result in an energy increase of $5/6\mu_B B$ instead of the expected decrease of $1/6\mu_B B$ from an $F=2$ collisions. The loss attributed to hyperfine-changing collisions described above prevented us from measuring this rate directly, but it can be estimated to be $0.25(7)\mu K$/sec for these conditions. This estimate is done using

$$R_{heating-hyperfine} = \frac{5Bn\zeta\mu_B f t_c}{6k_B t_{cycle}(3)(1+\chi_{87})} \tag{7.9}$$

where the average density $n = 3\times10^{11}cm^{-3}$, the collision rate $\zeta = 3\times10^{-11}cm^3$/s and the assumed time during which collisions can occur during the optical pumping cycle (based on the rate equation model) is $t_c=300\mu s$.

7.3.2 Final Cooling Rate

After subtracting these heating rates from the maximum cooling rate I obtain a net cooling rate of 7.54(82) μK/sec. All of the heating and cooling rates are summarized in Table 7.1. It is clear that the heating rates have reduced the cooling capacity significantly even at a gas temperature much greater than the recoil energy divided by k_B. I can convert the measured heating rates determined above to a value for κ in equation (7.4) using

$$\kappa = \Delta(1 - \frac{net\ cooling\ rate}{maximum\ cooling\ rate}) \tag{7.10}$$

Table 7.1: A table summarizing the heating rates and cooling rates associated with the 2-CAZ experiment.

Rate (Heating or Cooling)	Value
Maximum Cooling Rate	11.2(9) μK
Density Dependent Heating from Hyperfine Changing Collisions	1.19(8) μK
Heating from Random Photon Scatters	2.22(12) μK
^{85}Rb F=3 Spin-Exchange Collisions Resulting in Heating	0.25(7) μK
Final Net Cooling Rate	7.54(82) μK

This equation is fairly straight forward to derive. If we consider $\kappa=0$ in equation (7.4) then the cooling rate is equal to the maximum cooling rate and is proportional to Δ. The net cooling rate is then proportional to $\Delta - \kappa$. Thus, $(\Delta - \kappa)/\Delta=$(net cooling rate)/(maximum cooling rate) and this can then be solved for κ, as shown above. This calculation results in $\kappa/k_B=7.31(68)\mu$K. Using this value, equation (7.4) predicts a net cooling of 7.78±2.1 μK/sec, again in agreement within statistical uncertainty. The implications for this value of κ will be discussed in section 7.4 below.

7.3.3 Additional Check of Heating

To help insure that I did not miss a significant heating or cooling factor, I performed an additional experiment. I loaded the FORT with ^{85}Rb and ^{87}Rb at a reduced optical trap depth of about 1/3 the typical depth and held the atoms there for 1 second before adiabatically ramping up the FORT to its full depth. Following this sequence radically reduced the evaporative cooling rate at the expense of a factor of 5 in the number of the atoms in the FORT. I then applied 60, 17 ms duration 2-CAZ cycles. At the end of the 2-CAZ cycles there were $0.24(1)\times10^6$ ^{85}Rb atoms and $0.21(1)\times10^6$ ^{87}Rb atoms. While not optimum for a 2-CAZ cooling rate, these conditions were sufficient to compare a measured amount of 2-CAZ-related cooling to predictions generated from a differential equation model. This differential equation model was much like the one detailed in Chapter 5 of [1], adapted to include the optical pumping timing and explicit scrambler rebalancing. I measured a temperature reduction of 1.92(27) μK as compared to a model prediction of 1.98(50) μK. This provides evidence that I have not left out any substantial heating or cooling considerations.

7.4 Future of 2-CAZ

Initially, the goal of this work was to use 2-CAZ for efficient cooling of an $^{85/87}$Rb mixture to few μK temperatures. This was not achieved in part because of the difficulty in creating sufficient initial conditions, particularly sufficiently high initial density, due to difficulties in simultaneous $^{85/87}$Rb optical trap loading [5]. In principle this limitation can be overcome through the use of different trapping techniques such as hybrid magnetic/optical trap loading [6], pre-cooling, or possibly trap geometry modification to increase initial density. However, the measurements reported above indicate that sufficient initial densities will not be the only critical factor in an $^{85/87}$Rb mixture for efficient 2-CAZ cooling. This in turn has implications for evaluating when 2-CAZ may be useful in other systems with other types of atoms.

Once k_BT has been lowered to be on the order of κ, the cooling rate will start to decrease exponentially. Thus, κ is an indication of the lowest practical achievable temperature. Ideally, κ would be on the order of a few photon recoil energies $((\hbar k)^2/(2m) = (k_B)0.19\mu K$ for Rb). The measured value of κ presented above is far above this ideal case. There are three main contributing factors. First, more efficient optical pumping (i.e. not having so many atoms end up in the m_F=-1 or 0 state rather than the m_F=-2 state at the end of an optical pumping cycle) would reduce κ by about a factor of 2 overall. Second, the heating contribution from photon recoils for the actual implementation of the optical pumping is much higher than reasonable theoretical limits. This is due to the component of the optical pumping beam that was along the axis of the trap. The required scattering rates associated with this beam meant that multiple photon scatters pushed the atom in a single direction along that axis causing a more than just random walk in the atom's motion rather than contributing random heat. The relevant beam alignment would have been difficult to change in this system without a radical change to the apparatus. Finally, the ^{85}Rb atoms are spending "too long" in the F=3 state, resulting in significant heating and atom loss from hyperfine-changing collisions. The second problem can be improved though multiple, although non-trivial, modifications to the apparatus. The final problem likely poses a severe challenge for the utility of 2-CAZ for $^{85/87}$Rb as it is density-dependent. For instance, if the cooling were made to be more effective and the densities increased by an order of magnitude over the conditions reported above, an order of magnitude reduction in time the ^{85}Rb atoms spend in the F=3 state during optical pumping would be required just to maintain the current contribution from hyperfine-changing collisions, let alone reduce it.

The time the ^{85}Rb atoms spend in the F=3 state is currently limited by the microwave power, but the timescales associated with scattering photons from L2 and L3 are less than an order of magnitude away from this microwave limit. While there are no reabsorption effects observed for the conditions reported above, I did observe degradation in optical pumping efficiency at an order-of-magnitude more intensity for L2 and L3. Thus, the window of sufficiently high density for effective cooling and sufficiently low time spent in

the F=3 state appears to be small. A potential solution to this problem would be to perform 2-CAZ by optically pumping an atom that had no hyperfine structure but a non-zero electron spin ground state (e.g. ^{52}Cr). This avoids the issues associated with the hyperfine changing collisions and would likely lead to better performance as long as the atom used did not suffer the unusually high light-assisted collision rate observed for low intensities in the implementation of the all-optical optical pumping of ^{85}Rb. In order for 2-CAZ to be effective, the other atom or molecule besides the no hyperfine structure atom in such a cooling situation would have to have hyperfine structure to produce an energy barrier (Δ) for spin-exchange collisions.

While $^{85/87}$Rb mixture did not work, there is nothing fundamental to the cooling technique that was a problem. It was instead the presence of the F=3 hyperfine state in the optically pumped ^{85}Rb that was the most insurmountable problem. This means that the problems with ^{85}Rb could likely be avoided by using a different atom, such as ^{52}Cr, that did not have hyperfine structure as the optically-pumped atom. Therefore, this technique is still viable, just not in the $^{85/87}$Rb system. More detail regarding the application of this technique to a different atom can be found in [7].

7.5   Conclusion

In this experiment I was able to probe the limitations of 2-CAZ cooling for the experimental configuration. Unfortunately, cross-isotope interference in optical trap loading, an unexpectedly large initial evaporation rate from the optical trap and the hyperfine-changing collision rate in the $^{85/87}$Rb mixture prevented the observation of robust 2-CAZ cooling. Working within the limitations of the experimental apparatus a 2-CAZ cooling rate was measured and evaluated. The results indicate that 2-CAZ cooling would be better suited for an atom without hyperfine structure as the optically pumped atom. Although this experiment did not lead to the hoped for cooling results it did lead us, although indirectly, to the STOP cooling technique which has significant promise.

References for Chapter 7

[1] Mathew Hamilton, Ph. D. Thesis, Colorado State University (2013).

[2] Kokoouline S 2001 Private Communication

[3] Burke J P Jr, Bohn J L, Esry B D and Greene C H 1998 Phys. Rev. Lett. 80 2097-2100

[4] Burke J P Jr 1999 Theoretical Investigation of Cold Alkali Atom Ph.D. Thesis (University of Colorado)

[5] Hamilton M S, Gorges A R and Roberts J L 2012 J. Phys. B: At. Mol. Opt. Phys. 45 095302

[6] Y.-J. Lin, A. Perry, R. Compton, I. Spielman, and J. Porto, Phys. Rev. A 79, 063631 (2009).

[7] Hamilton M S, Wilson R F and Roberts J L Eur. Phys. J. D (2014) 68: 14.

Chapter 8

Review and Future Measurements

Although the 2-CAZ cooling experiment did not result in the cooling we had hoped for when we first began the experiment, we were able to learn several interesting things about the nature of two isotope interactions [1, 2], as well as demonstrate the first extension of CAZ cooling to two isotopes [3]. We discovered that the two isotopes interfere in such a way as to greatly reduce the initial atom number of each isotope. This load rate reduction in addition to the large evaporation rate inherent in our FORT prevented us from achieving the initial conditions that we had originally planned on. Despite this we were still able to evaluate the cooling and heating rates that occur during 2-CAZ cooling. Through the investigation into the individual contributions to the heating and cooling rates we were able to discover that not only are ^{87}Rb and ^{85}Rb poor isotopes to work with because of the initial loading problems, but that during the cooling ^{85}Rb, for reasonable experimental parameters that avoid reabsorption problems, spends too much time in the upper hyperfine ground state causing a large amount of heating and loss. This discovery helped shed light on what types of atoms would be better suited for use in this cooling scheme.

After spending years working towards a less than satisfying conclusion with this 2-CAZ experiment, we were quite pleased to have great success with the STOP cooling technique after only a few short months. As reported in Chapter 3, we saw one-dimensional cooling rates of close to 250 μK/sec from a single cycle of STOP cooling. We only investigated single cycle STOP cooling largely due to limitations in the experimental setup. The next step in this experiment is to modify the experimental apparatus to reduce or eliminate the large evaporation rate in the optical trap.

We feel confident that the steps that are being taken to modify this experiment, as discussed in Chapter 4, will greatly reduce the evaporation rate in our FORT. With this improvement in the evaporation rate and the other experimental modifications mentioned, we are optimistic that the next round of STOP cooling measurements will allow us to measure multiple cycles of STOP cooling. In addition to investigating the success of many cycle STOP cooling with ^{87}Rb, this measurement should shed light on the potential limitations of this technique. Additional information about the limitations of this technique should allow us to explore the possibility of using this cooling method

to cool molecules. Theoretical evaluation of the details of such a molecular cooling scheme are under way, as is the next round of STOP cooling measurements.

References for Chapter 8

[1] Mathew Hamilton, Ph. D. Thesis, Colorado State University (2013).

[2] Anthony Gorges, Ph. D. Thesis, Colorado State University (2010).

[3] Hamilton M S, Wilson R F and Roberts J L Eur. Phys. J. D (2014) 68: 14.